

TALLINN UNIVERSITY OF TECHNOLOGY  
DOCTORAL THESIS  
69/2018

**Mathematical Modelling and  
Optimization of Erosion and Corrosion  
in Tribology**

FRANCISCO JOSE CASESNOVES GRANADO



TALLINN UNIVERSITY OF TECHNOLOGY

School of Engineering

Department of Mechanical and Industrial Engineering

This dissertation was accepted for the defence of the degree 26/06/2018

**Supervisor:** Senior research scientist, Professor emeritus Priit Kulu  
Department of Mechanical and Industrial Engineering  
Tallinn University of Technology  
Tallinn, Estonia

**Co-supervisor:** Senior research scientist Maksim Antonov  
Department of Mechanical and Industrial Engineering  
Tallinn University of Technology  
Tallinn, Estonia

**Opponents:** PhD Arkadi Zikin  
Technology Leader, Application Development,  
Laser Surface Engineering, Oerlikon Metco AG  
Wohlen, Switzerland

Associate professor Ella Puman  
Institute of Mathematics and Statistics  
University of Tartu  
Tartu, Estonia

**Defence of the thesis:** 14/12/2018, Tallinn

**Declaration:**

Hereby I declare that this doctoral thesis, my original investigation and achievement, submitted for the doctoral degree at Tallinn University of Technology, has not been submitted for doctoral or equivalent academic degree.

Francisco Jose Casesnoves Granada

-----  
signature



European Union  
European Social Fund



Investing in your future

Copyright: Francisco Jose Casesnoves Granada, 2017

ISSN 2585-6898 (publication)

ISBN 978-9949-83-356-6 (publication)

ISSN 2585-6901 (PDF)

ISBN 978-9949-83-357-3 (PDF)

TALLINNA TEHNIKAÜLIKOOL  
DOKTORITÖÖ  
69/2018

**Erosiooni ja korrosiooni matemaatiline  
modelleerimine ja optimeerimine  
triboloogias**

FRANCISCO JOSE CASESNOVES GRANADO



# Contents

|   |     |
|---|-----|
| List of Publications .....  | 6   |
| Author's Contribution to the Publications .....   | 7   |
| Introduction .....  | 8   |
| Abbreviations .....   | 11  |
| Symbols .....   | 12  |
| 1 Literature Review .....   | 14  |
| 1.1 Erosion and corrosion models .....  | 14  |
| 1.2 Review of optimization methods .....  | 23  |
| 1.2.1 Generic multi-objective optimization (MO) .....   | 23  |
| 1.2.2 Specific optimization algorithms .....  | 23  |
| 1.3 Aim and objectives of the study .....   | 25  |
| 2 Materials and Methods .....   | 26  |
| 2.1 Experimental .....  | 26  |
| 2.2 Software development tools used .....   | 28  |
| 3 Mathematical Modelling, Computational Results, and Nonlinear Optimization .....                 | 29  |
| 3.1 Classifications of tribology mathematical models for optimization framework... 29             |     |
| 3.2 Stratified construction of Beckmann and Gotzmann equations in discrete tribology models ..... | 32  |
| 3.3 Integral-differential model construction .....  | 33  |
| 3.4 Graphical optimization in 2D and 3D .....   | 34  |
| 3.5 Bioengineering tribological simulations and applications .....                                | 36  |
| 3.6 Inverse problems .....  | 38  |
| 3.6.1 Inverse problems theory and its applications in modelling .....                             | 38  |
| 3.7 Stochastic corrosion methods .....  | 41  |
| 3.8 Computational comparison of WC-Co hardness reinforcements .....                               | 42  |
| Conclusions .....   | 50  |
| References .....  | 52  |
| Acknowledgements .....  | 57  |
| Abstract .....  | 58  |
| Lühikokkuvõte .....   | 59  |
| Appendix 1 .....  | 61  |
| Appendix 2 .....  | 63  |
| Paper I .....   | 63  |
| Paper II .....  | 75  |
| Paper III .....   | 91  |
| Paper IV .....  | 99  |
| Paper V .....   | 129 |
| Curriculum vitae .....  | 139 |
| Elulookirjeldus .....   | 141 |

## List of Publications

The list of author's publications, on the basis of which the thesis has been prepared:

- I Surzhenkov, A., Viljus, M., Tarbe, R., Casesnoves, F. Wear resistance and mechanisms of composite hardfacings at abrasive impact erosion wear. *Journal of Physics: Conf. Series*, 2017, pp. 1-10 (843 012060 DOI :10.1088/1742-6596/843/1/012060).
- II Casesnoves, F., Surzhenkov, A. A mathematical model for abrasive erosion wear in composite Fe-based matrix with WC-Co reinforcement. *Materials and Contact Characterization*, 2017, 116, pp. 99-111. WIT PRESS. Section 2 Computer Methods: Computer and Simulation.
- III Kulu, P., Casesnoves, F., Simson, T., Tarbe, R. Prediction of abrasive impact wear of composite hardfacings. *Solid State Phenomena, Proceedings of 26<sup>th</sup> International Baltic Conference on Materials Engineering*. 2017, 267, pp. 201-206. (DOI:10.4028/www.scientific.net/SSP.267.201). 2017 Trans Tech Publications, Switzerland Online: 2017-10-10.
- IV Casesnoves, F., Surzhenkov, A. Mathematical models in biotribology with 2d-3d erosion integral-differential model and computational-optimization/simulation programming. *International Journal of Scientific Research in Computer Science, Engineering and Information Technology*, 2017, 2,3, pp. 329-356.
- V Casesnoves, F., Surzhenkov, A. Inverse methods for computational simulations and optimization of erosion models in power plants. *IEEE Proceedings of RUTCON2017 Power Engineering Conference*. 2017, paper 139. (DOI:10.1109/RTUCON.2017.8125630. Electronic ISBN: 978-1-5386-3846-0. USB ISBN: 978-1-5386-3844-6. ISBN: 978-1-5386-3847-7).

## Author's Contribution to the Publications

Author's work/contribution to the papers in this thesis is:

- I All computational-mathematical calculations of the proposed model. The modeling and programming software was made by thesis author, used was both FreeMat and MATLAB, and Fortran 77-95 subroutines. Numerical calculations were done by author with MATLAB and F# designed subroutines.
- II Article plan, numerical verification, manuscript writing principal part, modeling were performed by author. Mathematical model design, programming software in 3D surfactal optimization and global optimization graphs.
- III Mathematical model calculations and programming. All computational-mathematical calculations of the proposed model. The programming software used was special contribution design both in FreeMat and MATLAB, and Fortran 77-95 subroutines.
- IV Article plan, numerical verification, manuscript writing principal part, modeling and supervising by author. Mathematical model design, programming software in 3D surfactal optimization and global optimization graphs.
- V Article plan, numerical verification, manuscript writing principal part, modeling and supervising by author. Mathematical model design, programming software in 3D surfactal optimization and global optimization MATLAB graphs.

## Introduction

*Nonsense. Space is blue and birds fly through it.* Werner Heisenberg

To date, mathematical modelling (MM) constitutes one of the most important research methods in all fields of science, engineering and technology—but not limited to these areas, since it can be applied in many other field. In this thesis research, the mathematical model is defined as follows: Definition 1: A mathematical model is a cognitive abstraction of any natural and/or artificial phenomena, with an exact/approximated numerical-equational terminology.

A mathematical model could be specified in a number of explicit formulas/determinations, a group of engineering constraints for variables and even in an implicit function or formulation [1-4]. Along a series of subsequent references [4, 5], mathematical modelling concepts, results, programming and optimization were presented and analyzed. Model construction and specifications depend on the criteria of many authors throughout the historical stages in research. In Figure 1, a basic concept-caption of the importance of erosion models is presented. Namely, the impact particle, kinetic energy, speed, and impact angle variations along curved pipe regions determine constraints for modelling.

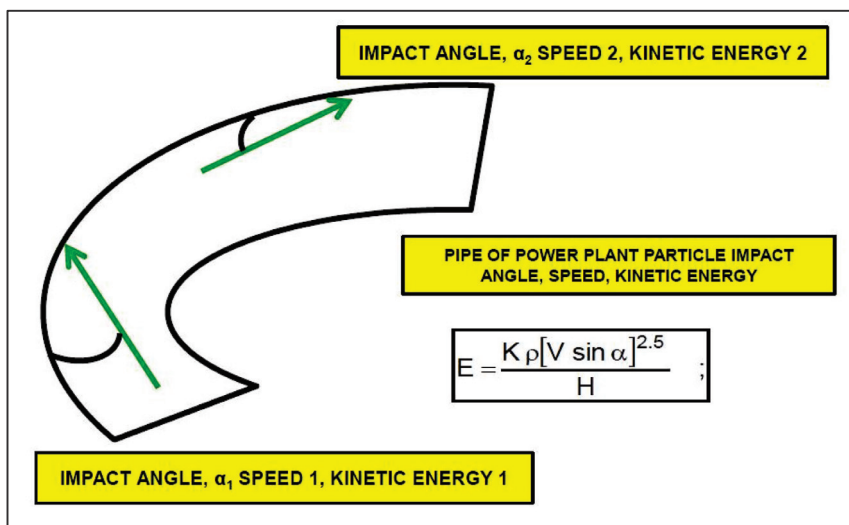


Figure 1 Concept of usage of an erosion mathematical model in a pipe.

Statistics [3, 4] could be considered a branch of mathematics or an independent science itself. Occasionally, mathematical models are mixed up, i.e., with mathematical equations with discrete parameters and statistical functions. The functionality of a model is evaluated by its usage and empirical validation. The functionality of a model is also determined in final stages by its precise match with the real experimental database. It is very unusual to find absolute precision in a mathematical model, although high accuracy is reached by the best built group of tribology models that have been improved and constantly updated/adapted to new materials, which happens also in many fields of science and technology.

Although the common technical concept of wear, erosion, and corrosion is usually related to materials in mechanical engineering/physics, these physical-chemical phenomena are widely extended both in nature and artificial world. Erosion, corrosion, tribocorrosion, and biotribology are concepts that belong to any kind of compounds of materials that constitute any type of engineering/bioengineering system.

“Trial and error” methods [5, 6] to determine, quantity, and model construction methods in E/C (erosion and/or corrosion), tribology and biotribology, i.e., the forward problem technique was found expensive, imprecise and time consuming. In consequence, applications of the Inverse Problems Theory, (Paper V), were used to determine *a posteriori* the computational possibilities, validation/refinement of an initial theoretical mathematical model previously approximated. In doing so, the optimization methods are developed in order to carry out an initial mathematical approximation for a subsequent experimental choice of the most convenient materials - from experimental to model through inverse optimization methods.

Statistically (Paper V), [72], a rate higher than 90 %, of mechanical machine failures is linked to fatigue, friction, stress, and wear. The general causes of degradation are wear, corrosion, oxidation, temperature, gas-particle size/velocity, and any combination of these factors. Mathematical modelling is essential for determination of engineering probability of failure of any mechanical or electromechanical system in power plants. To date, a number of mathematical models are available for erosion, biotribology, tribocorrosion, corrosion, and combinations of these phenomena.

A large-scale statistical determination of worldwide energy consumption due to tribological origin [7] sets the approximate rate of 23 % loss of energy caused by wear and friction. This fact implies serious consequences in engineering, economy, and environmental science and engineering. What is more, the loss and/or unfunctional use of energy cause a thermodynamic increase of entropy in the planet, with subsequent consequences in environmental damage increment rate along the years/decades. In other words, as sketched in Figure 2, the reduction of the rate increase-entropy/time on the earth is linked directly to losses of energy unrelated to/dispersed from any practical use.

The objective of this research is to adapt existing E/C models [8] for specific conditions and to develop new models for wear – specifically, the integral-differential general model. Additionally, it is required to build techniques for model optimization by using numerical methods. An objective in computational simulations is to present 2D and 3D simulations series of selected models, and show new results in graphical optimization methods. Subsequently, it is necessary to apply models for simulation of a series of experimental lab database obtained in the thesis research.

A complementary objective, in the line of circular economy linked to mathematical modelling in tribology, was introduced. In this research, specific materials were calculated, modelled and compared to recycled ones, to prove the engineering utility of circular economy with real laboratory data.

All these results in tribology applications, both theoretical and experimental, have been implemented in a series of internationally peer-reviewed and recognized journals. The verification of the tribology models, were presented also in lectures and conference contributions to support and validate the quality of the investigation. The projection for further research of these papers can be considered promising, since, for example, the determination of the basis for the second generation of tribology/biotribology modelling opens a new research line towards the improvements of modelling construction. In Figure 2, the real and necessary energy demanding factors are biased by inefficient factors related to waste/loss of energy in tribology. Mathematical modelling in tribology holds important consequences in optimization at minimum waste in this improper energy spending.

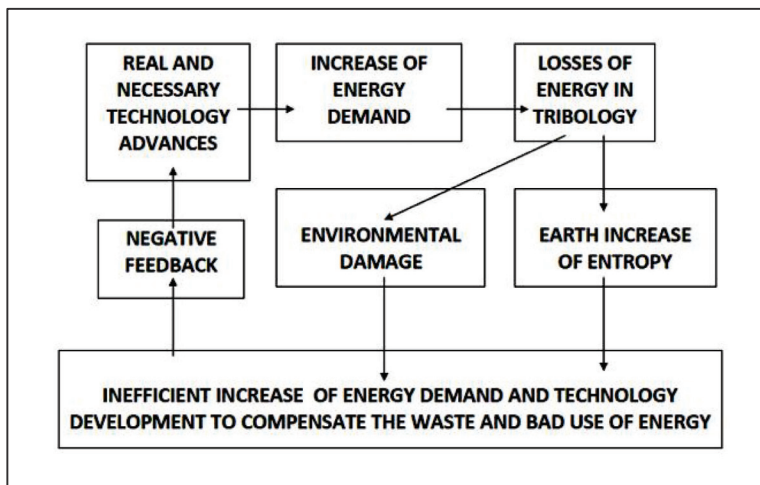


*Figure 2 Illustration of the earth entropy consequences of tribology-energy improvements-advantages and justification of correct modelling design/approaches, a development based on statistics [7].*

## Abbreviations

|                      |                                      |
|----------------------|--------------------------------------|
| CG                   | Conjugate gradient methods           |
| DM                   | Deterministic optimization method    |
| E/C                  | Erosion and/or corrosion             |
| GA                   | Genetic algorithms                   |
| GPL                  | General public license               |
| HGA                  | Hybrid genetic algorithms            |
| IP                   | Inverse problems theory/applications |
| K                    | Proportionality constant             |
| LO                   | Linear optimization                  |
| NLO                  | Nonlinear optimization               |
| M                    | Metal                                |
| MC                   | Monte Carlo (methods)                |
| MM                   | Mathematical model                   |
| MO                   | Multi-objective optimization         |
| MSDM                 | Microscale dynamic model             |
| OF                   | Objective function                   |
| ROI                  | Region of interest                   |
| RT                   | Random optimization techniques       |
| SD                   | Steepest descent (method)            |
| SA                   | Simulated annealing (method)         |
| SO                   | Stochastic optimization              |
| TUT, TTÜ,<br>TalTech | Tallinn University of Technology     |

## Symbols

|              |  |
|--------------|--|
| $A$          | <i>Cross-sectional area used in the formulation</i>  |
| $A(t)$       | <i>Wave amplitude</i>  |
| $A_t$        | <i>Cross sectional area of cutting tool</i>  |
| $a$          | <i>Mean half diagonal length of an abrasive or<br/>Quotient between <math>T</math> and <math>\Delta t</math></i> |
| $b$          | <i>Burger vector</i>   |
| $B$          | <i>Particle velocity for unit of force applied</i>   |
| $c$          | <i>Size of median of lateral crack</i>   |
| $C_s$        | <i>Ratio of effective contact length to the mean diameter of abrasives</i>                                       |
| $C$          | <i>Volumetric concentration of abrasives</i>   |
| $C'$         | <i>Specific constant of material</i>   |
| $C_K$        | <i>Proportionality constant</i>  |
| $d_m$        | <i>Average diameter of abrasive grain</i>  |
| $d_{max}$    | <i>Average maximum diameter of abrasive grain</i>  |
| $d_{min}$    | <i>Average minimum diameter of abrasive grain</i>  |
| $E_{name}$   | <i><math>E</math> is erosion rate, and the subscript is the initial<br/>of the author of the model</i>           |
| $E_t$        | <i>Young modulus of tool</i>   |
| $f$          | <i>Cyclic frequency of vibrations</i>  |
| $G$          | <i>Gibbs energy</i>  |
| $G_w$        | <i>Shear modulus of work surface</i>   |
| $H$          | <i>Hardness</i>  |
| $K$          | <i>Proportionality constant or Erosion wear constant/coefficient</i>   |
| $K_{O_2}$    | <i>Temperature coefficient</i>   |
| $K_1$        | <i>Constant of proportionality</i>   |
| $L_t$        | <i>Contact length</i>  |
| $M$ or $M_a$ | <i>Mass of abrasive particle</i>   |
| $M_a$        | <i>Mass flow rate of abrasive particles</i>  |
| $N$          | <i>Number of abrasive particle by time unit</i>  |
| $N$          | <i>Number of active abrasive grains in the working gap in Lee model</i>  |
| $n$          | <i>Flaw parameters corresponding to different models</i>   |
| $O_2$        | <i>Oxygen molecule</i>   |
| $p$          | <i>Nozzle pressure</i>   |
| $P_{atm}$    | <i>Atmospheric pressure</i>  |
| $q_w$        | <i>Work hardening capacity</i>   |
| $r$          | <i>Position of particle or geometrical distances</i>   |
| $R$          | <i>Surface roughness</i>   |
| $R_g$        | <i>Constant of gas</i>   |

## Symbols (continued)

|                         |  |
|-------------------------|--|
| $R_f$                   | <i>Particle roundness factor</i>                                 |
| $r_m$                   | <i>Average radius of particle</i>                                |
| $T$                     | <i>Time period of vibrations</i>                                 |
| $T1$                    | <i>Type 1 model</i>  |
| $T2$                    | <i>Type 2 model</i>  |
| $t_a$                   | <i>Time corresponding to abrasive contact</i>                    |
| $V_a$                   | <i>Volumetric removal rate</i>                                   |
| $V_a$                   | <i>Conical volume removed by a single particle</i>               |
| $v$                     | <i>Particle velocity</i>   |
| $v_a$                   | <i>Particle impact velocity</i>                                  |
| $V_{wg}$                | <i>Volume of tool-work gap</i>                                   |
| $v_n$                   | <i>Normal component of velocity</i>                              |
| $W$                     | <i>Specific mass of corroded metal, wear rate in Section 3.2</i> |
| $w$                     | <i>Angular frequency</i>   |
| $\vartheta$ or $\alpha$ | <i>Particle impact angle</i>                                     |
| $\delta$                | <i>Depth at which crack originates</i>                           |
| $\rho_a$                | <i>Density of abrasive particles</i>                             |
| $\sigma_f$              | <i>Flow strength of work piece</i>                               |
| $\sigma_{fw}$           | <i>Flow of stress</i>  |
| $\varphi$               | <i>Chemical potential (Nerst equation)</i>                       |
| $\phi_c$                | <i>Material dependent wear factor</i>                            |

# 1 Literature Review

This section is focused on the erosion and corrosion models and review of optimization methods.

## 1.1 Erosion and corrosion models

This section contains a bibliographic description of E/C models, setting advantages, inconveniencies, and prospective considerations. However, the citations are presented in brief. Most of this modelling review comes from [72]; however, the brief was extended to recently published models whose applicability is not complicated. In general, formulation and description are simplified and the description of the model is practical and simple. A classification of models is proposed in [72].

The interaction of materials [9-13], whether they are liquid, gas, metastates, or varieties of them, is rather difficult for study. It is possible to simplify the classification(s) on the following basis: given a rather large number of models, it is assumed that the extensive complexity of E/C causes the necessity to design particular models almost for every type of interaction. In other words, the lack of existence of widely applicable general models for E/C constitutes the main reason for a variety of such kind of mathematical models, [14]. In Section 3.1, a group of classifications frames was set to both erosion and corrosion, in terms of simplification and fast practical use/selection of models in each particular material choice. In the following, a series of mathematical formulas of selected models is presented. The author of the current thesis has proposed a classification of models in T1 (general models), and T2 (specific models) in [71] and Section 3.1.

**Miller model (T2, 1957).** This model is for ductile-cutting [1, 2] and its equations are formulated for abrasive particles with cubic shape. However, it can be considered simple in structure as follows:

$$E_M = K \times \frac{A d_m f F P_{atm}}{b_w G_w q_w R V_{wg} \rho_a} \times \frac{C}{C+1} \quad (1.1)$$

*depth of cut per unit time is,*

$$DE_M = K \times \frac{A d_m f p P_{atm}}{b_w G_w q_w R V_{wg} \rho_a} \times \frac{C}{C+1} ,$$

where  $E_M$  is material removal rate ( $\text{mm}^3/\text{s}$ ),  $DE_M$  - depth of cut per time unit ( $\text{mm}/\text{s}$ ),  $K$  - constant of proportionality,  $A$  - cross-sectional area ( $\text{mm}^2$ ),  $b_w$  - Burger vector work surface (mm),  $d_m$  - mean diameter of abrasive (mm),  $P_{atm}$  - atmospheric pressure (MPa),  $F$  - mean static force over a period (N),  $f$  - cyclic frequency of vibrations (cycles/s),  $G_w$  - shear modulus (MPa),  $q_w$  - work hardening capacity (MPa),  $R$  - surface roughness ( $\mu\text{m}$ ),  $V_{wg}$  - volume of tool-work gap ( $\text{mm}^3$ ),  $C$  - volumetric concentration of abrasives (adimensional). The first equation is to determine the erosion rate, the second is to calculate the depth of cut per unit time caused by erosion. This model is applicable for ductile materials, and has similar applications than Finnie model (1.3). In general, the units can be adapted on specific laboratory requirements [1, 2].

**Lee and Chan model** for brittle fracture (**T1-T2, 1997**). This nonlinear model [15] is very specific for a hemispherical indentation fracture. Abrasives are assumed as spherical particles and rigid. The formulation is:

$$E_L = \frac{2\pi K_1^2 f}{3N} \times (aF + bA)^2; \quad (1.2)$$

where,

$$a = \frac{T}{\Delta t}; b = \frac{A_t E_t}{L_t} \left( 1 + \frac{T}{\pi \Delta t} \cos(\omega t_a - \varphi) \right);$$

$$\text{and, } A(t) = A \sin(\omega t - \varphi),$$

where  $E_L$  is material removal rate ( $\text{mm}^3/\text{s}$ ), and  $\varphi$  - the phase of the amplitude equation (radians),  $A$  and  $A(t)$  - wave amplitudes (mm),  $K_1$  - constant of proportionality,  $F$  - mean static force over a period (N),  $f$  - cyclic frequency of vibrations (cycles/s),  $N$  - number of active abrasive grains in the working gap,  $a$  - quotient between  $T$  and  $\Delta t$  adimensional,  $b$  - Burger vector (mm),  $T$  - time period of vibrations (s),  $A_t$  - cross sectional area of cutting tool ( $\text{mm}^2$ ),  $E_t$  - Young modulus of tool (MPa),  $L_t$  - contact length of tool (mm),  $\omega$  - angular frequency (cycles/s),  $t_a$  - time corresponding to abrasive contact (s). This model specific for brittle can be considered less general than Parbhakar model (1.5).

**Finnie model (T1, 1958, 1960)**. This model was one of the first models invented [1] for quantification of eroded material magnitude. It is a cutting considering model, which sets a rigid-plane surface. Today Finnie algorithm is used as a formal reference for improved models. The formulation reads:

$$E_f = c \times \frac{MV^2}{\psi p K} \times f(\alpha); \quad \text{with,} \quad (1.3)$$

$$f(\alpha) = \sin(2\alpha) - \frac{6}{K} \sin^2(\alpha), \quad \alpha \leq \arctan\left(\frac{K}{6}\right);$$

$$f(\alpha) = \frac{K \cos^2(\alpha)}{6}, \quad \alpha \geq \arctan\left(\frac{K}{6}\right),$$

where  $E_f$  is the material removal ( $\text{mm}^3/\text{mass of abrasives in kg}$ ),  $K$  - the geometrical ratio between vertical to horizontal forces adimensional,  $V$  - the particle speed ( $\text{mm/s}$ ),  $p$  - material flow stress,  $M$  - mass of abrasives (kg),  $c$  - a correction factor for impact failure/mutual-particle-impact,  $\psi$  - the ratio of depths, contact to cut, adimensional,  $\alpha$  is the attack angle (radians or degrees). Note the factor  $MV^2$  that corresponds to a kinetic energy magnitude inserted implicitly within the formula. This model is classical, and erosion is characterized by high flow stress compared to others for both ductile materials and brittle materials, such as (1.4).

**Bitter model (T1, 1963).** This model [1, 2] sums erosion for plastic deformation ( $E_{Bd}$ ) and cutting erosion ( $E_{Bc}$ ). Principal equations are as follows:

$$\begin{aligned}
 & \text{Deformation wear erosion,} \\
 E_{Bd} &= \frac{M[V \sin(\alpha) - V_{el}]^2}{2\varepsilon_b} \text{ for } V \sin(\alpha) \geq V_{el} \text{ and} \\
 & \text{null if } \leq V_{el}; \\
 & \text{and subsequent, cutting wear erosion,} \\
 E_{Bc} &= \frac{2MC'[V \sin(\alpha) - V_{el}]^2}{2\varepsilon_b} \times \\
 & 2MC' V \cos(\alpha) \frac{C' \times [V \sin(\alpha) - V_{el}]^2}{\sqrt{V \sin(\alpha)}} \varphi_C \\
 & \text{if } \alpha \leq \alpha_0 \text{ or} \\
 M V \cos(\alpha) & \frac{M[V^2 \cos^2(\alpha) - K_1[V \sin(\alpha) - V_{el}]^{3/2}]}{2\varphi_C} \\
 & \text{for } \alpha \geq \alpha_0 ,
 \end{aligned} \tag{1.4}$$

where  $\alpha$  is the impact angle (degrees or radians),  $\varepsilon_b$  - the deformation wear factor obtained experimentally ( $\text{J}/\text{mm}^3$ ), and  $V_{el}$  - the threshold velocity (velocity at collision at which the elastic limit of the workpiece material is just reached), (m/s).  $V_{el}$  can be calculated from the Hertzian contact theory.  $V_{el}$  depends on several factors, and some approximations were carried out. Parameter  $\varphi_c$  is a material dependent wear factor obtained experimentally ( $\text{J}/\text{mm}^3$ ) and  $C'$  and  $K_1$  are constants of a specific material. This model has similar advantages compared to (1.3).

**Parbhakar model (T2, 1993)**, [16]. This model was designed for brittle fracture with spherical particles and Hertz fracture theory was applied. The equation of this model is:

$$\begin{aligned}
 E_p &= N f V_a C_s ; \\
 \text{where, } V_a &= \frac{1}{3} \pi c^2 \delta ,
 \end{aligned} \tag{1.5}$$

$E_p$  - is volume removal rate , ( $\text{mm}^3/\text{s}$ )  $V_a$  - volumetric removal rate ( $\text{mm}^3/\text{s}$ ),  $N$  - number of active abrasive grains in the working gap,  $f$  - cyclic frequency of vibrations (cycles/s),  $C_s$  -ratio of effective contact length to the mean diameter of abrasives, adimensional,  $V_a$  - conical volume removed by a single particle ( $\text{mm}^3/\text{s}$ ) ,  $c$  - radial extension of crack (mm),  $\delta$  - depth at which crack originates (mm). Parameters are also described with more detail in [16]. This model is simple and specific for brittle compared to (1.3) and (1.4) is more simple to apply and for indentation fracture.

**Bitter simplified model (Neilson and Gilchrist's Model, T1, 1968).** Neilson and Gilchrist simplified the Bitter model [1], combined to express a ductile erosion model and using this Bitter model for brittle erosion as follows:

$$E_N = \frac{MV^2 \cos^2(\alpha)^2}{2\phi_C} + \frac{M [V \sin(\alpha) - V_{el}]^2}{2\varepsilon_b};$$

$\alpha \geq \alpha_0$  ; and, (1.6)

$$E_N = \frac{MV^2 \cos^2(\alpha)^2 \sin(n\alpha)}{2\phi_C} +$$

$$+ \frac{M [V \sin(\alpha) - V_{el}]^2}{2\varepsilon_b}; \alpha \leq \alpha_0 ,$$

where  $\alpha$  - is the impact angle (degrees or radians),  $\varepsilon_b$  - the deformation wear factor obtained experimentally ( $J/mm^3$ ),  $V_{el}$  - the threshold velocity (velocity at collision at which the elastic limit of the workpiece material is just reached), (m/s).  $V_{el}$  can be calculated from the Hertzian contact theory.  $V_{el}$  depends on several factors, and some approximations were carried out. Parameter  $\phi_c$  - is a material dependent wear factor obtained experimentally ( $J/mm^3$ ) and  $C'$  - and  $K_1$  - are constants of a specific material. Experimental work is required to determine the erosion constants  $\varepsilon_b$  and  $\phi_c$ . This model is a simplified evolution of (1.4), and applicable in brittle and ductile erosion. Compared to (1.4), it results in formulation very similar and efficacious.

**Hutchings models (T1, 1981)** [1, 2, 17]. There are several types of this model and this is a primary one. In Paper III, the classical equation was calculated for discrete models. It was designed for erosive wear by plastic deformation, without deformation factors. The specific formula for normal impact is:

$$E_H = \frac{K\rho v^2}{2H} , \quad (1.7)$$

where  $E_H$  is erosion rate ( $mm^3/kg \text{ s}$  in this study),  $\rho$  - the density of the material being eroded ( $kg/mm^3$ ),  $v$  - the initial particle velocity ( $mm/s$ ) and  $H$  - the target surface hardness (MPa to mm and kg).  $K$  represents the fraction of material removed from the indentation as wear debris and is also known as the wear coefficient. The value of  $K$  can be thought of as a measure of the efficiency of the material removal process. Derivations of this model inserting the impact angle have been developed and constitute a specific variety. This model was used to make an optimization example with software-subroutine in Section 3.3. It cannot be considered a good model compared to (1.3) and (1.4), because it is a generalization.

**Sheldon model (T2, 1996)** [18]. This model is for brittle materials, particles are set as rigid, spherical and angular. Constraints of the impact angle are always normal.

$$E_s = K_4 \frac{r_m^6}{r^4} \frac{0.6n}{n-2} \times (v_a)^{\frac{2.4n}{n-2}}, \quad (1.8)$$

where  $K_4$  forms a series of consecutive equations with products and exponentials,

where  $E_s$  is volume of material removed by particle,  $v_a$  - article impact velocity,  $r$  parameters - geometrical distances,  $K_4$  - proportionality constant,  $n$  - flaw parameters.

**Hashish modified model for erosion (T2, 1987).** This model [1] is based on the Finnie model and includes the velocity term and the conditions of the particle shape. Basic formulation is as follows:

$$E_{HM} = \frac{7}{\pi} \times \frac{M}{\rho_a} \times \frac{V}{C_K} \frac{5}{2} (\sin(2\alpha) \times (\sin(\alpha))^{1/2}); \quad (1.9)$$

and,

$$C_K = \sqrt{\frac{3 \sigma_f R_f^{3/5}}{\rho_a}},$$

where  $R_f$  is the particle roundness factor (mm), alpha - the impact angle (radians or degrees),  $C_k$  - the characteristic velocity factor defined by the second equation (mm/s),  $M$  - particle mass (kg),  $\rho_a$  - particle density (kg/mm<sup>3</sup>),  $\sigma_f$  - flow strength of the work piece (MPa). This model requires no experimental constants. It is uniquely based on the ductile properties of the eroded material, and therefore useful/focused for shallow impact angles for ductile materials, T2. It is an improved Finnie model specific for deformation wear.

**Computational fluid dynamics models (T1, 2000, 2009).** This method [1] is used for solid particle erosion inside pipe geometries, rather for T2 but since it could be applied on several kinds of materials, for T1 as well. Its weakness is that this technique is complicated and time consuming and as such is most appropriate for complex, non-standard geometries.

Additional difficulties are the determination of particle percentage on a fixed surface, their impacting angle, and specific/individual velocity. An example of formulation for this type of modelling is:

$$E_{CD} = A F_s V_0^n f(\vartheta), \quad (1.10)$$

where,  $E_{CD}$  is the erosion rate (mm<sup>3</sup>/kg s),  $V_0$  - the particle impingement velocity (mm/s),  $A$  - a material adimensional dependent coefficient,  $F_s$  - a particle shape coefficient (mm),  $n$  - an empirical constant, and  $f(\vartheta)$  - a function dependent on the impact angle. Computational fluid dynamics models are used, for example, for pipe erosion.

**Neema model (T2, 1993)** [1]. This model is suitable exclusively for brittle materials at normal impact angle.

$$E_N (\text{Kg/s}) = 0.1156 \times \frac{\rho_a M_a v_n^2}{10^3 \sigma_{fw}} ; \quad (1.11)$$

*brittle and normal impact  
constraints,*

where  $E_N$  is the volume of material rate (kg/s),  $v_n$  - normal component of particle speed (mm/s),  $M_a$  - mass of abrasive particle (kg),  $\sigma_{fw}$  - flow stress of target of workpiece material (MPa or N/mm<sup>2</sup>),  $\rho_a$  - density of abrasive particles (kg/mm<sup>3</sup>). Neema model is very specific compared to (1.3), (1.4), and (1.9).

**Microscale dynamic model (MSDM, T1).** This model [2] is designed to be implemented with the FE method and is useful for erosion-corrosion. It is based on the equations of fundamental physical forces, such as:

$$\vec{F} = m \times \frac{d^2 \vec{r}}{dt^2} , \quad (1.12)$$

where  $m$  is mass defined in Newton's law (any convenient unit of mass),  $r$  - position of particle (any convenient unit of longitude),  $t$  - time (any convenient unit of time),  $F$  - force (any convenient unit of force related to equation). The MSDM approach is applied to modelling of an abrasion process compared to plastic-elastic mechanical elements, such as wheels or similar mechanical components. This tribotesting method is widely used to rank wear-resistant materials under low stress condition. Abrasive particles pass through the opened-gap between the mechanical sample and the specimen. As a result, the specimen surface is eroded/abraded. The mass loss of a tested material is dependent on the mechanical properties of the tested material and the abrasive particles as well as the wear conditions. All this is carried out with 2D modelling and the resulting equations have a physical mechanical frame and present no important complications.

**Beckmann and Gotzmann (T1-T2, 1985)**, [19]. These are discrete models in Equations (3.1) and (3.3). They were derived as an analytical expression for the erosion of metals from the hypothesis that in abrasive and erosive wear, the volume removed is proportional to the work of shear forces in the surface layer. The basic model was formulated from the study of deformation caused by a single spherical particle. A discrete extended model of this type was implemented completely in Paper III.

**Finite Element (FEM) and Monte Carlo/Quasi Monte Carlo models.** Broadly, FEM is a mathematical method [1, 2] and not a specific model. Therefore, what is included here is the FEM that has been applied on specific model equations to obtain practical results for erosion determination. The same consideration holds for Monte Carlo, i.e., Monte Carlo is a mathematical method that was used for erosion modelling, e.g., thermal barrier coatings or physical vapor deposition.

Monte Carlo simulation techniques [4-24] use continuous software random loops to reach an optimal value for particle size, properties, the material surface condition and the local dynamic impact condition. Monte Carlo methods were applied in the dynamics of deformable solids and radiotherapy delivery dosimetry optimization [25]. Monte Carlo methods are also applied in turbulence analysis for aerospace dynamics [26, 27].

In this section, corrosion models are explained with their main formulation. One difference between erosion modelling compared to corrosion is the relative complexity of the chemical process of corrosion equations. In the following, a series of corrosion models are presented. In corrosion, depending on the imperative condition of every chemical compound of the materials, T2 models are found very frequently in the literature. We recommend [72] to develop these concepts with formulation. Usually, the most frequent opinion is that erosion can accelerate corrosion, and less common that corrosion can accelerate erosion; oxidative-corrosion is an important engineering question in seawater technology and marine engineering. Corrosion in power plants [6] is caused principally by oxidation whose general chemical equation reads:



where  $a$ ,  $b$  are chemical reaction proportionality constants,  $O_2$  - oxygen molecule,  $M$  - the metal oxidized,  $G$  - Gibbs energy. Apart from that, recently, corrosion combined with wear/erosion, i.e., wear plus abrasion, has become a promising and applicable new investigation line – so called tribocorrosion. Tribocorrosion joins in applicable algorithms, both chemical and physical concepts and equations, and constitutes a simplification to share two simultaneous phenomena in one modelling-formulation. In the following, a series of erosion-corrosion models are presented whose references are detailed in [72].

**Chemo-hygro-thermo-mechanical model for concrete (T2, 1990).** This model [72] is developed in FEM and is used for reinforcement of concrete at any kind of special construction. It comprises chemical and mechanical characteristics. It can be considered a specific model of T2, and with features of corrosion-erosion duality.

**Pipe corrosion models based on neural-network theory (T2, 1996).** This model [6] works in pipes, based on neural-networks mathematical methods. It is applicable in power plants since pipes constitute an important structure in energy systems and corrosion in oil-gas pipelines. The internal corrosion of a pipeline is a multivariable nonlinear system, and Genetic Algorithms (GA), in combination with artificial neural network, are used in its optimization. The computational development of this model follows usual steps of the GA programming; it can be considered a specific T2 model.

**Stress corrosion model (T1, 1981).** Stress corrosion, in combination with environmental agents, causes cracks in a number of mechanical structures [72]. The environment component diffuses within the cracks and causes a positive feedback for the cracking-mechanical process.

The modelling is rather complex, and some approaches were used. The role of the geometry of the cracks added to fracture mechanics principles constitutes additional factors to increase the difficulties. Some equations for this kind of stress are published in the literature, as follows, for a hyperbolic notch:

$$\begin{aligned}
\sigma_x &= \frac{K}{(2\pi r)^{1/2}} \times \\
&\times \left[ \cos\left(\frac{\vartheta}{2}\right) \times \left(1 - \sin\left(\frac{\vartheta}{2}\right) \sin\left(\frac{3\vartheta}{2}\right)\right) - \frac{\rho}{2r} \times \cos\left(\frac{3\vartheta}{2}\right) \right]; \\
\sigma_y &= \frac{K}{(2\pi r)^{1/2}} \times \\
&\times \left[ \cos\left(\frac{\vartheta}{2}\right) \times \left(1 - \sin\left(\frac{\vartheta}{2}\right) \sin\left(\frac{3\vartheta}{2}\right)\right) - \frac{\rho}{2r} \times \cos\left(\frac{3\vartheta}{2}\right) \right],
\end{aligned} \tag{1.14}$$

where  $\vartheta$  is the polar angle of  $r$ ,  $K$  - a geometrical constant, and  $\rho$  - the curvature parameter. The study and modelling of the interrelation among cracks (mechanical) and corrosion (chemical) is a complex mathematical-geometrical challenge.

**Three-dimensional geometric models of corroded steel bars (T2, 1996).** This geometrical model, T2, is based on the experimental fact that a corrosion pit can be given with a hyperbola [72]. The effects/physical consequences of geometric parameters for a hyperbola on the mechanical properties of corroded steel bars are applied. Therefore, there is a link with any kind of energy plant applications. It is a rather empirical model based on simple hyperbolic geometry of pits and steel bars. Stress and strain parameters are fundamental in the implementation of this model.

**Wagner model and derived equations for oxidative corrosion (T2, 1996).** This equation is basic for the mathematical analysis of the kinetic process of oxidation-corrosion rates [6]. Oxidative corrosion rate usually has two stages: the initial stage (formation of superficial layer) and the main stage (the growth of the thickness of oxidative layer and formation of the multilayer of oxide), with an intermediate stage between both. The Wagner primary equation is used to derive practical formulas for high-temperature corrosion and low-temperature corrosion, and a series of intermediate approximations. Wagner's differential equation reads

$$J = CB \frac{d}{dx} + ze \frac{dE}{dx}, \tag{1.15}$$

where  $J$  is the rate of number of particles through oxide layer,  $C$  - particle concentration,  $B$  - the particle velocity for unit of force applied,  $\varphi$  - the chemical potential (we refer to Nerst fundamental equation),  $z$  - the valence of the particle,  $e$  - the electron charge, and  $x$  - the thickness of the oxide layer. From this Wagner equation, a series of models for different oxidative stages have been developed in the literature, mainly in an exponential differential equation frame or integral equation. This model is a milestone for power plant functionality Survival Time Function  $R(t)$  in the reliability determination of the plant.

In classic contributions, Ots in [6] developed corrosion models both in metal in general at low, high, discrete or continuous temperature, and in metal pipes with the same variations, but under the effect of oil shale combustion.

The series of equations/approximations is rather large; nevertheless, it is possible to refer to some fundamental formulas that could be modified according to specific metal material or geometry of basic plant components. For general metal corrosion at high temperature, the following equation holds:

$$\begin{aligned} & \text{Amount of oxidized metal, } W, \\ & W = K_{O_2} e^{\frac{Ez}{RT}} \times t^n, \end{aligned} \quad (1.16)$$

where  $t$  is time (s),  $T$  - absolute temperature (Celsius degrees),  $K_{O_2}$  - derived from a temperature-dependent coefficient,  $R$  - chemical constant of gas,  $n$  - a corrosion rate factor. Variations of these formulas are detailed in [6], i.e., specific for diffusion-controlled region of the oxide layer, particular for the kinetic region of the layer, etc.

**Models of corrosive-erosive wear of heat-transfer tubes (T1, 1996).** In the literature [6], a series of equations/approximations for Erosion-Corrosion Models preferably/more-specific for oil shale combustion have been developed. In order to refer/show a basic equation with differential-frame of a function of several variables, which is  $W$ , the specific mass of corroded material, in the function of, namely,  $P$ , force acting on the layer,  $K$ , corrosive activity of the deposit (e.g., a boiler), and  $t$ , the time.

That formulation reads:

$$W(P,K,t) \text{ differential,} \\ dW(P,K,t) = \left[ \frac{\partial W(P,K,t)}{\partial t} \right]_{P,K} + \left[ \frac{\partial W(P,K,t)}{\partial P} \right]_{t,K} + \left[ \frac{\partial W(P,K,t)}{\partial K} \right]_{P,t}, \quad (1.17)$$

where  $W$  is mass of corroded metal (kg),  $P$  – pressure (MPa),  $K$  - gas constant,  $t$  - temperature. A similar mathematical observation is applicable, this and these formulas in general, could be modified according to a specific metal material or geometry of basic plant components.

**Todinov synergic model of erosion and corrosion (T2).** This is a model for erosion and corrosion for powdered material coatings developed by Todinov [72, 78]. The synergism between erosion and corrosion reads:

$$E_T = E + C + S, \quad (1.18)$$

where  $E_T$  is the total mass loss rate from [72], i.e., the erosion–corrosion rate,  $E$  - the pure erosion rate,  $C$  - the pure corrosion rate, and  $S$  - the loss due to the synergistic effect between erosion and corrosion – the object of interest of this equation. This synergistic term may be separated into two terms:

$$S = S_{EC} + S_{CE}, \quad (1.19)$$

where  $S_{EC}$  represents the erosion-induced corrosion rate (i.e., increase in corrosion rate due to erosion) and  $S_{CE}$  represents corrosion-induced erosion rate (increase in erosion rate due to corrosion). This is the synergism modelling base, and further developments and approximations can be found in the literature. By way of explanation, it sharply differs from a corrosion process over a previously eroded powdered material surface,  $S_{EC}$  from an erosion with loss of material in a previous corroded area  $S_{CE}$ .

## 1.2 Review of optimization methods

This section addresses the subject of optimization techniques to optimize the modelling of E/C, [22, 23, 24, 29, 30]. There are two main subsections. The first contains the general optimization method used/selected for E/C, which is multi-objective; in general, the condition is not exclusive, since there are other types of applicable optimization methods. In [72] extent details about this part are described. The second is a series of modern/classical algorithms that can be used for this kind of multi-objective optimization, namely, from evolutionary algorithms to, e.g., Monte Carlo formulation. All in all, we refer in short to the most important methods/algorithms, and explain advantages, limitations, and their best area of use/applications. In the last subsection, the important probabilistic link between the group of E/C models and the statistical models/concepts of engineering reliability for power plants is analyzed concisely with formulation and mathematical lemmas.

### 1.2.1 Generic multi-objective optimization (MO)

Multi-objective optimization has developed in recent years toward large-scale optimization methods to determine a series [5] or a combination of series of optimal parameters for a number of variables into the Objective Function. MO with least squares  $L_2$  norm is the most frequent technique used in the literature for large-scale computational problems. MO function with  $L_1$  norm or so-called Chebyshev multi-objective, is also useful, although not so frequent.

### 1.2.2 Specific optimization algorithms

Specific optimization methods/algorithms can be divided into deterministic and stochastic. Deterministic methods (DM) are the steepest descent [5, 23, 24]; conjugate gradient, linear programming, maximum likelihood, dynamically penalized likelihood, quasi Newton methods, Broyden-Fletcher method, Davidson-Fletcher method and other techniques. Random techniques (RT) are principally Monte Carlo methods, Quasi-Monte Carlo, simulated annealing and genetic algorithms. All of them show advantages and weaknesses, and the aim of this section is to identify the most useful and practical of all these methods.

**Interior-reflective Newton method.** This DM method described in [5, 30] is an evolution of the classical good Newton/Newton-Raphson Method. We obtained acceptable results in multi-objective optimization with several variables in CAD modelling, and large-data/variables polynomial fits with results of high determination coefficients previously. According to the literature, it can be considered also suitable for mathematical models for E/C.

**Levenberg-Marquardt (DM).** This is a method whose objective function is the sum of squares of nonlinear functions. Levenberg-Marquardt algorithm is considered, in general, as an acceptable multi-objective method, and it has also been used efficiently in several of our contributions [22].

**Conjugate gradient (CG) algorithms (DM) and variations/refinements.** This group of CG methods is derived from the original Steepest Descent (SD) method with important mathematical improvements. SD can be considered useful but obsolete and with approximate solutions, and CG methods is still useful although it cannot be considered as the best. CG running time is acceptable. To date, CG methods are widely used.

**Genetic/evolutionary algorithms.** These methods [23, 24] are extensively used in many varieties and extensive branches of science, economy, and statistics. Evolutionary algorithms intend to resemble the nature selection process through continuous random generations of solutions (so-called chromosomes), at every program loop. Evolutionary algorithms have been improved in recent years by setting varied sub-methods, which are properly applied in

every type of optimization. The process is continuously repeated at any step, conditioned by a settled tolerance. These methods are considered good, although not extraordinary.

**Simulated annealing (SA).** This is a global optimization method (RT). The algorithm [5] searches for new values for input parameters in three ways: grid search, linear interpolation and discrete values. SA is a simple method that should, in principle, converge to a global optimal solution but parameters settings could be a problem and the time required could be too long for time critical applications. In our terms, SA is considered useful for a search of a primary useful approximation towards global minimum, and because of its proper random algorithm, the obtained optimal value does not match *necessarily* the global minimum of the objective function. For optimization of a large number of parameters, it is especially difficult to obtain optimal results. Inconveniences, as referred to above, are that the search point could be trapped in a deep concavity of the OF and the program call would give it as global minimum. Therefore, SA is useful for an accurate initial search.

**Stochastic optimization (SO) group.** This group comprises random methods in general, and SO denomination is used generically in the literature to characterize the applied method as a reference of its group of origin. Markov chain models are also considered stochastic and their variants are widely used to date.

**Monte Carlo methods (RT).** Generically [4], Monte Carlo (MC) is considered a random/stochastic method applicable in a large number of science specializations and mathematical statistics science. Basically, MC uses a continuous group of computational loops with a fixed/input closing-tolerance value for all the variables to be determined. Each loop is generating random values that can stop its circle when the tolerance value is accomplished for that/those variables. It is quite similar to evolutionary algorithms but not the same. In the past, computer's running time was rather slow compared to that today; so MC was a method only implemented for particular calculations with powerful computers. Today, with microelectronics advances in microprocessors and operating systems mainly, standard programs such as GEANT and many evolutions/variants of this type, e.g., GEANT-FLUKA, are computationally able to bring results after a reasonable running time - GEANT is an example among a large variety [25, 30]. MC is used in physics extensively, e.g., radiation therapy, numerical methods (numerical integral calculations), and several branches of science and mathematical statistics – in statistics, e.g., to select/optimize randomly samples, sorting the tedious task of collecting a large bulk of empirical data. MC methods are used also, for example, to determine the random reliability of a mechanical chain linked to probability calculations of the system or plant under certain conditions. Specific probabilities of each part are calculated algebraically and the plant complete probability of failure, for instance, is determined.

**Hybrid methods.** In order to provide both convergence to global optimum and reasonable computational speed, a number of hybrid methods were introduced [5]. For example, in several Hybrid genetic algorithms (HGA), the genetic algorithms (GA) are combined with gradient methods. In the first stage, the GA is applied, resulting in solutions near global optimum; next, the gradient method is applied, providing fast convergence to global optimum.

### **1.3 Aim and objectives of the study**

The main aim of this study is to develop mathematical models and optimization methods for tribology and biotribology for circular manufacturing. Objectives of this research are focused on the following stages:

1. To study current tribological modern and useful classical models.
2. To set a functional classification of the models.
3. To create a discrete stratified model based on Beckmann and Gotzmann equations.
4. To make an integral-differential model corresponding to the second generation of tribology models.
5. To develop and prove a graphical optimization method in 2D and 3D for the determination of optimal wear rate. To provide for further graphical optimization method development.
6. To apply graphical optimization to bioengineering models for optimization and simulations.
7. To apply inverse methods for modelling optimization and obtain a stochastic corrosion model. Numerical methods are to be complemented by graphical visualization.
8. To carry out a 2D computational-numerical comparison for two types of hardfacing reinforcements.

These objectives were reached in the publications and presentations at conferences during this thesis research, please refer to Papers I-V. References from all these publications in optimization methods, Section 1.1, and [72-78] are sufficient to obtain adequate information of mathematical techniques for numerical computational optimization.

## 2 Materials and Methods

The experimental materials were produced at TalTech Powder Metallurgy Laboratory, with the apparatus, specimens, samples, and tools available, and the computational compilers, software, and computer science facilities that were used for the whole programming framework.

### 2.1 Experimental

In this section, the principal materials and experimental used to set modelling are explained and we refer to all papers published for complete details of materials, experimental techniques and apparatus used [19, 33].

The materials were samples of FeCrSiB-alloy based hardfacings with commercial WC-Co spherical reinforcement (S3 notation in this paper) at 30 % volume fraction and polygonal/angular WC-Co reinforcement (R3) obtained by disintegrator milling from hardmetal scrap, both produced by sintering in vacuum. In Figure 2.1a, on the left, a microimage of S3 material hardface is presented with details, the circles correspond to the spherical WC-Co reinforcement and the zone among the circles is FeCrSiB matrix, on the right, angular reinforcement microimage, scale bars are shown in the lower, 2mm x 50. In Figure 2.1b, on the upper, a sketch of S3 material hardface is presented with details, and on the lower, the polygonal shape of R3, the dimensions are in the image, at the right side of the image the coating dimensions 4-5 mm. Scanning electron microscope (SEM) EVO MA-15 (*Carl Zeiss*) and *Hitachi* TM-1000 were used for imaging. The shape of the grains is clear, matrix parts and interface zones are well-defined. The shape and details of R3 polygonal recycled reinforcement are presented in a sketch in [19, 35-37, 75]. The basic geometry of the reinforcements with their average size and setting over the substrate—S235 steel are detailed. The universal hardness tester 2.5/TS (*Zwick*) was used to carry out the hardness measurements.

The experimental is detailed in Table 1, from Publications I and III. Vickers hardness (HV) and modulus of elasticity (E) were simultaneously determined according to the standard EN/ISO 14577-02. Using the tester, the applied load was 50 N.

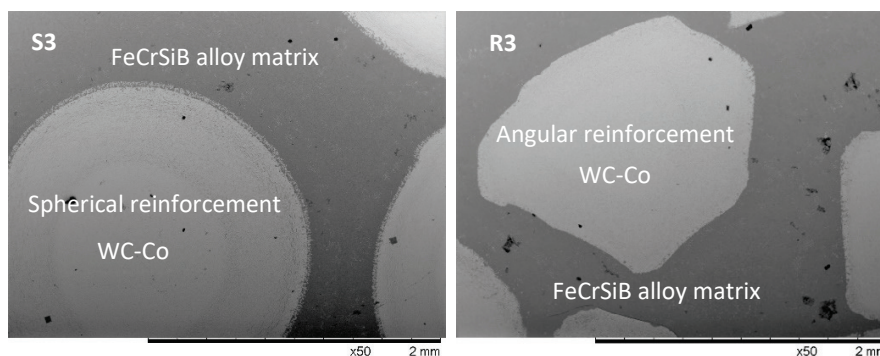


Figure 2.1a SEM image of hardface materials used in the experimental and geometrical description of reinforcements.

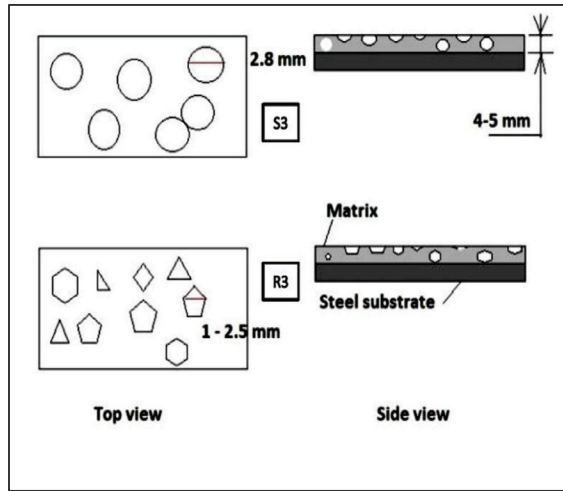


Figure 2.1b Schematic representation of hardface materials used in the experimental and geometrical description of reinforcements. The average diameter of grains is 2.8 mm, and the polygonal 1-2.5 mm, coating dept, right-upper, h is 4-5 mm.

Table 2.1 Basic description of hardfaces studied and geometrical description of reinforcements

| Ordered number of measurement of hardface (total is 100)   | Hardness [HV] S3 / R3 | Type of material  | Average hardness (HV) |
|--|-----------------------|---|-----------------------|
| 1  | 689 / 713             | S3<br>Matrix with spherical reinforcement                                   | 1574±486              |
| 10   | 981 / 981             |   |                       |
| 20   | 1051 / 1027           | R3<br>Matrix with rectangular-triangular reinforcement                      | 1447±483              |
| 30   | 1161 / 1081           |   |                       |
| 50   | 1559 / 1219           |   |                       |
| 80   | 2060 / 1995           | Average reinforcement conversion factor (CF) from HV to mm <sup>3</sup> /Kg | CF = 9807             |
| <b>Diameter of reinforcement at surface</b><br>Spheres average 2.8 mm<br>Triangles rank 1.0-2.5 mm<br>Rectangles rank 4.0-5.0 mm |                       |   |                       |
| <b>Substrate</b><br>Steel S235 of thickness 5-6 mm   |                       |   |                       |

## 2.2 Software development tools used

The methods, compilers, software designed extensively and special techniques used for modelling optimization, construction, simulation and surfactal optimization are included in the Papers I-V, [38]. In brief, the computational work was carried out with:

1. FORTRAN compilers 77-95 usually in double-precision designed programs [38], (Sections 3.2, 3.4, 3.5, 3.7)
2. FreeMat 4.1, 4.2, [39, 40], and subsequent versions [Samit Basu General Public License] (Sections 3.2, 3.4, 3.5, 3.7)
3. MATLAB 2009 and 2011, [20, 29, 41, 42], and within MATLAB:
  - 3.1. Optimization Toolbox (Sections 3.2, 3.4, 3.5, 3.7)
    - 3.1.1. Optimization special software programs (Sections 3.2, 3.4, 3.5, 3.7)
  - 3.2. Curve Fitting Toolbox (Sections 3.4, 3.5, 3.7)
  - 3.3. Signal Analysis toolbox
  - 3.4. Simulink Toolbox
  - 3.5. Visual Studio F# Station (Sections 3.2, 3.4, 3.5, 3.7)
4. Abramowitz classical mathematical tables for approximations, [3], (Literature review, Sections 3.2, 3.4, 3.5, 3.7, Conclusions, Abstract)
5. Complementary tables and specialized mathematical references in several branches [3, 5, 42-52], (Sections 3.2, 3.4, 3.5, 3.7)
6. Python programming in Visual Components Basic (Section 3.7)
7. Mathematical equations [3]:
  - 7.1. Beckmann (Section 3.2). For wear due to cutting
  - 7.2. Hutchings model (Sections 3.2, 3.4, 3.5, 3.7). For wear at surface due to fatigue
  - 7.4. Gotzmann (Section 3.2). For wear due to brittle fracture
  - 7.4. Menguturk model (Sections 3.2, 3.4, 3.5, 3.7, it was used in these sections also to compare the results).

### **3 Mathematical Modelling, Computational Results, and Nonlinear Optimization**

This section comprises the most important results of the original research obtained and published in the author's papers. Since the amount of numerical data, computational work, and graphical results is large [20, 29, 41, 42, 53], the results are selected in relation to the most significant engineering/practical topics. The study contains the basics of the methodology and programming task. This section comprises the principal results of algorithms that are linked to publications. Subsection 3.1 presents the conceptual classification of models applied in the thesis research, optimization, modelling, and simulations.

#### **3.1 Classifications of tribology mathematical models for optimization framework**

Along a series of publications corresponding to this thesis, an engineering-tribology group of model classifications was reviewed, explained and presented. A mathematical model could be set in a number of explicit formulas/determinations and even in an implicit function or formulation [19, 31-34].

MMs equations formed by parameters can be from the simplest to the highly/complicated ones. That is, they could be from basic operators to matrix algebra and differential/integral equations, or from discrete functions to continuous functions. Statistical models could be mathematical models depending on the criteria of many authors along the historical stages in research. It is also possible to insert statistical functions or operators, such as summatories within the model complete formulation.

Table 3.1 introduces the structural classification, mainly from [72]. This classification is focused on mathematical model composition, from simple discrete values to, e.g., functional or statistical parameters. This frame is especially useful for the second generation of models that are formed by integrable-differentiable functions.

Table 3.2 presents the most important functional criteria, defining Type 1 and Type 2 model strands, as a proposal of the study and author's publications. The criteria of this functional classification were applied to analyze the series of equations of diverse models of the literature review. The integral-differential model is based mainly on these two types of equations.

Table 3.1 Structural classification of mathematical models in tribology

| According to parameters |   | According to structure           |   |
|-------------------------|---|----------------------------------|---|
| Type                    | Description   | Type                             | Description   |
| Discrete                | Formed by integers values and simple operations usually   | Algebraic operators              | Matrix algebra operators main structure of the model, rather discrete values. The most simple model and less accurate |
| Real                    | Constituted by real numbers and simple operations   | Complex or real simple functions | Functions based on complex/real numbers and any type of sub-function, series included                                 |
| Functional              | Involving any kind of function within a parameter, with/without infinitesimal calculus operators, special functions, limits, series, etc. | Statistical                      | With statistical function of any kind or combinations of statistical parameters                                       |
| Mixed                   | Involving hybrid combinations of previous types   | Hybrid                           | Intermediate/combined models related to parameters. The most complicated models to be built                           |

The predominant criterion of the functional classification is the practical engineering selection, i.e., *for what every model is used*, and its advantages and limitations. The framework of classification is just the same for erosion, corrosion, biotribocorrosion, and tribocorrosion. Erosion-corrosion models can be included at its corresponding group. They are defined as follows:

**Type 1 (T1)** mathematical E/C models. Models that can be implemented for several applications/material interactions. Degree of usage is from 1 (lowest application range) to 4 (highest application range).

**Type 2 (T2)** mathematical E/C models. Models that can be implemented and are designed/optimized for a specific/super-specific physical application. Degree of usage is 1.

Table 3.2 Functional classification of E/C models

| Group/brand                 | Model type   | Definition/examples  |
|-----------------------------|--|--|
| <b>TYPE 1 (T1)</b>          | Models with several applications   | Models for several E/C interactions in different conditions  |
| <b>TYPE 2 (T2)</b>          | Specific and superspecific models with one application   | Precise or extremely-accurate design for a unique materials physical interaction   |
| <b>Mathematical methods</b> | Mathematical and optimization techniques applicable to characterize Type 1 and Type 2, linked to any model | Heuristic<br>Empirical<br>Random (Monte Carlo)<br>Deterministic<br>Mixed<br>Finite Element<br>Dynamic model<br>Others<br>Degree of usage (1-4) |

Finally, it is conceptually useful to establish a classification of model for an origin linked to erosion and corrosion. Table 3.3 classifies the causes of erosion and corrosion, those natural, artificial, or mixed. In papers I and IV, a series of tables with T1 and T2 models are presented.

Table 3.3 E/C modelling-classification according to physical origin

| <b>Classification of erosion and corrosion models for origin/cause</b> |   |
|--|---|
| <b>Type</b>  | <b>Examples</b>   |
| Natural  | Geophysical earth changes, rocks corrosion-erosion, human body wear for ageing and biomechanical movement, e.g., natural-chemical corrosion for environmental chemicals               |
| Artificial, the most frequent  | Coatings damage with particles in gas/vapor or gas/vapor, wear in machinery parts, corrosion of coatings after erosion.   |
| Natural-Artificial   | Degradation of concrete caused by natural impact, metal corrosion for natural air humidity, e.g., erosion model that combines environmental erosion with machinery-functional erosion |

### 3.2 Stratified construction of Beckmann and Gotzmann equations in discrete tribology models

This section shows the development of a discrete model based on Beckmann and Gotzmann equations and Weibull distribution. This model was modified by P. Kulu and R. Veinthal [54], and later by F. Casesnoves and A. Surženkov (Papers I, III). The model is classified as T1-discrete type. Figure 3.1 presents a basic sketch of the numerical procedure based on the experimental data. The experimental and theoretical data for this model are presented in Paper III.

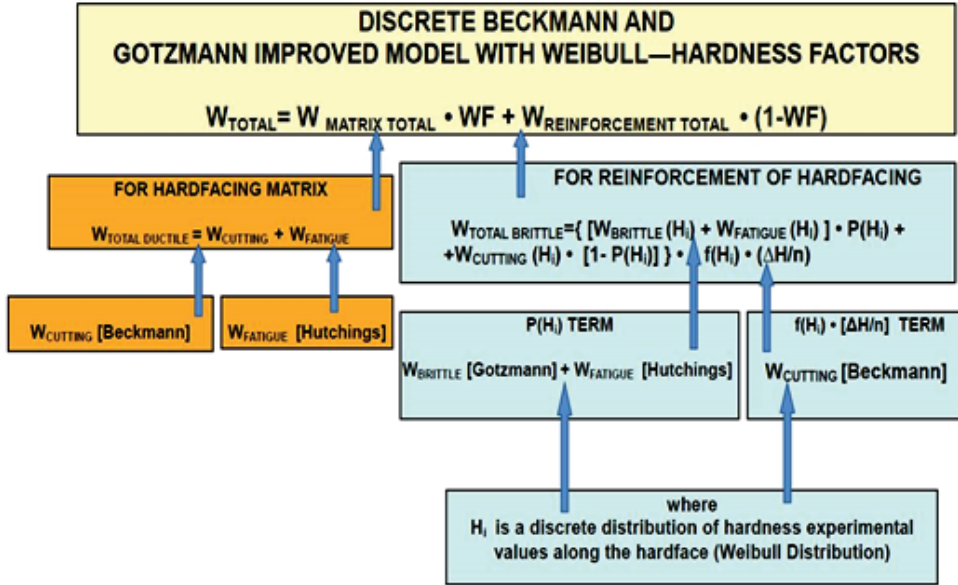


Figure 3.1 Basic structure of the discrete model.

In Figure. 3.1, the flow chart-equations shows the different parts of the model that constitute a summatory chain, from matrix and reinforcement parts, towards the determination of the total wear of the hardface as an addition of the partial wear rates of matrix and reinforcement. Although this modelling method was previously used, the proposed and developed stratification of the model, using Hutchings equation for fatigue, constitutes a new contribution. The formulation used for this model is as follows:

1. Beckmann model [19]. Wear due to cutting:

$$W_{cutting} = K_r \frac{3}{4\pi} \frac{\tau_0}{e_s} \left[ 6.81 \left( \frac{h_p}{R} \right)^{0.5} \frac{2\rho_2 v_0^2 \cos^2 \alpha}{3H_1} + 0.85 \left( \frac{h_p}{R} \right)^{0.5} \right], \quad (3.1)$$

where  $K_r$  is the dimensionless coefficient, (1.45),  $\tau_0$  – shearing stress in target material  $\tau_0/e_s$  - adimensional shear energy density,  $e_s$  - specific shear energy density (N/mm<sup>2</sup>),  $e_0$  – dynamic hardness of worn material (N/mm<sup>2</sup>)  $h_p$  - the depth of the impact crater (mm),  $R$  - average diameter of an erodent particle (mm),  $\rho_2$  - the density of the erodent (mg/mm<sup>3</sup>),

$v_0$  - the impact velocity (m/s),  $\alpha$  - the impact angle (degrees),  $H_1$  - the average static hardness of the target material (N/mm<sup>2</sup>).

2. Hutchings model [17]. Wear due to fatigue:

$$W_{fatigue} = 0.033 \frac{\alpha' \rho_1 \sqrt{\rho_2} v_0^3 \sin^3 \alpha}{e_c^2 H_{dynamic}^3 1/2}, \quad (3.2)$$

where  $\alpha'$  is the elementary volume removal ratio,  $e_c$  - the critical stress of the target material,  $\alpha'/e_c^2$  constitutes a dimensional factor,  $\rho_1$  - the density of target material in (mg/mm<sup>3</sup>),  $H_{dynamic}$  - the dynamic hardness of the target material (N/mm<sup>2</sup>).

3. Gotzmann [19]. Wear due to brittle fracture:

$$W_{brittle} = 0.75 \sqrt{3} \frac{\rho_1}{\rho_2} \left(\frac{C_r}{R}\right)^2 \left(\frac{h_p}{R}\right)^{0.5}, \quad (3.3)$$

where all parameters correspond to previous formulas with the exception of  $C_r$  the middle length of the radial crack.

The computational work for these large numerical calculations with laboratory and theoretical measurements and data was done with FreeMat and MATLAB basically. FORTRAN was used to re-check numerical data in double precision, and some graphs of complementary results were implemented in F#.

In Paper III, the complete setting of erosion wear rates obtained after application of this model is presented. Before the design of this stratified model, a series of simpler models of this structure were computationally calculated for other materials, e.g., such as Hardox 400 wear-resistant steel.

### 3.3 Integral-differential model construction

The construction of models and the Integral-differential model was detailed in Papers I-V and [72-78]. Here we explain one algorithm with the application of the Total Differential theorem for Hutchings model equation. Integral-differential model is classified as a general model T1 Type.

This basic type of a simpler formulation-model simulated/optimized in the publications (repeated Equation 1.7) is as follows:

$$W = \frac{K \rho v^2}{2H}, \quad (3.4)$$

where  $\rho$  is the density of the material being eroded,  $v$  - the initial particle velocity and  $H$  - the target surface hardness.  $K$  represents the fraction of the material removed from the indentation as wear debris and is also known as the wear coefficient. Hutchings models constitute a series of formulas from the simplest to the most complicated in terms of powers and constants—powers are in fractions amid the most complex models. All through this study, these models were used to demonstrate the optimization methods, graphical

optimization, and a series of simulations for their simplicity and sharp learning. The total differential from Equation (3.4) results as follows:

$$\begin{aligned}
 & \text{Setting the total differential,} \\
 dw &= \frac{\partial w}{\partial H} dH + \frac{\partial w}{\partial v} dv + \frac{\partial w}{\partial \rho} d\rho = \\
 &= \left( K\rho v^2 \right) \times \frac{1}{2H^2(s)} \times \frac{dH}{ds} \times ds + \\
 &+ \frac{K\rho}{2H} \times (2v)dv + \frac{Kv^2}{2H} \times d\rho;
 \end{aligned} \tag{3.5}$$

Integrating along all reinforcement [68] spots average radius length, and using weight factors for reinforcement we get:

$$\begin{aligned}
 W &= 2xF_R \int_{w_0}^w dw = \int_{s_0}^s \left( K\rho v^2 \right) \times \frac{1}{2H^2(s)} \times \frac{dH(s)}{ds} ds + \\
 &+ \int_{v_0}^v \frac{K\rho}{H} \times (v) \times dv + \int_{\rho_0}^{\rho} \frac{Kv^2}{2H} \times d\rho;
 \end{aligned} \tag{3.6}$$

Equations (3.5) and (3.6) show how to take partial derivatives in a total differential development to develop later the integral determination of the wear rate. Theoretically, it is proven that the use of functions for the determination of the wear rate can be carried out, provided these functions are well-known and verified. In this equation-algorithm, three functions, namely, hardness, particle velocity and density of surface, were considered. The introduction of this modelling part is shown in [76, 77, 78]. The Monte Carlo method to determine the range of distance-parameter  $s$  is included in Paper II. References from all these publications in optimization methods, Papers I-V, are sufficient to obtain comprehensive information of the mathematical techniques for numerical computational optimization.

The significance of this integration, i.e., the cumulative of erosion rate and/or erosion during a time interval when parameters of models are not constant, are functions, such as, velocity, impact angle, or surfactal hardness distribution. All of these functions are depending on variables, e. g., time or temperature. In Paper V and [55, 56, 57, 78], the second generation of tribology models with functions is demonstrated.

For example, if the impact speed  $v$  is not constant during a time interval, and is increasing during the experiment in a polynomial function, the total erosion during that interval can be calculated without errors with integrals. In [78] an extent mathematical demonstration is included.

### 3.4 Graphical optimization in 2D and 3D

This section comprises basic definitions in tribology for graphical matrix-algebra optimization and a graph with a ROI selection for learning [20, 24, 29, 41, 42]. Convexity concept of a 2D or 3D objective function [24] was applied in optimization development. In all the Publications and in [73-75, 77, 78], a large series of plots with model implementations of graphical optimization were included.

Definition 1: *Graphical nonlinear optimization<sup>1</sup> is a constructive approximated method to set the global/local minima/maxima of an objective function provided when two strict conditions are met:*

- (1) Computational graphical simulation of the objective function is precise and imaging software is sufficiently proved as accurate in its imaging algorithms.
- (2) Objective function of mathematical development and constraints is strictly mathematically linked to the graphical implementation.

A graph of ROI selection in graphical optimization is included in Figure 3.2. The algorithms of graphical optimization were developed in a series of programs, both in FreeMat and MATLAB. The subroutines for 3D implementation of the graph are given by those software options. The formulation of a model for graphical optimization is a rather complicated task and depends specifically on each type of the model. This means that to obtain appropriate size and congruent operations of the matrices, such as multiplications, powers, summatories, and division, it is mandatory to perform a model operations division in a number of parts. This original technique was developed along all series of papers published [58, 59]. In Figure 3.2, a ROI selection of Menguturk model with constraints is presented. Matrices are 1000x1000, and MATLAB sharpness of this image is very good, and running time is  $\leq 0.5$  s with a Linux Station 16.2 and AMD processor. Region of interest is velocity [61.6, 104.3]  $\text{ms}^{-1}$ , angle in degrees [42.9, 57.3], and erosion rate [0.1, 0.2]  $\text{mm}^3/\text{g}$ .

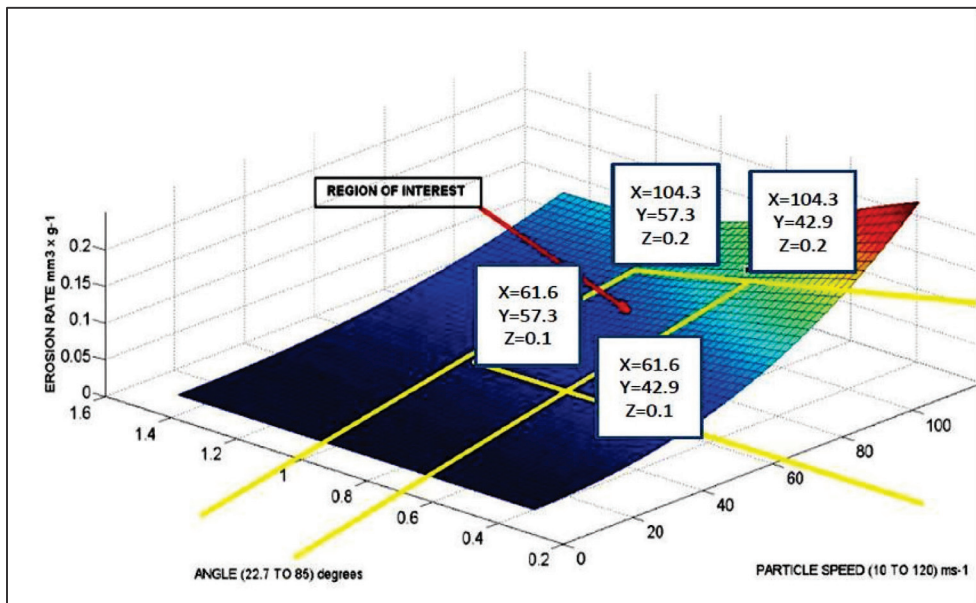


Figure 3.2 ROI selection of the Menguturk model with constraints.

<sup>1</sup> Graphical 3D Nonlinear Optimization method was created by Francisco Casesnoves at Tallinn University of Technology in December 2016. The method was a result of the numerical-mathematical study with Fortran and F# software of laboratory experimental data.

3D and 2D Graphical optimization of ROI selections are detailed in all contributions, and multiple graphical optimization methods are included in the conclusions specifically. To select a ROI, a specific tool is provided in MATLAB. When a ROI is selected graphically, the complete numerical matrices data is set at prompt. Therefore, the selection of the desirable values for the model can be easily chosen from the numerical data. FreeMat does not offer this option, and the matrices-values for a ROI have to be extracted with commands at prompt.

In plain language, suppose that the laboratory apparatus has some functional constraints (or the material that we would manufacture will only be exclusively exposed to a range of erodent velocities and impact angles). That is, the velocity of particles can be in the interval  $[61.6, 104.3] \text{ ms}^{-1}$ , the impact angle in radians at  $[1.0, 0.7]$ . Then, within that ROI it is possible to click the optimal minimum erosion approximately at  $0.1 \text{ mm}^3/\text{g}$  for a particular velocity and angle. This is possible if the model surface representation is sharply concave-concavity/convexity concept that is fundamental in the optimization. If it is necessary to see all the matrix values within the region of interest, set the vectors of the axes  $x,y,z$  at prompt, or more easily, use the MATLAB tool that automatically gives the ROI magnitudes at screen. With many variants and different algorithms, this method was previously used in the selection of optimal ROIs for the implementation of surgical prostheses at the selected surface parts of the vertebrae [58, 59].

### 3.5 Bioengineering tribological simulations and applications

The biotribological optimization and simulations were developed in Paper IV. Numerical computing was focused mainly on hip wear prostheses models. The wear of a hip prosthesis is highly complicated. Generally, it depends on the contact status between the ball and the cup (i.e., friction regime), characteristics of the tribocouple, anatomical and physiological conditions, age, type of physical activity, production quality of the prostheses, lubricants, diseases history, concomitant diseases, etc. There are prostheses made of metal, composites, metal with ceramics, metal with composites etc. [57, 58, 59, 60]. For example, despite a low friction torque, the polymer-on-metal configurations exhibit higher wear than those of metal-on-metal or ceramic-on-ceramic due to the boundary lubrication regime between the wearing surfaces. For the same reason, small-size metal-on-metal hip joints perform worse than large-sized ones. If properly designed and manufactured, metal-on-metal hip joint prostheses work, *vice-versa*, under mixed lubrication regime, and ceramic-on-ceramic hip joints function even under hydrodynamic lubrication conditions, which provide extremely low friction. It is related to the articular movement of acetabular hip that is estimated as the number of rotations in a day and it is high since arms and legs are basic in human daily movements. If sports or high physical effort/activity is added, the result in the modelling involves a large number of factors. Figure 3.3 presents a 3D Graphical optimization for a hip implant basic Archard's law model for abrasion. Matrices are  $1000 \times 1000$ , and MATLAB sharpness of this image is good, and running time is  $\leq 0.5 \text{ s}$  with a Linux station 16.2 and AMD processor. Maximum load is 2960 N, wear rate  $0.0040 \text{ mm}^3/\text{kg}$ , hardness 539.4 MPa. Minimum load is 1040 N, wear rate  $0.0004 \text{ mm}^3/\text{kg}$ , hardness 1787 MPa.

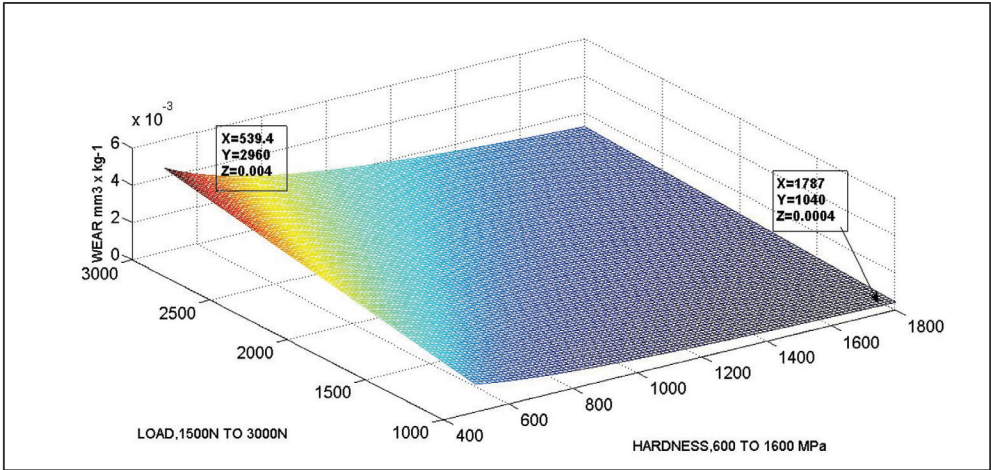


Figure 3.3 Model for hip implants with cursor inset showing numerical values of maximum and minimum.

For graphical optimization of hip implants, the following equation was applied:

$$W = K \frac{L \cdot X}{H}, \quad (3.7)$$

where  $K$  is the wear constant specific for each material,  $L$  - biomechanical load (N),  $X$  - sliding distance of the acetabular semi-sphere of the implant (mm), and  $H$  - the hardness of the implant material (MPa).  $X$  is measured as the number of rotations of the implant multiplied by half distance of its circular-spherical length. The number of rotations depends on the daily physical activity of the patient.

In Figure 3.3, the simulation presented comprises a range of loads between 500 and 300 N, and a range of implant-material hardness between 600 and 1600 MPa. The number of articular rotations selected was 1000. The constant  $K$  was chosen for a metal-composites type implant. The programming of this algorithm for graphical simulations was done with the subdivision method and 3D surfactal imaging subroutines both in FreeMat and MATLAB.

This equation was implemented computationally for graphical optimization with varied constants depending on the material of the hip implant. In Paper IV, a series of nonlinear constrained and non-constrained optimization results are shown. Among these hip implant materials selected were: ceramic implants, metal implants, metal-coated and mixed-implants such as metal-composites [Appendix 2 of Paper IV]. Additionally, in Table 3, Paper IV, important biotribological models are described in detail.

To date, in hip implants, tribological design constitutes an increasing bioengineering demand in the market and Health Services, both public and private. The increase of the population age in the European Union creates an increment of incidence/prevalence of surgical interventions for femoral-hip articulations replacement with artificial implants. In [58, 59], the objective functions for geometrical modelling of cloud data to a surface are set and developed with MATLAB and FreeMat subroutines. Specifically, in [58], a 3D hyperboloid geometry was fitted to ¼ million cloud data from a medical scanner with results of high values, (> 75 %), in statistical error determination coefficients.

### 3.6 Inverse problems

The study and applications of IP theory method(s) were focused on practical optimization and nonlinear inverse problem applications in erosion models useful for modelling and integral-differential new model design – see Papers I-V and [73-78]. The selected models for IP simulations/optimization are appropriate to be applied for wear, abrasive wear, and corrosion. In this study, the demonstration of the technique applicable to a large number of models is most important.

Heuristic methods (Paper VI) have been substituted mainly by IP methods for practical engineering reasons; among many other reasons was that the results obtained became better in a short-term [56, 57].

In general, most of the tribological models, mainly for impact wear, abrasive wear erosion, are nonlinear equations, since their research origin had to be fitted on an extent of an empirical/experimental database. As a consequence, it affects the choice of most appropriate subroutines for optimization.

#### 3.6.1 Inverse problems theory and its applications in modelling

This section is focused on simple examples to corroborate the work done along publications and mainly in Papers II and V.

If laboratory measurements data,  $D_i$  are trustworthy statistically and the objective is to fix the optimal parameters of a selected model,  $M$ , it can be made by using IPs with nonlinear optimization methods. Laboratory database numbers  $D_i$  are usually large series and the first step is to set them into statistical programs to apply several distributions and get information about the numerical setting of the main statistical parameters. The most accurate distribution is the Gaussian, although if the number of data is reduced, other types are also available. According to all these conditions, we get

$$D_i \text{ (database numbers)} = M_i \text{ (function of } x, y, z, \dots \text{ parameters of model)},$$

*x could be particle speed, y density of hardface, z impact angle, etc*

In these papers, the usual technique applied was the  $L_2$  norm least-squares optimization. Although new optimization methods are extensively applied today, e.g., evolutionary algorithms, nonlinear least-squares can be considered a classical-functional method with acceptable results [56, 57]. This technique was implemented with the series of hardness measurements. The computationally-implemented equation is:

optimize,

$$\sum_{i=1}^{i=N} \|D_i - M_i(x, y, z, \dots)\|^2 \quad ; \text{with, } M = \text{selected equation}; \quad (3.8)$$

with the objective to make,

$$D_i \approx M_i ;$$

This method was intended for many mathematical-optimization models to guarantee all the curves to be at the positive quadrants in 2D and 3D, and follow the most efficient literature techniques in nonlinear optimization. The applied real laboratory measurements were mainly hardness of S3 and R3 materials, and erosion rates or data of other parameters already published in [73-78].

In Table 3.4 and Figure 3.4, a model equation is implemented with one evolved-optimized algorithm shown [76, 77]. The mathematical development of any model begins with the formulation of some selected simple models, as was done in previous sections. It is intended to explain the technique that can be used for any other equation, no matter what kind of complication is.

A basic erosion model from Hutchings Equation (1.17), specifically for low impact angles is shown in Equation (3.9) model. This objective function with the model was numerically optimized in Paper II; however, without impact angle trigonometrical function and the velocity-parameter power unit, not being 2.5. In this section, the primary results/algorithms/methods of Paper II are presented/commented, and we refer to the following papers, both principal and additional, to obtain further developments of this method(s) and algorithms. The computational optimization was set as follows:

$$\begin{aligned}
 & \text{minimize,} \\
 & F(\bar{x}) = \sum_{i=1}^{i=N} \|H_i - f(\bar{x})\|^2 ; \text{subject to,} \\
 & a_1 \leq K \leq a_2 ; \\
 & b_1 \leq \alpha \leq b_2 ; \text{ with,} \\
 & f(\bar{x}) = \frac{K\rho \times [v \sin \alpha]^{2.5}}{2W},
 \end{aligned} \tag{3.9}$$

which is the determination of optimal angle and wear constants within intervals  $[a_1, a_2]$  and  $[b_1, b_2]$ .  $F(x)$  is the objective function and  $f(x)$  is the model,  $\rho$  - the density of the material being eroded,  $V$  - the initial particle velocity and  $H$  - the target surface hardness.  $K$  represents the fraction of the material removed from the indentation as wear debris and is also known as the wear coefficient. The construction of the model follows straightforward from this equation since the hardness measured at the matrix region is a continuous and differentiable function, instead of a series of discrete values.

Given the hardness function  $H(s)$ , at any other particular model, according to Paper II hypotheses, the insertion of the function into the model of wear or other parameters, subject to constraints, constitutes a new method for erosion/tribological-parameters rate determination. An example of inverse method algorithm is detailed and developed in Paper II (Equation (9)). This model in its differentiable equation was developed further in the next contributions from Paper II in all articles, lectures at conferences, and in [78], since to obtain useful calculations could be extended and its applications substantiated.

Weibull distribution was not initially applied for this type of modelling since an attempt was made to set a direct determination of the weight factors in hardface distribution to obtain particular functions for every kind of material, according to explanations in Figure 3.4 and Paper II.

The linear erosion rate is not constant. Measurement result are not dependent on the distance, but is the structure parameters (average grain size, grain contiguity, free binder path) dependent. For that reason, it is necessary to take derivatives. The hardness is taken in consideration as a function of distance measurements; it is not constant. There should be weight factors because the surface is divided into a matrix, interface and reinforcement. Every part has different hardness distribution, as proven in Section 3.8.

According to this, and the model of Equation (3.9), a subsequent application of the derivative chain theorem, supposed power of sine is 1, not 2.5 for simplification, which transforms this algorithm as follows:

*Direct application of chain theorem derivation,*

$$\begin{aligned} \frac{dw}{ds} &= \frac{dw}{dH} \times \frac{dH}{ds} = \\ &= \left( k\rho [V]^2 \sin\vartheta \right) \times \frac{1}{H^2(s)} \times \frac{dH(s)}{ds} ; \end{aligned} \quad (3.10)$$

*integrating along all reinforcement average radius length [x 2],*

$$2 \int_{w_0}^w dw = \int_{s_0}^s \left( k\rho [V]^2 \sin\vartheta \right) \times \frac{1}{H^2(s)} \times \frac{dH(s)}{ds} ds ;$$

However, hardface has weight factors for spatial-surface distribution, namely, matrix, interface and reinforcement:

$$W = 2F_R \int_{w_0}^w dw = \int_{s_0}^s \left( k\rho [V]^2 \sin\vartheta \right) \times \frac{1}{H^2(s)} \times \frac{dH(s)}{ds} ds , \quad (3.11)$$

with  $F_R$  as a weight-surfactal factor for reinforcement. Results obtained for the optimization of this algorithm are in Table 3.4 and Figure 3.4. Paper II contains further numerical data about this optimization exercise/simulation. There are two groups of optimization. In the first group, the algorithm is developed for the first velocity, namely 40 m/s, and graphical determination of this objective function is shown in Figure 3.4. All data and results of the running program are included in Table 3.4.

The second group of constrained-simulations with constraints (Paper II) shown in Table 3.4 is intended for the same hardness data but with an extended wear interval for the wear rate whose central point is the experimental value obtained during tribotesting. The determination of  $K$  in the constraints is also in an interval centered in the value of  $K$  determined without constraints. What is meant here is the multiple options available for nonlinear optimization of a model, a diverse determination of the optimal formula according to lab tribotesting. A search point in an optimization subroutine is the initial point that is provided to the program to find the optimal point of the objective function. The search points usually never coincide with the optimal point.

Table 3.4 Optimization results (Paper II), unconstrained and constrained

| Simulation group 1    |   |                                     |  |
|-----------------------|---|-------------------------------------|--|
| Search point<br>[K]   | Optimal K<br>value minimum<br>(inverse method)<br>V particles=40m/s,<br>Impact angle $\alpha$ is 30<br>degrees  | Residual of objective function (OF) |  |
| X=1                   | 0.9646  | 838.8507                            |  |
| X=5                   | 0.9646  | 838.8507                            |  |
| X=20                  | 0.9646  | 838.8507                            |  |
| COMMENTS              | Acceptable result for optimization of low residual of global minimum exact for any search point                 |                                     |  |
| Simulation group 2    |   |                                     |  |
| Search point<br>[K,W] | Optimal K/W<br>value minimum<br>(inverse method)<br>V particles=80m/s<br>Impact angle $\alpha$ is 30<br>degrees | Constraints<br>Intervals            | Residual of objective<br>function (OF) |
| [20,15]               | [0.7424,3.0787]   | LB=[0.5,0.2]<br>UB=[1.5,4]          | 838.8507                               |
| [10,15]               | [0.6334,2.6265]   | LB=[0.5,0.2]<br>UB=[1.5,3]          | 838.8507                               |
| [1,15]                | [0.7214,2.9915]   | LB=[0.5,0.2]<br>UB=[1.5,3]          | 838.8507                               |
| COMMENTS              | Constraints values are not equal, good residual   |                                     |  |

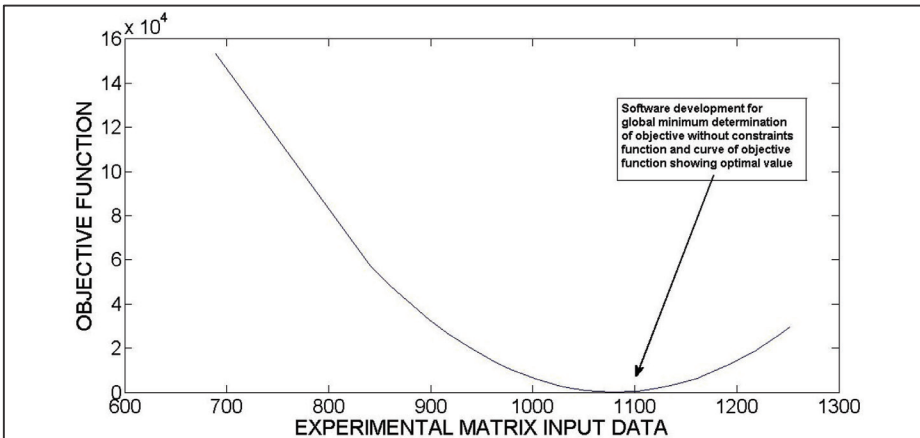


Figure 3.4 Global minimum of the results graph in Table 3.4 without constraints.

### 3.7 Stochastic corrosion methods

This subsection addresses stochastic corrosion methods related to [76, 77, 78]. The objective is to show the stochastic reasons because of which corrosion can be considered as a stochastic phenomenon. This fact is even more random when the hardface of the metal coating is formed by sharply separated parts of materials, such as a matrix and a reinforcement in Paper II. The model implementation is explained in this part.

Figure 3.5 shows the specimen of laboratory samples of coatings of Fe-based matrix with WC-Co reinforcement in spherical shape, S3 materials.

According to Markov Chain Optimization Methods, there is a sequence of probabilistic factors for the formation of corrosion spots, whether at matrix, binding zone, or at reinforcement surface, [2, 28, 29, 44]. Synergic Todinov corrosion model with modifications in Markov Chain can be applied for this type of corrosion [76, 77, 78]. In Figure 2.1, macro-image of specimens with sharp differentiation for this kind of random optimization is presented.

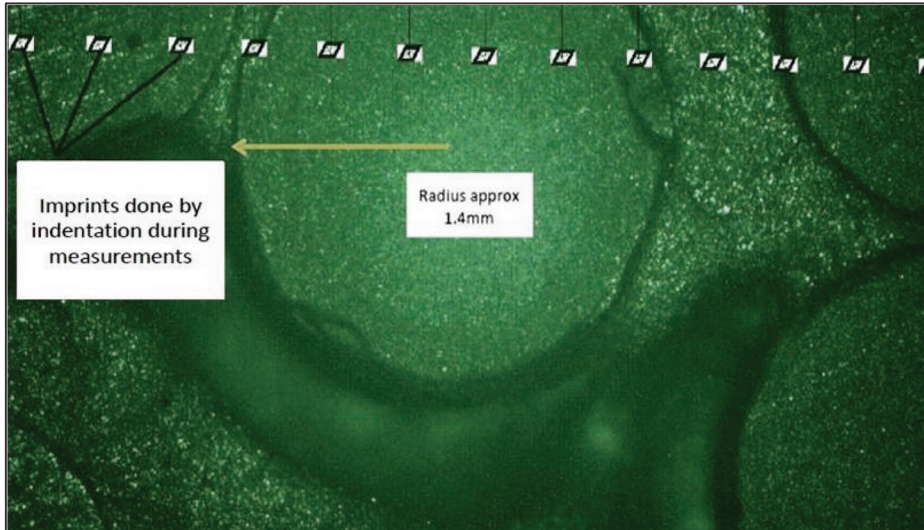


Figure 3.5 Basic S3 optical macro-images of hardfacings used in the experimental, every zone with different surface area proportion has its stochastic probability.

### 3.8 Computational comparison of WC-Co hardness reinforcements

In this section, the 2D computational modelling is studied with a series of graphical polynomial optimization determinations/simulations. Current hardface reinforcements present diverse geometrical shapes, reinforcement-particle size, chemical compounds proportions, volume-spatial distribution, and chemical composition—several kinds of manufactured material types or recycling ones. A series of experimental measurements for Fe-based hardfacing with WC-Co reinforcement were obtained from manufactured and recycled ones. The comparison of hardness distribution between these manufactured reinforcements, both spherical, and recycled-polygonal, obtained by powder materials techniques, is useful in any industrial manufacturing process. In terms of efficient engineering design, industrial cost, and environmental-geophysical consequences, all resulting data are applied for tribological modelling. We refer to [73-75, 77, 78] for a complete description of graphical optimization and results, extent numerical data and sharp-learning plots. In previous publications [4, 56, 57, 58, 59], the algorithm(s) to obtain a polynomial fitting optimization was set and explained with complementary statistics of coefficient of determination. The polynomial fitting to a large series of data is an inverse method to set the optimal polynomial coefficients to the experimental data; this procedure was performed for scanning cloud data in [58].

A series of nonlinear programming equations were obtained for both materials in order to visualize the 2D hardness distribution, and compare the advantages/disadvantages between

both. The first is spherical industrial reinforcement denoted as S3; the second is polygonal recycled reinforcement, R3 named because of its usual rectangular profile geometry.

For computational-programming algorithms, the classical algorithm to carry out a polynomial computational-numerical fitting reads:

given vectors,  $\bar{x}, \bar{y}$ ,

$$\text{find optimal } \bar{a} = \begin{pmatrix} a_0 \\ \vdots \\ \vdots \\ a_n \end{pmatrix} \quad \text{in approximation, } \bar{y} = p(\bar{x}), \text{ such as, } p(\bar{x}) = \sum_{n=0}^k a_n x^n, \text{ for all,}$$

(3.12)

$$x \in \begin{pmatrix} x_0 \\ \vdots \\ \vdots \\ x_n \end{pmatrix} = \bar{x}; \text{ and } y \in \begin{pmatrix} y_0 \\ \vdots \\ \vdots \\ y_n \end{pmatrix} = \bar{y};$$

and  $\bar{a}$  is the optimal vector of polynomial coefficients ;

The subsequent implementation in software for the compilers used in this study is detailed in Figure 3.6. This technique is equal both for MATLAB or FreeMat. In the following sections, the results framework of the paper is presented. The corresponding mathematical base for all these concepts related to the algorithm of Equation (3.12) can be found in the optimization literature and some examples are in the classical optimization and numerical analysis literature. All papers of this study hold a sufficient number of useful nonlinear/linear optimization methods available in the literature.

In previous optimization publications [59], this initial polynomial model was developed. In this study, the nonlinear algorithm was modified for tribology models. For [57], the algorithm was applied for deformation and kinematics of implants. For [20], the nonlinear subroutines were used in the optimization model for radiation dose delivery. In [8], a variation of least squares was applied for viscoelastic tissue deformation. In other words, the model of Equation (3.12) reads:

minimize,

$$F(\bar{x}) = \sum_{i=1}^{i=N} \|H_i - f(\bar{x})\|^2; \text{ subject to,} \quad (3.13)$$

$$H = [H_i];$$

$$f(\bar{x}) = a_0 + a_1x + a_2x^2 \dots + a_nx^n,$$

where  $H$  is experimental hardness values obtained during measurements in of TalTech, and  $x$  - distances from the measurements. The inverse method is to optimize the experimental data of hardness for the distances values within the polynomial model [3, 5, 42-52].

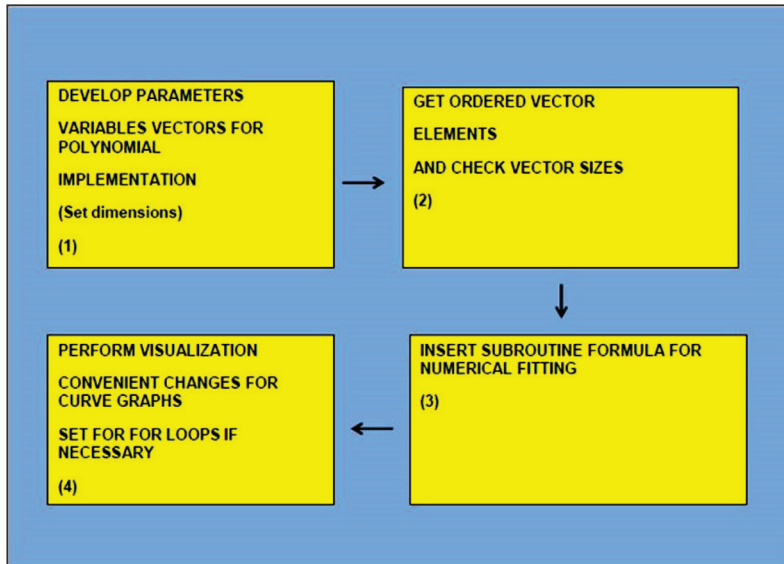


Figure 3.6 Flow chart of the graphical-numerical program (basic). This technique is equal both for MATLAB or FreeMat. Programming with F# was also used in this algorithm together with FORTRAN 77-95 compilers.

The following 2D reinforcement optimization results are both computational-graphical and numerical. The first part of this section deals with the results obtained in numerical-graphics by the developed software with experimental measurements in FreeMat. It is intended additionally to show the different features and similar advantages/disadvantages between MATLAB and FreeMat for this kind of programming. In such way, the results of the section are presented in a series of explained graphics for sharp/continuous learning. Each chart, when it corresponds to the point, is followed by its respective numerical-polynomial formula result. FreeMat software performs right and fast for this type of subroutines, in almost equal time compared to MATLAB. However, MATLAB tools are more varied and provide complementary features for graphical-computational work.

The graph in Figure 3.7 shows a FreeMat 4-degree polynomial fitting of R3 matrix plus transition zone for spatial hardness distribution of reinforcement with polygonal shape. The green curve is the fitted polynomial equation and the blue represents in splines the laboratory data. Visual Studio F# and FORTRAN 77-95 was also used to re-check the results. The difference in precision compared to S3 is significant, as shown in [75]. FreeMat software performs right and fast for this type of subroutines, ( $\leq 5$  s), and *for loops* can be included to improve the subroutines.

The running time of the program for the graph in Figure 3.7 was determined and is approximately half a second. Visualization is good. Polynomial results in five main terms, those with a low residual, using the algorithm of Equation (3.12), are shown in Equations (3.14). These computational results from the software running corresponding to this graph of Figure 3.7 shown in Equations (3.14) do not present at prompt of FreeMat the residual, and in MATLAB the residual is seen at prompt automatically after running the program. In these Equations (3.14), the first one corresponds to S3, and the second to R3 material shown in Figure 3.7.

The indentation forces the decomposition method presented in [74] that was used to analyze the mechanical increment of hardness along the hardfacings.

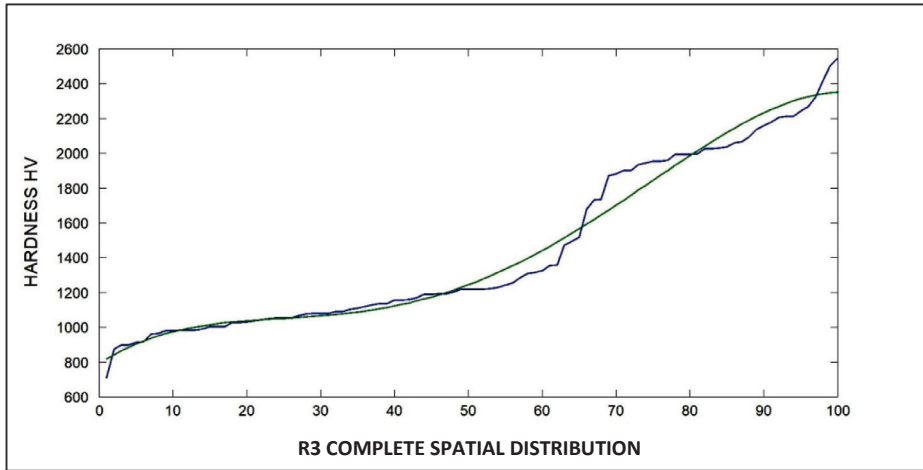


Figure 3.7 Complete polynomial distribution of R3 with FreeMat special software. In blue, laboratory data and in green, the polynomial fitted curves are shown.

FreeMat application in this graph of Figure 3.7 shows required additional programming commands to set the appropriate font size at axes, and the setting of the graph within the image. FreeMat has several options to get an optimal chart by using a series of commands. Polynomial results are in five main terms, with low residual in Equations (3.14).

The computational results from the software running corresponding to this R3 graph of Figure 3.7, and the equation corresponding to the same plotting for S3 are the following:

$$\begin{bmatrix} \vec{a} \end{bmatrix}^T = [651.7005, 63.5664, 3.4358, \dots, \dots, 0.0774, 0.0005]; \quad (3.14)$$

$$\begin{bmatrix} \vec{a} \end{bmatrix}^T = [851.8347, 6.6738, 0.4595, \dots, \dots, 0.0197, 0.0002];$$

residual  $\leq 500$ ;

Residuals are not represented in Equations (3.7) because in FreeMat, complementary commands are required. In Equations (3.13), the terms-order of the vector  $a$  corresponds to the Equations (3.7) algorithm.

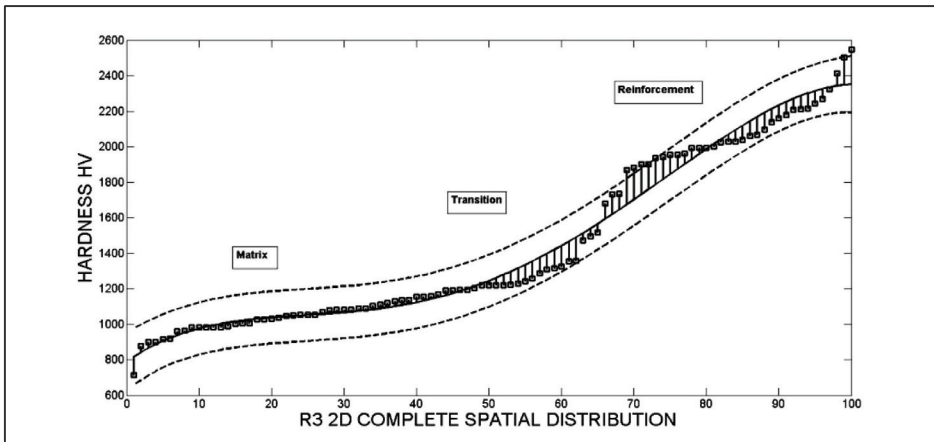


Figure 3.8 R3 MATLAB complete polynomial curve with residuals.

The curve in black in the graph in Figure 3.8 shows a MATLAB 4-degree polynomial fitting of R3 complete hardness spatial distribution—matrix, transition and rectangular reinforcement. The program here was designed to obtain more data at image, with errors. The curve with regression errors is detailed also. MATLAB software performs right and fast for this type of subroutines. In [75], a MATLAB 4-degree polynomial fitting of S3 complete hardness spatial distribution is also shown—matrix, transition and spherical reinforcement. The program for Figure 3.8 was designed to obtain more data at image, but a *for loop* was included with appropriate commands. Visual Studio F# and FORTRAN 77-95 were also used to re-check the results. The curve with regression errors is detailed also. For residuals, the square root of the summatory of differences at power 2 was calculated. MATLAB software performs right and fast for this type of subroutines, ( $\leq 5$  s), but FreeMat conforms to the same task efficiently.

In general, this type of graphs is not complicated if compared to 3D surfactal simulation/optimization of a model. The tools available in FreeMat and MATLAB to represent the splines and the polynomial are very varied in color selection, splines distribution, implementation of the curve errors at every point, linewidth of the curve at graph, etc. The running of the program for the graph in Figure 3.8 is approximately half a second ( $< 5$  s). It was necessary to perform a *for loop* at software. The numerical fitting shows low residual given to the extent data used. Equations (3.15) for Figure 3.8 have two principal weight terms. The computational results from the software running corresponding to this graph are shown in Equations (3.15). Firstly, for S3 and secondly for R3, the results are the following:

$$\begin{aligned}
 [\bar{a}]^T &= [872.0388, 5.0034, 0.1670, \dots \\
 &\dots 0.0007, 0.0000]; \\
 \text{Residual} & 679.8366 ;
 \end{aligned}
 \tag{3.15}$$

$$\begin{aligned}
 [\bar{a}]^T &= [789.9850, 28.0505, 1.1573, \dots \\
 &\dots 0.0208, 0.0001]; \\
 \text{Residual} & 706.8712 ;
 \end{aligned}$$

Subsequent imaging plots of Figure 3.9 show a MATLAB 8-degree polynomial fitting with double precision of S3 as a function of R3 complete-relative hardness spatial distribution corresponding to the matrix, transition and spherical reinforcement. S3 is the function of R3,  $S3=f(R3)$ , in the programming development technique.  $S3=f(R3)$  is the blue curve, and  $R3=f(S3)$  is the green one. Visual Studio F# and FORTRAN 77-95 were also used to re-check the results. When programming a double precision polynomial, it is useful to discard those terms that are high-negative exponentials of 10. In other words, it is preferential to keep significant digits. Discrete laboratory data for the polynomial is given in circles and is represented in blue-curve to show a variation in programming. The green curve is the strict mathematical function  $R3=f(S3)$ . The software here was designed to obtain more data at image. The transition-binding zone shows the sharp differences between the two functions implemented. The reason to compare S3 and R3 materials in Figure 3.9 is to visualize the differences at the transition zone and the coincidences at the matrix and the reinforcement.

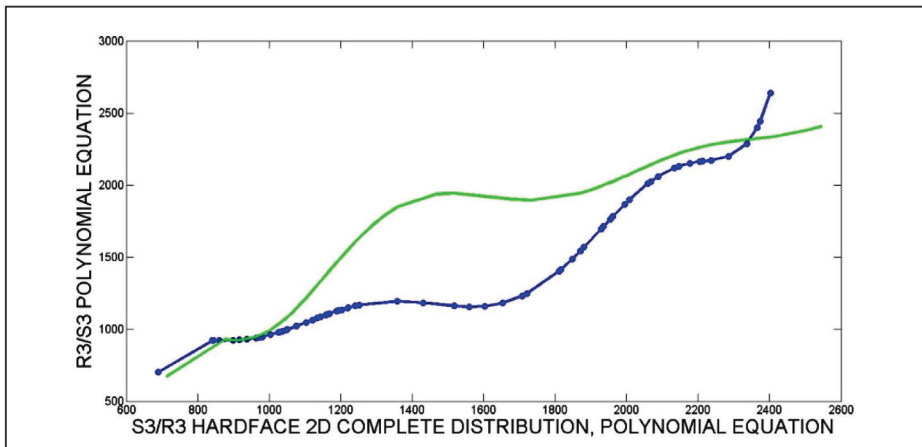


Figure 3.9 Programming  $S3=f(R3)$  in MATLAB with double precision (8 terms).

The numerical computation shows a larger residual given for the extent data used. This is due to the comparative analysis in both materials hardness values. Equations (3.16) set the principal weight terms and residuals, both for  $S3=f(R3)$  and  $R3=f(S3)$ . The computational results from the software running corresponding to this graph of Figure 3.9 and also  $R3=f(S3)$  are the following:

$$\begin{aligned}
 [\bar{a}]^T &= 10^5 [ 1.4204, 0.7742e2, 0.1732e5, \dots \\
 &\dots 0.2059e7, 0.1387e10 ; ] \quad (3.16) \\
 \text{Residual} & 6.3229 \times 10^2 ; \\
 [\bar{a}]^T &= 10^5 [ 4.0499, 0.2303e1, 05512e4, \dots \\
 &\dots 0.7281e7, 0.5801e10 ; ] \\
 \text{Residual} & 6.2549 \times 10^{12} ;
 \end{aligned}$$

The computational design of the program for the graph of Figure 3.9 is different because it is in double precision, and from the 8-degree polynomial solution, it is necessary to select the most significant digits. The numerical computation, Equations (3.16), shows a larger residual given for the extent data used. This is due to the comparative analysis in both materials hardness values. The main equations have two principal weight terms; the other ones are high-negative powers.

In the following, Figure 3.10 is intended to show a Double-Numerical-Computational comparison between S3 and R3 polynomials fittings and two options of similar software compilers. The graph of Figure 3.10 is performed in MATLAB (2010), [20, 29, 41, 42], where the imaging tool permits setting labels before saving the image. For FreeMat, [39, 40], the graph of Figure 3.11 is presented without labels.

The verification of imaging smoothness is almost equal in both but it is not possible at first prompt result to set labels within the image in the FreeMat case, but it can be added manually to the chart. Visual Studio F# and FORTRAN 77-95 were also used to re-check the results. Specifically, FORTRAN numerical results are highly significant  $\leq 450$  with double precision. However, F# resulted in residuals  $\geq 800$ .

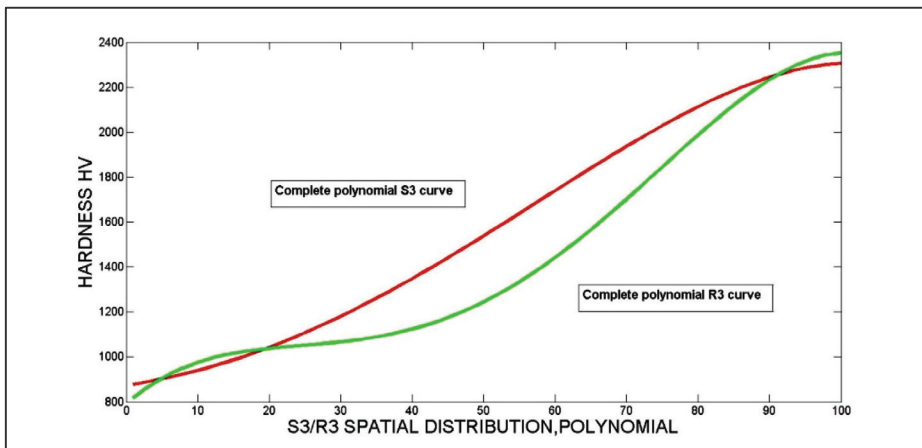


Figure 3.10 Complete dual polynomial distribution of R3 and S3 with MATLAB special software.

The consequences and practical information that can be assumed from graphs of Figures 3.10 and 3.11 are included in [75]. Recycling engineering approximations in modelling for erosion impact wear are feasible from this extent data-plotting.

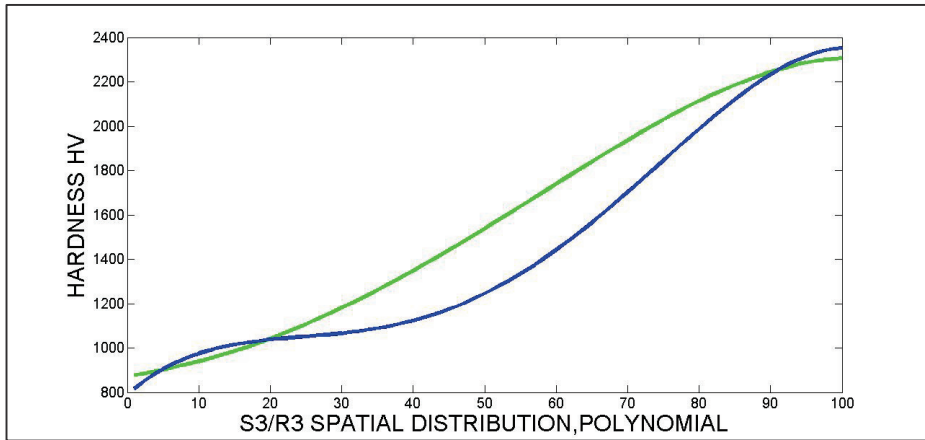


Figure 3.11 Complete dual polynomial distribution of S3 (green) and R3 (blue) with FreeMat program. Residuals in FreeMat are  $\leq 500$ .

Experimental and theoretical data obtained from the stratified model of the section for S3 and other materials corresponding to Paper II are presented in Table 3.5 and 3.6. The best results matching between theory and experimental are obtained for low energy and 30 degrees of impact angle.

Table 3.5 Theoretical and experimental results for low energy erosion rate ( $\text{mm}^3/\text{Kg}$ ) of H400 (Hardox 400 steel), P1 (unreinforced FeCrSiB), C3 (70 % FeCrSiB+30 % WC-Co; recycled), S3 (70% FeCrSiB+30 % WC-Co; spherical) for stratified model of Paper III

| Velocity, m/s      | 40              |      | 80      |      |
|--------------------|-----------------|------|---------|------|
|                    | Impact angle, ° |      |         |      |
|                    | 90              |      |         |      |
| Material/Data Type | Calc.           | Exp. | Calc.   | Exp. |
| H400               | 6.0e-12         | 26.1 | 4.8e-11 | 85.4 |
| P1                 | 2.7e-12         | 9.3  | 2.1e-11 | 29.5 |
| C3                 | -               | -    | -       | -    |
| S3                 | 0.4             | 85.2 | 3.2     | 25.7 |

Table 3.6 Theoretical and experimental results for high energy erosion rate ( $\text{mm}^3/\text{Kg}$ ) of the same materials as in Table 3.5

| Velocity, m/s      | 40              |      |         |      | 80    |      |         |      |
|--------------------|-----------------|------|---------|------|-------|------|---------|------|
|                    | Impact angle, ° |      |         |      |       |      |         |      |
|                    | 30              |      | 90      |      | 30    |      | 90      |      |
| Material/Data Type | Calc.           | Exp. | Calc.   | Exp. | Calc. | Exp. | Calc.   | Exp. |
| H400               | 3.8             | 7.9  | 6.0e-12 | 3.8  | 21.8  | 37.0 | 4.8e-11 | 30.0 |
| P1                 | 4.6             | 3.2  | 2.7e-12 | 10.0 | 25.7  | 12.0 | 2.2e-11 | 1.5  |
| C3                 | -               | -    | 1.1     | 3.7  | 42.9  | 12.9 | 23.4    | 16.7 |

## Conclusions

Erosion/Corrosion (E/C) models available in the literature are presented with a simplified classification. This categorization is based on practical applications, mathematical framework, optimization of modelling and functionality. The most important E/C models were examined, pointing out advantages, combinations, particular details, applications, variants, approximations, and weaknesses. Optimization methods to fit E/C models and mathematical models in general have been explained specially in all the publications presented.

The studies conducted, especially those focused on graphical optimization methods for modelling, proved how complicated it is to obtain well-optimized erosion models with computational programming codes and subroutines and generalized models for E/C. The reasons for this rather significant mathematical-empirical hurdle have been explained in this contribution. However, as a result, the current models could be improved towards a continuous generalization process. The second generation of models could provide more general models of Types 1 and 2 by programming/experimentally. In the future, this kind of techniques of nonlinear optimization using the large computational work performed can be implemented for other models with a larger number of parameters, such as angle in the case of erosion, particle density, particle size, kinetic energy of impacting particle, etc. In summary, the results of the study are as follows:

1. Current erosion and corrosion models were analyzed.
2. A functional classification of erosion and corrosion mathematical models was developed.
3. A discrete stratified model was created with laboratory experimental measurements.
4. An integral-differential model was presented and developed with formulation.
5. Graphical Optimization model was detailed and explained in 3D and 2D, [20, 29, 41, 42].
6. The Graphical Optimization model and the method were applied to bioengineering erosion models.
7. The application of Inverse Problems methods in tribology models was demonstrated.
8. A 2D computational-numerical comparison for two types of hardfacing reinforcements was carried out.

An innovative graphical optimization method was developed both in FreeMat [39, 40] and MATLAB. F# programming was introduced also in bioengineering simulations papers. FORTRAN programming was used to re-check the numerical results of simulations and nonlinear optimization methods. A large variety of computational examples with the selected models for erosion optimization—indicative computational illustration and biomedical tribology computational approaches/simulations were provided. This type of graphical optimization is not reduced to 3D with two variables at plane x-y, several techniques with matrix algebra permit to implement an unlimited number of variables for graphical-surfactal optimization.

The variables were determined with software specially designed in a high-dimensional matrices of Nonlinear Optimization subroutine. It can be considered as an E/C modelling-programming instance for future contributions to be developed/published. The high-degree polynomial fittings presented in single/double-precision are significantly useful for environmental engineering applications/consequences and future second generation of models.

Additionally, this advanced research was focused on nonlinear optimization and direct applications of inverse problems theory. Inverse methods, specifically for wear in the mechanical structure of power plants, were introduced extensively in Paper V. The models presented for optimization were detailed to demonstrate the method of inverse nonlinear optimization with specific software. All the selected models in this study are appropriate/suitable to be implemented on any other more complicated equation, independent of the number of variables to be optimized. Large-scale multi-objective optimization could be carried out with the programming designed properly for Hutchings, and Archard models. In particular, graphical 3D optimization/simulation surfaces were shown for sharp learning of this new technique.

Results are considered accurate and acceptable, conditioned to extensive serial laboratory experimental validation in future research. The practical applications in erosion/corrosion models for mechanical systems, power plants, energy industry, and circular production, follow straightforward from the proven method with software and subroutines of optimization in FreeMat and MATLAB. Practical conclusions related to the functionality of the experimental data and simulations were drawn for environmental engineering and economic-cost reduction. For the hard metal R3 produced from recycling powder [66, 68, 71], results were proven theoretically and experimentally with real laboratory database.

## References

1. Eitobgy, M., Elbestawi, M. Finite element modelling of erosive wear. *International Journal of Machine Tools and Manufacture*. 2005, 45, pp. 1337-1346.
2. Crocker, L. A Review of Current Methods for Modeling Erosive Wear. NPL Report. 2011.
3. Abramowitz, M., Stegun, I. Handbook of Mathematical Functions. Applied Mathematics Series. 55. 1972.
4. Casesnoves, F. A Monte-Carlo optimization method in Numerical Reuleaux Method for the movement analysis of pseudo-rigid bodies. *Proceedings 10th SIAM Conference in Geometric Design and Computing joint to Approximation Theory Conference*. 2007, pp. 4-5.
5. Luenberger, G. Linear and Nonlinear Programming. Fourth Edition. Springer. 2008.
6. Ots, A. Oil Shale Combustion. TUT Press. Tallinn. 2004.
7. Holmberg, K., Erdemir, A. Influence of tribology on global energy consumption, costs, and emissions. *Friction*. 2017, 5, 3, pp. 263-284.
8. Casesnoves, F. 3D Improved mathematical model for lumbar intervertebral ligaments (LILs). *Proceedings SIAM Life Sciences Conference joint to SIAM Annual Conference San Diego*. 2012, pp. 25-27.
9. Antonov, M., Veinthal, R., Huttunen-Saarivirta, E., Hussainova, I., Vallikivi, A., Lelis, M., Priss, J. Effect of oxidation on erosive wear behaviour of boiler steels. *Tribology International*. 2013, 68, pp. 35-44.
10. Antonov, M. Assessment of Cermets Performance in Aggressive Media. Doctoral Dissertation. Thesis on mechanical and instrumental engineering e29. TUT Press. 2006.
11. Mellor, B. Surface Coatings for Protections Against Wear. CRC Press. Woodhead Publishing in Materials. 2006.
12. Huttunen-Saarivirta, E., Antonov, M., Veinthal, R., Tuiremo, J., Mäkelä, K., Siitonen, P. Influence of particle impact conditions and temperature on erosion–oxidation of steels at elevated temperatures. *Wear*. 2011, 272, pp. 159-175.
13. Antonov, M., Michalczewski, R., Pasaribu, R., Piekoszewski, W. Comparison of a tribological model and real component test methods for lubricated contacts. *Estonian Journal of Engineering*. 2009, 15, 4, pp. 349-358.
14. Ashby, F. Materials Selection in Mechanical Engineering. Butterworth-Heinemann. 2000.
15. Lee, T., Chan C. Mechanism of ultrasonic machining of ceramic composites. *J. Mater. Process. Technol.* 1997, 71, pp. 195-201.
16. Pabhakar, D., Pei, Z., Ferreira, P., Haselkorn, M. A theoretical model for predicting material removal rates in rotary ultrasonic machining. *Trans. NAMRI/SME XXI*. 1993, pp. 167-172.
17. Hutchings, I. A model for the erosion of metals with spherical particles at normal incidence. *Wear*. 1981, 70, pp. 269-281.
18. Sheldon, G., Finnie, I. The mechanism of material removal in the erosive cutting of brittle materials. *Trans. ACME, J. Eng. Ind.* 1996, 88, pp. 393-400.
19. Kleis, I., Kulu, P. Solid Particle Erosion. Springer. 2008.
20. Casesnoves, F. An Optimization Method for Static Wedge-Radiation Filters in Radiation Therapy. Master in Physics Thesis. Eastern Finland University. 2001.

21. Balamanikandasuthan, K., Arun, K., Palam, S. Design and fabrication of erosion protection shield for boiler tubes and its analysis. *International Journal of Mechanical and Materials Engineering*. 2015, 1, 1, pp. 39-52.
22. Bartholomew-Biggs, M. Nonlinear Optimization with Engineering Applications. Springer Optimization and its Applications. 2008.
23. Bertsekas, D. Nonlinear Programming. Second Edition. Athena Scientific. 2003.
24. Borwein, J. Convex Analysis and Nonlinear Optimization. Second Edition. CMS Books In Mathematics. Springer. 2000.
25. Casesnoves, F. Large-Scale multiobjective MATLAB optimization toolbox (mot) computing methods in radiotherapy inverse treatment planning. *High Performance Computing Conference*. Nottingham University. 2007.
26. Casesnoves, F. Geometrical/computational dynamics approximations for helicopter-rotor instantaneous rotation center in turbulence with Numerical Reuleaux Method. *International Journal of Engineering and Innovative Technology*. 2014, 4, 3, pp. 175-184.
27. Casesnoves, F. Geometrical algorithms for civil helicopter (CH) rotor blades instantaneous rotation center (IRC) determination in deformable/turbulence conditions using the Numerical Reuleaux method (NRM): a nonlinear optimization method in aerospace engineering dynamics. *Proceedings SIAM Conference on Applied Algebraic Geometry Fort Collins*. 2013, pp. 112-114.
28. Hildebrand, F. Introduction to Numerical Analysis. Second Edition. Dover Publications, Inc. 1987.
29. Fausett, L. Applied Numerical Analysis using MATLAB. Pearson International. 2008.
30. Casesnoves, F. A new radiological optimization method for lumbar artificial disc imaging in biomechanics. *UK Doctoral Conference*. Nottingham University. 2007.
31. Hussainova, I., Kubarsepp, J., Shcheglov, I. Investigation of impact of solid particles against hardmetal and cermet targets. *Tribology International*. 1999, 32, pp. 337-344.
32. Hussainova, I. On micromechanical problems of erosive wear of particle reinforcement composites. *Proc. Estonian Acad. Sci. Eng*. 2005, 11, pp. 46-58.
33. Kajdas, C., Harvey, S., Wilusz, E. Encyclopedia of Tribology. Elsevier. 1990.
34. Liao, H., Normand, B., Coddet C. Influence of coating microstructure on the abrasive wear resistance of WC-Co cermet coatings. *Surface and Coatings Technology*. 2000, 124, pp. 235–242.
35. Kulu, P., Zimakov, S. Wear resistance of thermal sprayed coatings on the base of recycled hardmetal. *Surface and Coatings Technology*. 2000, 130, pp. 46-51.
36. Kulu P., Tarbe R., Zikin A., Sarjas H., Surženkov A. Abrasive wear resistance of recycled hardmetal reinforced thick coating, *Key Eng. Mat*. 2013, 527, pp. 185-190.
37. Kulu, P. Selection of powder coatings for extreme erosion wear conditions. *Advanced Eng. Mater*. 2002, 4/6, pp. 392-397.
38. Harland, D. STEM. Student Research Handbook. NSTA Press. 2011.
39. FreeMat v4.0 Documentation. Samit Basu. 2009.
40. FreeMat v4.0 Documentation. Samit Basu. 2010.
41. Moler, C. Numerical Computing with MATLAB. SIAM. 2004.
42. Gherpade, S. Introduction to Algebraic Geometry. Department of Mathematics Publications. Indian Institute of Technology Bombay. 2014.
43. Casesnoves, F. A Gaussian Mathematical Model for Optimization Methods of Absorbed Dose in Radiation Therapy. Bachelor in Physics and Natural Sciences Thesis. Eastern Finland University. 2001.

44. Cheney, W., Light, W. A Course in Approximation Theory. Graduate Studies in Mathematics. Am. Math. Soc. Vol. 101. 2000.
45. Crowell, A., Slesnicks, J. Calculus with Analytic Geometry. Version 3.03. 2008. GNU Free Documentation License. Free Software Foundation. 2008.
46. Wilson, P. Curves Spaces. Cambridge. 2008.
47. Heinbockel, J. Introduction to Calculus. Volume I. Lectures of Electronics. Copyright by J H Heinbockel. 2012.
48. Heinbockel, J. Introduction to Calculus. Volume II. Lectures of Electronics. Copyright by J H Heinbockel. 2012.
49. Serway, R., Jewett, J. Physics for Scientists and Engineers with Modern Physics. Seventh Edition. Thomson Higher Education. 2008.
50. Strauss, W. Partial Differential Equations. Second Edition. Wiley. 2008.
51. Mackerle, J. Finite-element analysis and simulation of machining: a bibliography (1976–1996). *Journal of Materials Processing Technology*. 1999, 86, pp. 17-44.
52. Chen, Q., Li, D. Computer simulation of solid-particle erosion of composite materials. *Wear*. 2003, 255, pp. 78–84.
53. Casesnoves, F. Experimental simulations of the Numerical Reuleaux method (NRM) for lumbar artificial disk implants IRC determination. *Proceedings SIAM Conference in Computational Science and Engineering*. 2009, PP1 Section, pp. 1-2.
54. Veinthal, R. Characterization and Modelling of Erosion Wear of Powder Composite Materials and Coatings. PhD thesis. TUT Press. 2005.
55. Casesnoves, F. Theory and primary computational simulations of the Numerical Reuleaux method (NRM). *International Journal of Mathematics and Computation*. 2011, 13, D11, pp. 90-110.
56. Casesnoves, F. Applied inverse methods for deformable solid dynamics/kinematics in Numerical Reuleaux method (NRM). *International Journal of Numerical Methods and Applications*. 2013, 9, 2, pp. 109-131.
57. Casesnoves, F. Applied inverse methods for optimal geometrical-mechanical deformation of lumbar artificial disks/implants with Numerical Reuleaux method. 2D comparative simulations and formulation. *Ethan Publishing Computer Science Applications*. 2015, 2, 4, pp. 1-10.
58. Casesnoves, F. Computational simulations of vertebral body for optimal instrumentation design. *ASME Journal of Medical Devices*. 2012, 6, 2, pp. 14-25.
59. Casesnoves, F. Computational simulations of anterior vertebral body for optimal surgical instrumentation design. *ASME Journal of Medical Devices*. 2010, 4, 2, pp. 25-26.
60. Camomilla, V., Cereatti, A. An optimized protocol for hip joint centre determination using the functional method. *Journal of Biomechanics*. 2006, 39, 6, pp. 1096-1106.
61. Casesnoves, F. Spinal biomechanics mathematical model for lumbar intervertebral ligaments. *Proceedings SIAM Conference on Computational Science and Engineering*. 2011, pp. 227-229.
62. European Textbook on Ethics in Research. European Commission, Directorate-General for Research. Unit L3. Governance and Ethics. European Research Area. Science and Society. EUR 24452 EN.
63. Li, L., Li, D. Simulation of corrosion-erosion of passive metals using a micro-scale dynamical model. *Wear*. 2011, 271, pp. 1404-1410.
64. Matthews, S., Franklin, A., Holmberg, K. Tribological coatings: contact mechanisms and selection. *Journal of Physics D: Applied Physics*, 2007, 40, pp. 5463-5475.
65. Miller, G. Special Theory of ultrasonic machining. *J. Appl. Phys.* 1957, 28, pp. 146-156.

66. Notes, References, and Lectures. *CEE SIMP Conference*. Raw Materials and Circular Economy. Institute of Geology, Tallinn University of Technology. Mektory Technology Innovation Center. 2017.
67. Ožbolt, J., Sola, E., Balabanić, G. Accelerated corrosion of steel reinforcement in concrete: experimental tests and numerical 3D FE analysis. *ASCE Conference Proceedings*. Concreep 2010.
68. Shin, J., Jeon, Y., Maeng, A. Kim, J. Analysis of the dynamic characteristics of a combined-cycle power plant. *Energy*. 2002, 2, pp. 1085-1098.
69. Simson, T., Kulu, P., Surženkov, A., Tarbe, R., Viljus, M., Tarraste, M., Goljandin, D. Optimization of reinforcement content of powder metallurgy hardfacings in abrasive wear conditions. *P. Est. Acad. Sci.* 65. 2016, pp. 90-96.
70. The European Code of Conduct for Research Integrity. Revised Edition. ALLEA. 2017.
71. Kulu, P., Tumankov, A., Arensbürger, D., Pihl, T., Mikli, V., Kaerdi, H. Recycling of hard metals. *P. Est. Acad. Sci. Eng.* 1996, 2, 1, pp. 49-60.

### **Additional author's publications**

72. Casesnoves, F., Antonov, M., Kulu, P. Mathematical models for erosion and corrosion in power plants. A review of applicable modelling optimization techniques. *IEEE Proceedings of RTU CON201 Power Engineering Conference*. 2016, paper 51. (DOI:10.1109/RTU CON.2016.7763117. Electronic ISBN:978-1-5090-3732-2. USB ISBN: 978-1-5090-3730-8. ISBN: 978-1-5090-3722-2).
73. Casesnoves, F., Surzhenkov A. Mathematical models in mechanical and biomedical tribology with computational simulations/optimization methods. *International Journal of Scientific Research in Computer Science, Engineering and Information Technology, IJSRCSEIT*. 2017, Volume 2, Issue 1. (ISSN : 2456-3307).
74. Casesnoves, F. Erosion wear mathematical model for WC-Co reinforcement hardness distribution in Fe-based alloy matrix with evolved algorithms. *International Journal of Scientific Research in Science, Engineering and Technology, IJSRSET*. Section Engineering and technology. 2017, Volume 3, Issue 5, pp. 336-344. (Print ISSN : 2395-1990. Online ISSN : 2394-4099).
75. Casesnoves, F. 2D computational-numerical hardness comparison between Fe-based hardfaced with WC-Co reinforcements for integral-differential modelling. *Proceedings of Materials Science and Applied Chemistry 58<sup>th</sup> International Conference*. 2017 Trans Tech Publications.
76. Casesnoves, F. Stochastic Optimization/simulations of corrosion models for Fe-based hardfaced with WC-Co reinforcements with nonlinear programming methods in integral-differential model. Submitted and accepted for *International Journal of Scientific Research in Computer Science, Engineering and Information Technology*. 2018. IJSRCSEIT.
77. Casesnoves, F. 2D computational-numerical hardness comparison between Fe-based hardfaced with WC-Co reinforcements for integral-differential modelling. *Key Engineering Materials Journal. Trans Tech publications*. 2018, Vol 762, pp 330-338. (DOI: 10.4028/www.scientific.net/KEM.762.330.ISSN: 1662-9795).
78. Casesnoves, F. Inverse methods and Integral-Differential model demonstration for optimal mechanical operation of power plants –numerical graphical optimization for second generation of tribology models. *Electrical, Control and Communication Engineering*. Riga Technical University. 2018, Vol 14, 1, pp. 39-50. (DOI: 10.2478/ecce-2018-0005).

79. Casesnoves, F. Nonlinear comparative optimization for biomaterials wear in artificial implants technology. Presented in Applied Chemistry and Materials Science RTU2018 Conference Proceedings. 2018.
80. Casesnoves, F. Optimization of probability of failure with erosion Integral-Differential model for power plants mechanics2018 IEEE 59th International Scientific Conference on Power and Electrical Engineering of Riga Technical. Section Information and Communication Technologies in Electrical and Power Engineering. Paper 34. 2018. (ISBN: 978-1-5386-6902-0).
81. Casesnoves, F. Primary Modeling For Electromagnetic Waves Transmission In Extreme Weather Conditions. International Journal of Innovative Research in Science, Engineering and Technology, volume 7, issue 10, 2018. (ISSN Online: 2319-8753. DOI:10.15680/IJIRSET.2018.0710022).

## Acknowledgements

*To Natashka Kamarova, the best of my life*

Senior researcher Maksim Antonov (project B56, ETAG 18012) is gratefully acknowledged for facilities and information required for the thesis research. The teaching and facilities for the PhD program and continuous experienced advice of Professor Priit Kulu is recognized. Associate Professor Fjodor Sergejev also contributed to the development of the project with facilities for the PhD program. Professor Jakob Kübarsepp is acknowledged for his support in publications related to project IUT 19-29. Professor Jüri Majak is acknowledged for his computational teaching and facilities. Teaching Assistant Andrei Surženkov is recognized for his collaboration along a significant number of articles and reviewing the experimental framework of some of the thesis papers. Specialists in Centre for Open Education at TalTech Katrin Saadre and Enelii Kirschinger have given important facilities for the participation in mandatory doctoral courses during PhD program. TalTech Accommodation Services Merje Meister, Helen Türkson and Helge Marks are gratefully acknowledged. TalTech Library is gratefully acknowledged for facilities.

## Abstract

# Mathematical Modelling and Optimization of Erosion and Corrosion in Tribology

This study is focused on tribological modelling with nonlinear computational optimization methods and specific approaches of software engineering. The database was implemented to develop the modelling methods and the optimization tools.

The thesis includes computational, theoretical and experimental study. The theoretical study covers development and application of the mathematical modeling methods and tools, also graphical optimization techniques. The experimental study is related to the management of large laboratory data to set and optimize/simulate computationally a series of models for hardfacings with WC-Co reinforcement together with Monte Carlo approaches. This type of simulations and optimization methods are also applied to biotribological models, namely hip wear prostheses equations.

3D optimization problems with at least three variables and any kind of objective function are studied. A series of simulations were carried out always with the perspective of tribological, biotribological or tribocorrosion applications. The simulation techniques based on the matrices and polynomial programming codes are developed for specific tribological applications. The modelling with 3D surfactal optimization is not necessarily defined for two parameters. Since the parameters within the 3D surfactal optimization model can be joined in variables groups, the surfactal representation can be extended for a number of parameters. In 2D it is easier to find the geometrical locus for convergence of several functions with different parameters.

Another part of the study covers the application of Inverse Problems methods to data analysis, which was carried out for hardness laboratory data. The stochastic optimization model for corrosion is introduced.

The interrelation between hardness of hardfacings produced from commercial self-fluxing alloy and recycled hardmetal powders is proved. These findings show important consequences related to the development of materials and prediction of wear rate.

In conclusion, the research results published in peer-reviewed papers are focused mainly on development and application of mathematical models and optimization techniques covering tribology, biotribology and tribocorrosion.

**Keywords:** Mathematical Modelling, Tribology Models, Nonlinear Optimization, Constrained Graphical Optimization, Wear Rate Prediction

## Lühikokkuvõte

### Erosiooni ja korrosiooni matemaatiline modelleerimine ja optimeerimine triboloogias

Antud uurimustöö on keskendunud triboloogiliste protsesside modelleerimisele mittelineaarsete arvutuslike optimeerimise meetoditega ja spetsiifiliste tarkvaratehnika lähenemisviisidega. Modelleerimise meetodite ja optimeerimise vahendite arenduseks ja rakendamiseks koostati katseandmete andmebaas.

Töö sisaldab nii arvutuslikku, teoreetilist ja eksperimentaalset osa. Teoreetiline osa katab peamiselt üldistatud integraal-diferentsiaalmodelite ja graafilise optimeerimise arendamisest. Eksperimentaalne osa on seotud mahukate laboratoorsete andmete haldamisega, et optimeerida / simuleerida erinevaid mudeleid paksude kulumiskindlate WC-Co kõvapinnete jaoks. Seda tüüpi simulatsioone ja optimeerimismeetodeid on rakendatud ka biotriboloogilistele mudelitele puhul, nimelt puusa proteeside kulumist kirjeldavates võrrandites.

Antud töös on uuritud 3D optimeerimise probleeme, mis sisaldavad vähemalt kolme muutujat ja eri tüüpe sihifunktsioone. Viidi läbi simulatsioonide seeria triboloogiliste, biotriboloogiliste või tribokorrosiooni valdkonna probleemide jaoks. Töö tulemusena töötati välja maatriksarvutusel ja polünoomide rakendamisel põhinevad simulatsioonitehnikad. 3D pinnalise optimeerimisega modelleerimine ei ole tingimata määratletud kahe parameetriga. Kuna mudelis olevaid parameetreid saab grupeerida muutujate rühmadesse, saab pinna esitust laiendada mitmele parameetrile. 2D ruumis on erinevate parameetritega funktsioonide jaoks geomeetrilist asukohta - koonduvuspunkti lihtsam määrata.

Üks osa uurimistööst käsitleb pöördülesannete lahendusmeetodite rakendamist andmeanalüüsi probleemidele, mis viidi läbi komposiitmaterjali kõvaduse laboratoorsete andmete jaoks. Korrosiooniprotsessi kirjeldamiseks rakendati stohhastilist optimeerimise mudelit.

Antud töös on toodud välja tavapärase tööstuslike pihustuspulbrite ja ümbertöödeldud kõvasulami baasil valmistatud komposiitpinnete kõvaduste jaotuse ja kulumiskindluse vaheline seos. Saadud uurimistulemused on olulised kulumiskindlate materjalide arendamiseks ja kulumiskindluse prognoosimiseks.

Kokkuvõtteks võib öelda, et eel-retsenseeritud artiklites avaldatud uurimistulemused keskenduvad peamiselt matemaatiliste mudelite ja optimeerimistehnikate arendamisele ja rakendamisele triboloogia, biotriboloogia ja/või tribokorrosiooni valdkonnas.

**Märksõnad:** matemaatiline modelleerimine, triboloogia mudelid, mittelineaarne optimeerimine, kitsendustega graafiline optimeerimine, kulumise prognoosimine.



## Appendix 1

It is important to include a graphical optimization programming image in the thesis section to set clearly the results of the software nonlinear programming designed. The model is sharp in its global minimum and maximum in Figure 1 and corresponds to the model of Papers II, III and IV. In Figure 1, velocity interval is  $[50, 230] \text{ ms}^{-1}$ , angle interval is  $[22.7, 85]$  degrees, matrices are  $20 \times 20$  with higher tessellation.

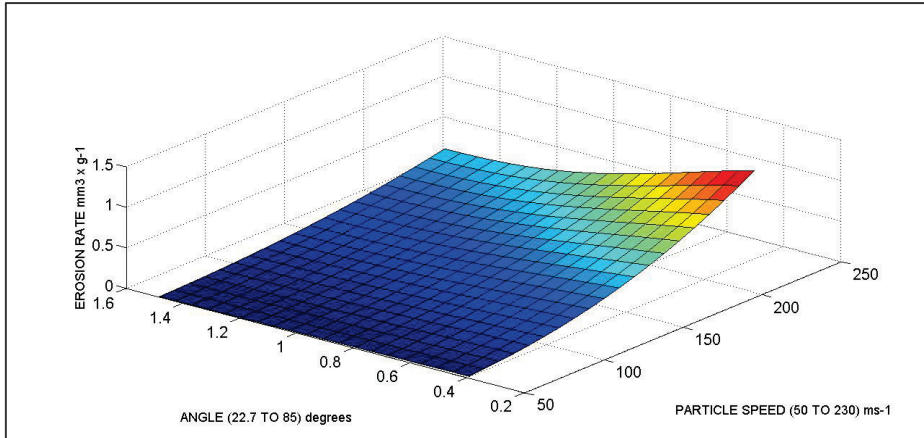


*Figure 1 Complete surfactal 3D image of Menguturk model with a sharp definition of optimization data, namely, global minima and maxima.*

The image of Figure 1 is sharp, for this model, the location of a global maximum and a global minimum is shown. Matrices in this program were not taken too large because it was intended to show how the tessellation of the subroutine constructs the 3D surface. In Papers I-V, and in [72-80], there are a series of graphical-surfactal optimization and simulation images in an extent variety.



## Appendix 2

### Paper I

Surzhenkov, A., Viljus, M., Tarbe, R., Casesnoves, F. Wear resistance and mechanisms of composite hardfacings at abrasive impact erosion wear. *Journal of Physics: Conf. Series*, 2017, pp. 1-10 (843 012060 DOI :10.1088/1742-6596/843/1/012060).



# Wear resistance and mechanisms of composite hardfacings at abrasive impact erosion wear

A Surzhenkov, M Viljus, T Simson, R Tarbe, M Saarna and F Casesnoves

Department of Mechanical and Industrial Engineering, Tallinn University of Technology, Ehitajate tee 5, 19086 Tallinn, Estonia

andrei.surzenkov@ttu.ee

**Abstract.** Tungsten carbide based hardmetal containing sprayed and melted composite hardfacings are prospective for protection against abrasive wear. For selection of abrasive wear resistant hardfacings under intensive impact wear conditions, both mechanical properties (hardness, fracture toughness, etc.) and abrasive wear conditions (type of abrasive, impact velocity, etc.) should be considered.

This study focuses on the wear (wear rate and mechanisms) of thick metal-matrix composite hardfacings with hardmetal (WC-Co) reinforcement produced by powder metallurgy technology. The influence of the hardmetal reinforcement type on the wear resistance at different abrasive impact erosion wear (AIEW) conditions was studied. An optimal reinforcement for various wear conditions is described. Based on wear mechanism studies, a mathematical model for wear prediction was drafted.

## 1. Introduction

Abrasive impact erosion wear (AIEW) of materials depends on their mechanical properties and on wear parameters. The dominating mechanisms at AIEW may generally be predicted on the grounds of the material / abrasive hardness ratio ( $H_m/H_a$ ) and the impact angle ( $0..90^\circ$ ). Depending on the first ratio, these mechanisms are [1,2]:

- $H_m < H_a$ : microcutting or plastic deformation with surface fatigue;
- $H_m \approx H_a$ : deformation with microcutting and/or surface fatigue;
- $H_m > H_a$ : deformation with surface fatigue and direct fracture.

Toughness of a material is another important mechanical characteristic that determines the behavior of a material at impact erosion. Depending on fracture toughness, the following mechanisms of wear may occur [3,4]:

- in brittle materials (low  $K_{Ic}$ ): plastic deformation with surface fatigue and great probability of direct fracture;
- in ductile materials (high  $K_{Ic}$ ): deformation with microcutting and/or surface fatigue [3,4].

Thick metal matrix composite (MMC) hardfacings are recommended for extreme abrasive wear conditions (i.e., high abrasivity, hardness and impact velocity of abrasive particles) due to their optimal hardness-toughness ratio. In this case, different wear mechanisms may simultaneously exist.



Such hardfacings may be produced, for example, by casting, plasma transferred arc (PTA) welding and submerged arc welding (SAW), vacuum sintering (VS), spray-fusion (SF), and high velocity spraying (HVS) [5–10].

The concept of plastic deformation and brittle fracture and a combined model of erosion were proposed to calculate the wear of composite structure materials [11]. A relatively soft metal matrix allows for use of the energetic theory of wear with the mean hardness and dimensionless specific energy parameter  $\tau_0/e_s$ . In the wear calculations of hardphase, the models of plastic deformation and brittle fracture using hardness distribution and fracture probability must be taken into consideration [2,11].

The calculated and the experimental results showed that the wear rates of the Ni-based matrix composite coating with a relatively low hardness ( $H_m < H_a$ ) have very good coincidence [12].

In the analysis of the abrasive wear resistance of HVOF-sprayed, PTA-welded and PM hardfacings in different wear conditions (abrasion at rubber wheel, impact erosion) in [13], potential application areas of selected composite hardfacings were proposed.

Wear of matrix material at impact erosion is contributed from erosion by microcutting [1,2]. As not all impacts lead to the formation of a clean machined chip that is removed, at multiple impacts within the plastic strain field of the previous impacts, it may be possible for material to be removed. In [14] that kind of wear is classified as fatigue wear for only two overlapping impacts.

The aim of the present research was (a) to study wear resistance and wear mechanisms of surface damage of thick MMC hardfacings at different AIEW modes (oblique and normal impact), and (b) to propose criteria for selection of hardfacings for the above-mentioned conditions based on the mechanical properties (hardness-toughness ratio) and microstructure (reinforcement content, size and shape).

## 2. Experimental

### 2.1 Materials

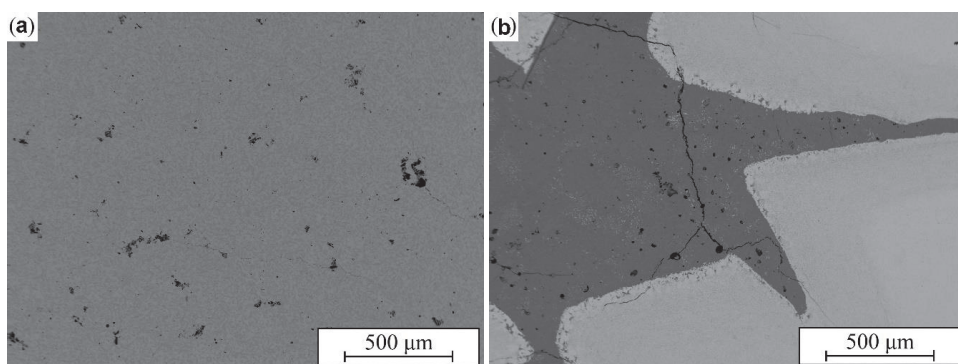
Metal matrix composite hardfacings were produced by powder metallurgy (PM) technology using vacuum liquid-phase sintering. For matrix iron based self-fluxing alloy powder Höganäs 6AB with composition, wt.%: 13.72 Cr, 2.67 Si, 0.32 Mn, 2.07 C, 0.02 S, 3.40 B, 6.04 Ni, bal. Fe was used. As a reinforcement, WC-15Co hardmetal powder produced by mechanical milling using a disintegrator milling system [15], with a particle size of 1.0–2.5 mm (coarse), 0.16–0.315 mm (fine) and their mixture (50% coarse + 50% fine) was used. The amount of 50% (optimal) was determined in our previous studies [8].

Table 1 shows the composition and hardness and Figure 1 – the microstructures of the studied hardfacings. As a reference material, Hardox 400 steel was used.

**Table 1.** Designation, composition and hardness of studied hardfacings.

| Designation | Reinforcement      |                | Hardness [16] |                  |
|-------------|--------------------|----------------|---------------|------------------|
|             | Particle size, mm  | Content, vol.% | HV30          | HV1 <sup>a</sup> |
| P1          | –                  | 0              | 870 ±30       | 1035 ±70         |
| C5          | Coarse angular (C) | 50             | 1260±435      | 1005±40/1855±65  |
|             | 1.0–2.5            |                |               |                  |
| F5          | Fine angular (F)   | 50             | 830±160       | 900±90/1445±135  |
|             | 0.160–0.315        |                |               |                  |
| M5          | Mixture 50C + 50F  | 50             | 1715±295      | 815±65/1480±125  |
| H400        | Reference steel    | –              | 425±25        | –                |
|             | Hardox 400         |                |               |                  |

<sup>a</sup> metal matrix/hard phase



**Figure 1.** Microstructures of the studied hardfacings: a – P1 (unreinforced), b – C5 (50 vol.% WC-Co angular reinforcement) [16].

## 2.2 Abrasive wear studies

Abrasive impact erosion wear (AIEW) tests were used to determine the wear resistance of the hardfacings. At the low-energy wear test, granite and quartz sand of fraction 0.2–0.3 mm and centrifugal type tester CAK were used; at the high-energy wear test, granite gravel of fraction 3.0–5.6 mm and a disintegrator type tester DESI (Figure 3) were used.

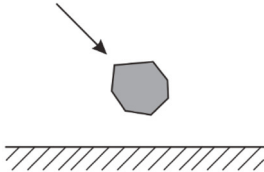
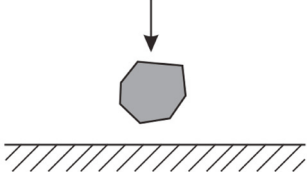
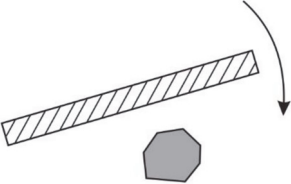
The schemes and parameters of AIEW are given in Tables 2 and 3.

Based on the weight loss of abraded hardfacings, the volumetric wear rate (loss of volume per 1 kg of abrading material) in mm<sup>3</sup>/kg was determined.

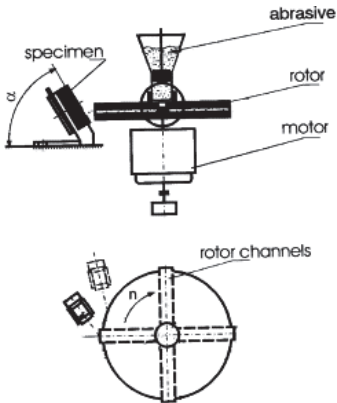
The relative wear resistance  $\varepsilon$  was calculated as the ratio of volumetric wear rates of the reference material (Hardox 400) to the wear rate of the studied hardfacing.

Mechanisms of the impact erosion wear were studied using a scanning electron microscope (SEM) EVO MA-15 (Carl Zeiss, Germany).

**Table 2.** Abrasive impact erosion wear (AIEW) modes.

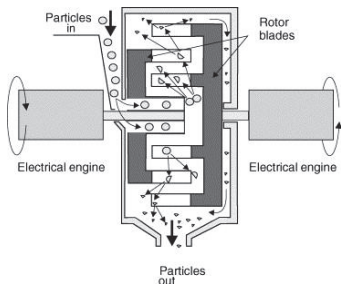
|             | Oblique impact erosion wear<br>$0^\circ > \alpha < 90^\circ$                      | Normal impact erosion wear<br>$\alpha = 90^\circ$   |
|-------------|---|---|
|             |   | Abrasive 0.2–0.3 mm   |
| Low energy  |  |                     |
|             |   | Kinetic energy $E_k$ at $v = 40$ m/s $3.0 \times 10^{-5}$ J<br>at $v = 80$ m/s $1.2 \times 10^{-4}$ J |
|             |   | Abrasive 3.0–5.6 mm   |
| High energy | —   |                     |
|             |   | Kinetic energy $E_k$ at $v = 40$ m/s $1.4 \times 10^{-2}$ J<br>at $v = 80$ m/s $5.6 \times 10^{-1}$ J |

**Table 3.** Abrasive impact erosion wear (AIEW) parameters (a).

| Scheme of wear tester   | Wear test parameters   |
|---|--|
|  | <p>Quartz sand 0.2–0.3 mm, 1000–1100 HV<br/>                     Granite sand 0.2–0.3 mm, 900–950 HV<br/>                     Impact angle <math>\alpha = 30^\circ</math> and <math>90^\circ</math><br/>                     Impact velocity <math>v = 40</math> m/s and <math>80</math> m/s<br/>                     Quantity of abrasive <math>Q = 6</math> kg</p> |

**Figure 2.** AIEW tester CAK.

**Table 3 (continues).** Abrasive impact erosion (AIEW) parameters (b).

| Scheme of wear tester   | Wear test parameters   |
|---|--|
|  | <p>Granite gravel 3.0–5.6 mm; 900–950 HV<br/>                     Impact angle <math>\alpha \approx 90^\circ</math><br/>                     Impact velocity <math>v = 40</math> m/s and 80 m/s<br/>                     Quantity of abrasive <math>Q = 15</math> kg</p> |

**Figure 3.** AIEW tester DESI.

### 3. Results and discussion

#### 3.1 Wear resistance of hardfacings at AIEW

3.1.1 *Influence of abrasive hardness.* Results of low-energy AIEW are given in Table 4 and Figure 4. As it follows from Figure 4, the wear resistance of hardfacings is better with a softer abrasive – granite (abrasive hardness is comparable with matrix hardness); relative wear resistance exceeds that of steel Hardox 400 by about 3 times. With a harder abrasive – quartz sand ( $H_a \approx 1.2 H_m$ ), the wear resistance of the studied hardfacings is low; relative wear resistance is at the same level or below that in comparison with Hardox 400.

**Table 4.** Wear rate ( $\text{mm}^3/\text{kg}$ ) of hardfacings at low-energy AIEW.

| Designation | Granite sand HV 900–950 | Quartz sand HV 1000–1100 |
|-------------|-------------------------|--------------------------|
| P1          | 12.0                    | 26.9                     |
| C5          | 11.7                    | 30.2                     |
| F5          | 30.2                    | 90.3                     |
| M5          | 21.9                    | 76.3                     |
| H400        | 37.0                    | 32.8                     |

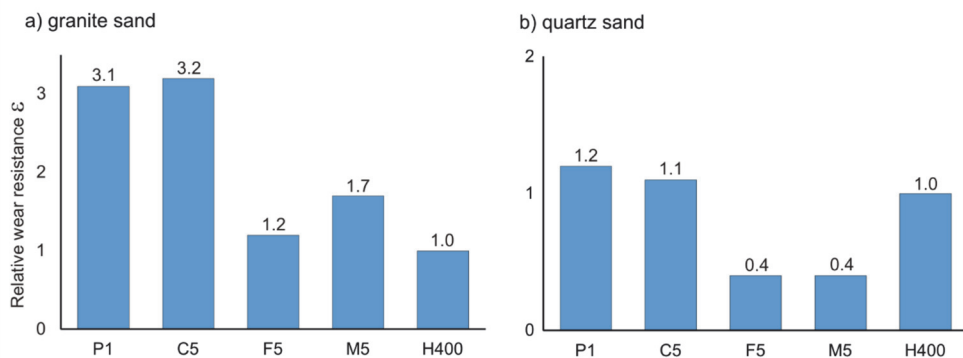


**Figure 4.** Relative wear resistance of hardfacings at low-energy AIEW with different abrasives (reference material – steel Hardox 400).

**3.1.2 Influence of impact angle at AIEW.** The results of wear resistance comparison of studied hardfacings at oblique impact ( $\alpha = 30^\circ$ ) and at normal impact ( $\alpha = 90^\circ$ ) show that the wear rate at straight impact is approximately 1.5 times higher (see Table 2). The relative wear resistance of the best hardfacing (C5) at  $\alpha = 30^\circ$  was 3.2 times higher, at normal impact ( $\alpha \approx 90^\circ$ ) it is only 1.9 times higher (Figure 5).

**Table 5.** Wear rates ( $\text{mm}^3/\text{kg}$ ) of hardfacings at different impact angles at low-energy AIEW (abrasive – granite sand, impact velocity  $v = 80 \text{ m/s}$ ).

| Designation | Impact angle, $\alpha$ |                     |
|-------------|------------------------|---------------------|
|             | $\alpha = 30^\circ$    | $\alpha = 90^\circ$ |
| P1          | 12.0                   | 21.5                |
| C5          | 11.7                   | 15.5                |
| F5          | 30.2                   | 41.0                |
| M5          | 21.9                   | 40.4                |
| Hardox 400  | 37.0                   | 30.0                |

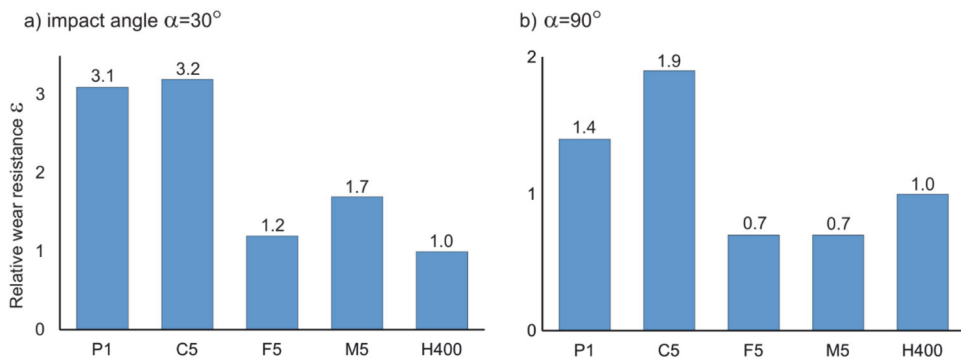


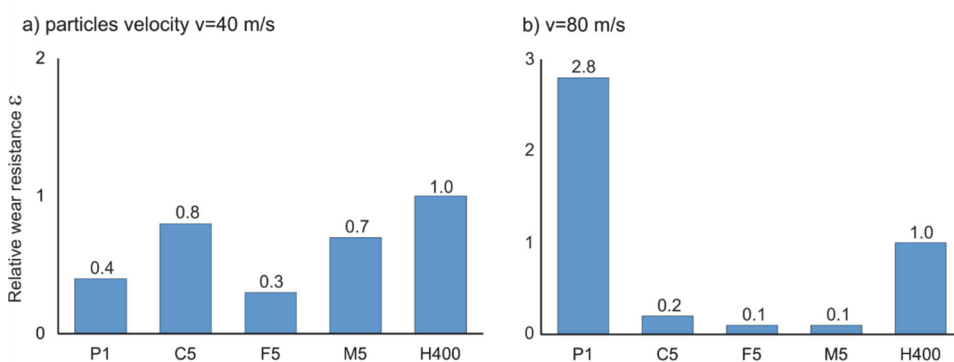
**Figure 5.** Relative wear resistance of hardfacings at low-energy AIEW under different impact angles (abrasive – granite sand, reference material – Hardox 400).

**3.1.3 Influence of abrasive particle velocity.** The results of wear rate comparison of studied hardfacings at 40 m/s and 80 m/s (Table 6 and Figure 6) show that the wear rate of reinforced hardfacings at higher velocities is 3–4 times higher when the wear of the reference steel Hardox 400 is 7–8 times higher.

Thus, at low velocity (in the range  $\epsilon = 0.3\text{--}0.8$ ), the relative wear resistance is lower to compare with Hardox 400; at high velocity, wear resistance of composite hardfacings is very low (in the range  $\epsilon = 0.1\text{--}0.2$ ). It can be explained by the differences in the wear mechanisms of hardened steel as compared with metal matrix composite hardfacings.

**Table 6.** Wear rates ( $\text{mm}^3/\text{kg}$ ) at different velocities at low-energy AIEW (abrasive – granite sand, impact angle  $\alpha = 90^\circ$ ).

| Designation | Velocity of abrasive particles, $v$ |                      |
|-------------|-------------------------------------|----------------------|
|             | $v = 40 \text{ m/s}$                | $v = 80 \text{ m/s}$ |
| P1          | 10.0                                | 21.5                 |
| C5          | 4.8                                 | 15.5                 |
| F5          | 13.8                                | 41.0                 |
| M5          | 5.6                                 | 40.4                 |
| H400        | 3.8                                 | 30.0                 |

**Figure 6.** Relative wear resistance of hardfacings under different impact velocities (abrasive – granite sand, reference material – steel Hardox 400).

**3.1.4 Influence of impact energy of abrasive particles.** As the difference in studied impact energies is high (ratio of kinetic energies of high and low energy impact at  $v = 40 \text{ m/s}$  is about 500 times), it influences the wear resistance significantly (see Table 7 and Figure 7). Wear rates of best hardfacing C5 differ about 23 times while the difference of the reference steel is only about 7 times.

**Table 7.** Wear rates ( $\text{mm}^3/\text{kg}$ ) at different impact energies (abrasive – granite,  $v = 40 \text{ m/s}$ ,  $\alpha = 90^\circ$ ).

| Designation | Low energy (sand)                    | High energy (gravel)                 |
|-------------|--------------------------------------|--------------------------------------|
|             | $E_k = 3.0 \times 10^{-4} \text{ J}$ | $E_k = 1.4 \times 10^{-2} \text{ J}$ |
| P1          | 10.0                                 | 9.3                                  |
| C5          | 4.8                                  | 108.6                                |
| F5          | 13.8                                 | 215.2                                |
| M5          | 5.6                                  | 348.6                                |
| Hardox 400  | 3.8                                  | 26.1                                 |

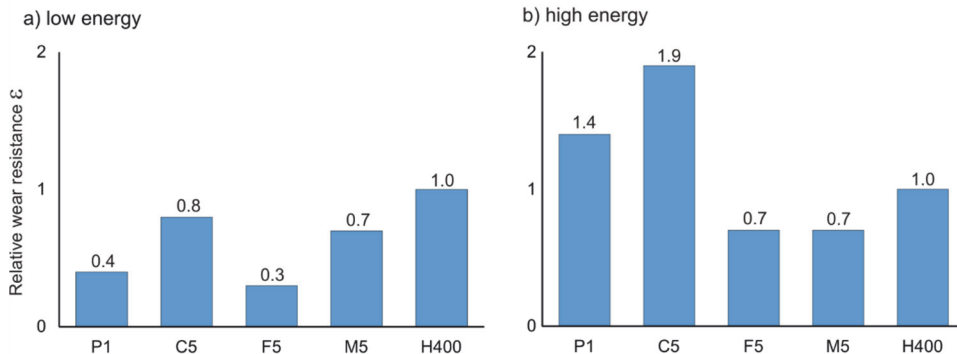


**Figure 7.** Relative wear resistance of hardfacings at low-energy and high-energy AIEW (abrasive – granite, reference material – steel Hardox 400).

### 3.2 Mechanisms of AIEW

As the unreinforced hardfacing (P1) and the hardfacing reinforced with the coarse hardmetal (C5) exhibited the lowest wear among the studied hardfacings, they were taken as the object for our analysis of wear mechanisms. Both under low-energy and under high-energy AIEW conditions, the general wear process took place in two stages: firstly, destruction of the matrix and secondly, loss of loose WC-Co particles (Figures 8 and 9). Because the wear of the matrix was much more intensive than the wear of the reinforcement, higher magnification pictures of the first are demonstrated separately.

Under the low-energy AIEW conditions, the wear of both the FeCrSiB matrix (both in unreinforced and composite hardfacing) and the WC-Co reinforcement occurred by the low-cycle fatigue mechanism (Figure 8) [2]. In the first case, it included the stages of work hardening by the impact particles, resulting in the formation and development of lateral cracks [17] and, finally, spalling of flat fragments. It is interesting to note that the wear of the FeCrSiB matrix was more extensive in the composite hardfacing, and in the proximity of the reinforcing particles (Figure 8 b,c), it became most remarkable. The most probable cause for that is the thermally induced tensile stresses at the matrix-reinforcement interface [8], which favor the removal of the material [18]. At reinforcement, the wear started with the extrusion of the binder and continued by the subsequent chipping of the exposed carbide particles, as described in [4] (not shown in Figures 8, 9).

Under high-energy AIEW conditions, the wear mechanism of the reinforcement was identical to that under the low-energy AIEW conditions. However, the wear mechanism of FeCrSiB alloy underwent some changes (Figure 9). In addition to lateral cracks, median ones [17] may be seen (Figure 9). Thus, the wear mechanism of the FeCrSiB matrix may be described as a combination of low-cycle surface fatigue and direct fracture. As at the low-energy AIEW, the wear of the FeCrSiB matrix was higher at the composite hardfacing (Figures 8 b,c) for the same reason.

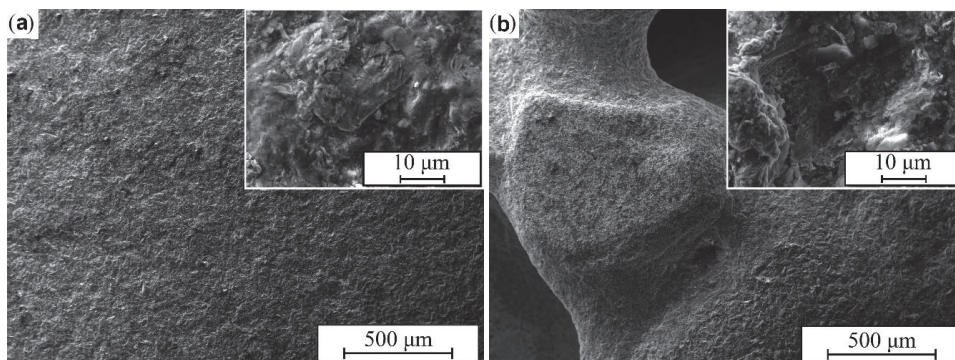


**Figure 8.** Worn surfaces of the hardfacings under low-energy AIEW conditions ( $v = 80$  m/s): a – P1 (unreinforced), b – C5 (50 vol.% angular WC-Co reinforcement).

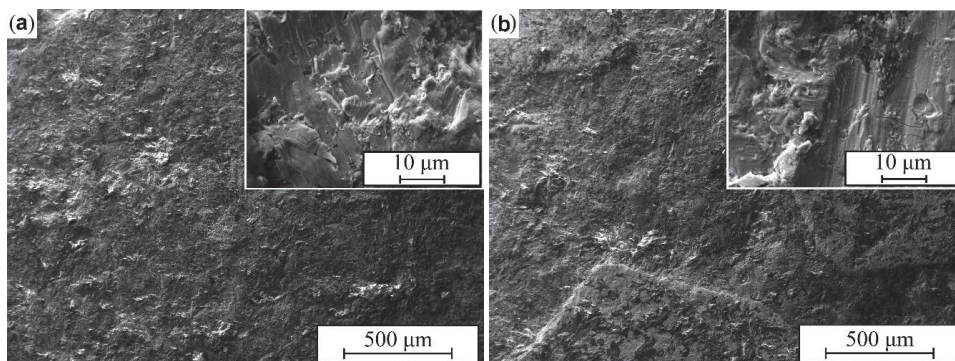


**Figure 9.** Worn surfaces of the hardfacings under high-energy AIEW conditions ( $v = 40$  m/s): a – P1 (unreinforced), b – C5 (50 vol.% angular WC-Co reinforcement).

#### 4. Conclusions

1. Wear rate of AIEW of studied composite WC-Co containing hardfacings depends first on the wear parameters (type and hardness of abrasive, velocity and kinetic energy of particles). Relative volumetric wear resistance of better hardfacings (coarse angular reinforcement, C5) exceeds that of the reference steel Hardox 400 about 3 times at low-energy AIEW with the abrasive – granite sand. At high velocity, AIEW relative wear resistance is low.
2. The dominating wear mechanism of both matrix and reinforcement at the low-energy AIEW was surface fatigue, at the high-energy AIEW – a combination of surface fatigue and direct fracture at the matrix and surface fatigue at the reinforcement.
3. The criteria for coating selection by composition and hardness-toughness ratio for hardmetals containing hardfacings are the following:
  - a) at oblique impact AIEW – maximal hardphase content and higher hardness of the composite;
  - b) at normal impact AIEW – lower hardphase content and hardness of metal matrix and higher toughness of hardphase.

#### 5. References

- [1] Hutchings I M, Winter R E and Field J E 1976 *Proc. Roy. Soc. London A* **348** 379–92
- [2] Kleis I and Kulu P 2008 *Solid Particle Erosion. Occurrence, Prediction and Control* (London:

Springer Verlag) p 206

- [3] Kulu P 2002 *Adv. Eng. Mater.* **4** 392–7
- [4] Hussainova I, Kübarsepp J and Pirso J 2001 *Wear* **250** 818–25
- [5] Rojacz H, Varga M, Kerber H and Winkelmann H 2014 *J. Mater. Process. Tech.* **214** 1285–92
- [6] Kulu P, Tarbe R, Saarna M, Surženkov A, Peetsalu P and Talviste K 2015 *Int. J. Microstructure and Materials Properties* **10** 101–13
- [7] Bendikiene R, Ciuplys A and Kavaliauskiene L 2016 *Proc. Est. Acad. Sci.* **65** 117–22
- [8] Simson T, Kulu P, Surženkov A, Tarbe R, Viljus M, Tarraste M and Goljandin D 2016 *Proc. Est. Acad. Sci.* **65** 90–6
- [9] *Reparation and wear protection technologies*. Product Catalogue, Castolin Eutectic, 2010
- [10] Surzhenkov A, Vallikivi A, Mikli V, Viljus M, Vilgo T and Kulu P 2012 *Proc. 2nd Int. Conf. Manufacturing Engineering & Management 2012 (Prešov, Slovak Republic)* ed S Hloch et al. (Prešov: Udulibri) 34–7
- [11] Kulu P, Veinthal R and Kaerdi H 2007 *Int. J. Mater. Prod. Tech.* **28** 425–47
- [12] Veinthal R 2005 *Characterization and Modelling of Erosion Wear of Powder Composite Materials and Coatings* PhD Thesis (Tallinn: TUT Press) p 61
- [13] Kulu P, Surženkov A, Simson T and Sarjas H 2016 *Proc. European Conf. Heat Treatment 2016 & 3rd Int. Conf. Heat Treatment and Surface Engineering in Automotive Applications*, 11–13 May 2016, Prague, Czech Republic (Prague: Asociace pro tepelné zpracování kovů)
- [14] Andrews D R 1980 *The Erosion of Metals* PhD Thesis (London: Cambridge Press) p 156
- [15] Goljandin D and Kulu P 2015 *Disintegrators and Disintegrator Treatment of Materials* (Lambert Academic Publishing) p 162
- [16] Simson T, Kulu P, Surženkov A, Goljandin D, Tarbe R, Tarraste M and Viljus M 2017 *Key Eng. Mat.* **721** 351–5
- [17] Sheldon G L and Finnie I 1966 *Am. Soc. Mech. Eng. Trans. J. Eng. Ind.* **88** 393–9
- [18] Stewart D A, Shipway P H and McCartney D G 1998 *Surf. Coat. Tech.* **105** 13–24

### Acknowledgements

This work was supported by institutional research funding IUT19-29 “Multi-scale structured ceramic-based composites for extreme applications” of the Estonian Ministry of Education and Research and by the project AR12132 “Development of advanced coatings and polymer-ceramic composites for road construction machinery wear parts (WearHard)” of Archimedes Foundation. This work was also supported by the Dora Plus activity 1.1 (Archimedes Foundation).

## **Paper II**

Casesnoves, F., Surzhenkov, A. A mathematical model for abrasive erosion wear in composite Fe-based matrix with WC-Co reinforcement. *Materials and Contact Characterization*, 2017, 116, pp. 99-111. WIT PRESS. Section 2 Computer Methods Computer and Simulation.



# A MATHEMATICAL MODEL FOR ABRASIVE EROSION WEAR IN COMPOSITE FE-BASED MATRIX WITH WC-CO REINFORCEMENT

FRANCISCO CASESNOVES<sup>1</sup> & ANDREI SURZHENKOV<sup>2</sup>

<sup>1</sup>IEEE (Electrical and Electronics Engineering Institute), Mechanical Engineering,  
Tallinn University of Technology, Estonia

<sup>2</sup>Mechanical Engineering, Tallinn University of Technology, Estonia

## ABSTRACT

This paper presents a new functional-computational model for metal-matrix composites (MMC), specifically for coatings with coarse spherical WC-Co reinforcement. We have developed, simulated and optimized the model based on previous classical approximations. The experimental data to validate this model are the laboratory tribotest-abrasion measurements and complementary appropriate numerical reports published internationally. Programming software was designed both with nonlinear optimization and curve-fitting subroutines. Results comprise the model construction from theory to computational validation on the laboratory statistical and numerical database. Additional simulations/optimization related to other models are also shown together with conceptual details of the next generation of functional models.

*Keywords: mathematical modelling, nonlinear optimization, inverse methods, reinforced metal-matrix coatings, optimization software.*

## 1 INTRODUCTION

In previous publications, a series of mathematical models for tribology, erosion, corrosion, and tribocorrosion models are presented and optimized by Casesnoves et al. [1], [4], Casesnoves and Surzhenkov [2] and Suzenkov et al. [3]. In general, and to date, general simulation methods of modelling have been improved and tested.

When the second stage is concluded/verified, it is possible to proceed to tribotesting and begin to implement completely new/specific laboratory data and new findings when performing the experimental. The theoretical final phase is to optimize the mathematical framework and to prepare for the period of validation. In this key point, the inverse and forward methods are strictly applied, i.e., from empirical data towards the model and from theoretical simulations of the model to comparisons with lab database [2], [4].

The second generation of functional models in tribology comprises a series of new mathematical modelling methods based on derivable and integrable functions [2], [3]. In other words, the surfactal variety of particular reinforced metals makes it convenient to adapt the modelling on the proper stochastic distribution of compounds along the surface that is exposed to abrasive wear, plastic deformation, cutting wear, erosion of other types, corrosion or tribocorrosion. We consider here the new generation of models that can be subject to a wide number of mathematical operations as a promising field in the investigation of tribological and biotribological algorithms.

This article uses a recently published integral-differential model for matrix of Fe-based alloy with WC-Co reinforcement, and develops a series of inverse optimization simulations based on laboratory experimental data.

## 2 MATHEMATICAL METHOD(S) IN MODEL DEVELOPMENT

This section is focused on the fundamental steps to develop a mathematical model, starting from experimental and heading towards the theory. A new functional model is presented both



within the theory and experimental framework. The engineering-rationale of the method is established on the following materials mechanics statements:

An approximation-modelling technique for the tribological, tribocorrosion, and biotribological precision measurements should involve the continuous functions of surfactal volume distribution of each well-defined constituent, i.e., the part exposed to abrasive erosion/corrosion and tribological consequences. This implies a specific range of constants and parameters for a particular mixed-material.

The validation/optimization methods for these models are related to the mathematical distribution of every element/part. Probability distributions, stochastic methods, together with several types of weight factors distribution, and specialized optimization methods are important for precision/refinements of modelling.

The wear of a material under the abrasive impact erosion conditions generally depends on its hardness and fracture roughness, and specifically on abrasive particle kinetic energy, momentum, mass/density, shape and size. All these factors are crucial to optimize the wear under the mixed impact angle (e.g., from 20 to 90 degrees) with defined kinetic energy. Metal-matrix alloys with double-cemented structure are manufactured according to these conditions.

The matrix abrasive wear mechanism studied at Tallinn University of Technology has resulted in the following outcome: abrasive wear in this type of materials-matrix may be modelled through micro-cutting wear and surface fatigue wear due to the horizontal/vertical components of the impact velocity. Micro-cutting phenomenon happens in practice when impact angles are not 90 degrees, that is, the specific applied formulation for micro-cutting rate calculation does not result in zero rate since it depends of the impact angle cosine.

In metallurgy industry, metal-matrix alloys with the double-cemented structure are manufactured by a variety of methods, including thermal spraying, cladding, and powder metallurgy techniques. The powder metallurgy method, according to this study, results to be more advantageous, as it allows to manufacture hardfacings with coarser reinforcement and significantly strong binding zone. As a practical consequence in terms of industrial production, this specific technique has shown a higher abrasive wear impact resistance.

In this study, the model construction is detailed for Fe-based self-fluxing alloy (FeCrBSi) with spherical WC-Co hard metal reinforcement extensively studied and experimented in Materials Laboratories of Tallinn University of Technology during decades. In the development of the model based on the conceptual mathematical, and analytic geometry problem present in this kind of coatings is the non-constant hardness spatial distribution in the composite material: generally, hardness of matrix, reinforcement and matrix-reinforcement interface may be distinguished. As hardness has a major influence on the wear properties, its non-homogeneous distribution would mean that the actual wear rates of the matrix, reinforcement and the matrix-reinforcement interface would be different. Therefore, the material modelling is more complicated. What is meant here is a method to construct a model that can be generalized with different equations/algorithms.

In Fig. 1, the method to calculate the average stochastic distance between the half point of the matrix and interface around the reinforcement is shown and graphically explained. This method is justified according to the rationale of Fig. 2, i.e., a sharp defined border/geometry between the principal components of the hardface of the composite implies that the discontinuity is at least sufficiently defined to separate the erosion rate that occurs in both parts. Fig. 1 shows the image of matrix, hardface and transition zone in Fe-based Technology Lab]. Direct Monte-Carlo imaging-random-calculations of average distance-width of matrix related to spherical reinforcement parts are detailed in the method (inset, black arrows). Monte-Carlo method is applied taking computational-imaging random points

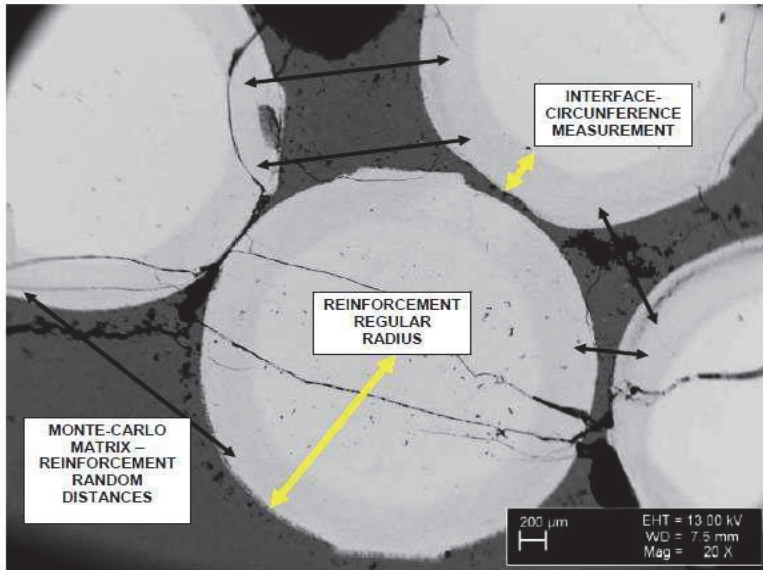


Figure 1: Image of matrix, reinforcement, and transition-binding zone in Fe-based hardfacings with coarse WC-Co reinforcement.

at interface, and afterwards calculating the average distances between each pair of points. The radius of the spherical reinforcement could be approximated as constant (inset, yellow arrow). The interface-binding zone external-circumference is also considered approximately constant (inset, yellow arrow). Distances proportion in image is provided by the Omnimet software accurately. Images of the composite were obtained with scanning electron microscope (SEM) EVO MA-15 at Tallinn University of Technology Lab [Optical microscope Axiovert 25 (Carl Zeiss) and Buehler® Omnimet® software].

Weibull distribution is considered more applicable, in our criterion, for those hardfacing that have sufficiently mixed materials whose reinforcement grains are small enough. In those hardfacing, there are a minimum of two compounds, and the total composition can be approximated to a mixture with different proportions of its constituents, spatially distributed along the surface. For this type of structure-composition, eqns 1 and 2 are applicable, see Fig. 2. This concept is also illustrated and explained graphically in Fig. 2. Weibull distribution, Kleis and Kulu [5], has been extensively used at Tallinn University of Technology, Materials Engineering Division, in a large series of contributions and is expressed as follows:

$$F(H) = 1 - e^{-\left[\left(\frac{H}{H_0}\right)^m\right]}, \quad (1)$$

$$F(H) = 1 - e^{-\left[\left(\frac{H - H_{\text{minimal}}}{H_0}\right)^m\right]}, \quad (2)$$

where  $H$  is hardness, and  $m$  is the Weibull shape factor, while  $H_0$  is the mean hardness value. The constant  $m$  varies according to the type of statistical distribution, e.g., exponential, normal, log-normal, etc. However, in metals the second approximation is also used. In that formula, the minimum hardness value,  $H_{\text{minimal}}$ , is used. These are basically the mathematical

concepts employed to obtain more advanced equations/models for combining the different types of erosion, such as brittle, fatigue, cutting that could occur.

The more Monte-Carlo calculations, are performed to obtain average distances, the higher the number of samples of hardface stochastic measurements, the better accuracy/refinement is reached for erosion/tribology modelling. In other words, instead of using previous statistical distributions, each different hardface well-defined in shape and geometry has a matrix and reinforcement hardness spatial distributions that can be transformed in continuous functions integrable and derivable. This is the core of the model of this research. Table 1 presents, details of experimental samples and composition, i.e., the initial lab measurements group to develop/justify the theory of the model and subsequent additional modelling simulations/optimizations.

The theoretical concepts/fundamentals to develop this Integral-Differential model are shown in Fig. 2. The most complicated models are those in hybrid-definition zone, i.e., they have features of geometrical/volume/shape nearly-clear characteristics and at the same time, composition-weight is distributed almost regularly along the hardface. Proportional methods, Luenberger [8], based on the combined equations derived from eqns 1 and 2 have also been developed. In Table 2, examples of experimental data of matrix hardness carried out at Tallinn University of Technology Mechanics Lab. These 43 values were implemented to construct the mathematical model for the matrix.

Fig. 2 shows the flow-chart-captions of the modelling ideas/concepts for the second generation of tribology mathematical modelling. When the volume/geometrical definition is sharp, the functional models are applicable. At the opposite level, is the rather proportionally-mixed material framework would be better using proportional rates of compounds. At the middle, in-between of those well-defined types, are the hybrid hardfaces whose separation among components could be approximated to both previous kinds and their model-construction involves more mathematical difficulties [7].

It is postulated that hardness is not constant as a result of the polynomial fitting of data in Table 2; the resulting polynomial equation development is described in Section 2 of results. Therefore, for the model in the matrix, it is suggested that hardness, has a nonlinear spatial distribution according to the distance from WC-Co reinforcement spherical spots. The model used in this section shows that the functional method is a simple nonlinear Hutchings model [14] whose formulation results are modified, provided hardness is not constant. In this way, a continuous and differentiable function providing the determination of a polynomial

Table 1: Composition of experimental.

| Type of component | Composition and proportion of experimental |  |  |
|-------------------|--|--|--|
|                   | Type of material                           | Chemical composition [wt.%]  | Comments   |
| Matrix            | Fe-based self-fluxing alloy (FeCrBSi)      | 13.72 Cr, 2.67 Si, 0.32 Mn, 2.07 C, 0.02 S, 3.40 B, 6.04 Ni, bal. Fe | Matrix distribution is reduced by high-size of spherical reinforcement |
| Reinforcement     | Spherical WC-Co hard metal                 | 85 WC, 15 Co   | Size of reinforcement about 1mm (rather high)                          |



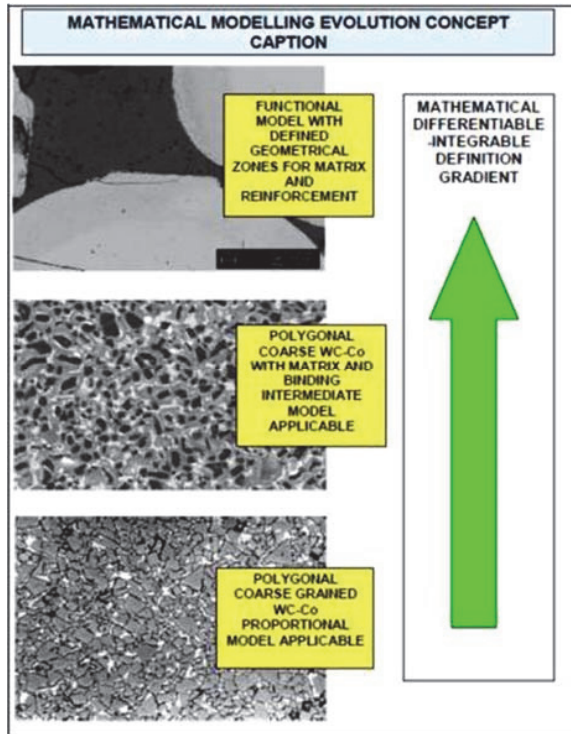


Figure 2: Graphical Imaging-Flow-Chart of concepts in the Nano-Micro-Macro tribology modelling.

Table 2: Numerical experimental data.

| Number of measurement | Examples of experimental data for model development [TUT laboratory, Estonia] |  |
|-----------------------|---|--|
|                       | Hardness [HV]   | Experimental Observations  |
| 4                     | 861   | Steady gradient of the polynomial fitted equation from half part of database sample, instead the lab measurements do not show a regular distribution at initial parts of the measurements group. Polynomial equation detailed in eqn 5 and Fig. 3. |
| 12                    | 1027  |  |
| 30                    | 1161  |  |
| 40                    | 1219  |  |

equation  $H(s)$  can be obtained through numerical analysis. The equation reads as follows:

$$E = \frac{K\rho[V \sin \alpha]^{2.5}}{H(s)}; \tag{3}$$

where  $E$  is erosion rate,  $\rho$  is the density of the material being eroded,  $V$  is the initial particle velocity and  $H$  is the target surface hardness.  $K$  represents the fraction of the material removed from the indentation as wear debris and is also known as the wear coefficient.  $\alpha$

is the impact angle of particles. As a first approximation, let us assume that density is constant, and K value is well-known. Since the hardness along the surface covered by the matrix is a function determined previously, it is practical to take derivatives of wear in relation to the distance. Therefore:

$$\frac{dw}{ds} = \frac{dw}{dH} \times \frac{dH}{ds} = (K\rho[V \sin \alpha]^{2.5}) \times \left(\frac{-1}{H^2(s)}\right) \times \left(\frac{dH(s)}{ds}\right);$$

integrating along all matrix average length,

$$\int_{w_0}^w dw = \int_{s_0}^s (k\rho[V \sin \alpha]^{2.5}) \times \left(\frac{-1}{H^2(s)}\right) \times \left(\frac{dH(s)}{ds}\right) ds; \tag{4}$$

which is the total wear for the whole matrix length, and a part of the total wear of the composite metal. This type of numerical-differential modelling is applicable to composite Fe-based hardfacings with coarse WC-Co reinforcement, and extrapolated also prospectively for other types, e.g., in titanium-varieties histocompatible coatings, usually Titanium-Boride composites, for hip or knee implants. The shape-conditions are explained in the previous figures of modelling design, where the geometrical differentiation between the matrix and the reinforcement is a necessary prerequisite.

The construction of the model follows straightforward from this equation since the hardness spatial distribution at matrix is a continuous and differentiable function, instead of a series of discrete values. Given the hardness function H (s), at any other particular model, according to Fig. 2 hypotheses, the insertion of the function into the model of wear or other parameters subject to constraints, constitutes a new method for the determination of erosion/tribological-parameters rate.

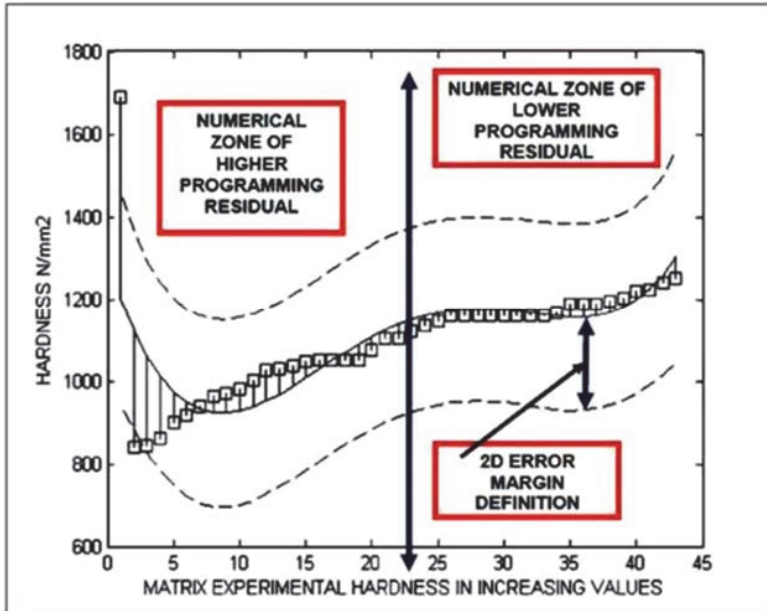


Figure 3: Computational-numerical determination of polynomial hardness distribution from the center towards the binding zone.

Weibull distribution was not initially applied for this type of modelling since the aim was to determine the weight factors in the hardface distribution to obtain particular functions for every kind of material, according to explanations in Fig. 2. In the subsequent, the computational optimization/simulations of this model type are developed with further mathematical framework.

### 3 COMPUTATIONAL RESULTS AND 2D-3D OPTIMIZATION/SIMULATIONS

In the mathematical computational results, first, it is suggested that hardness is not constant as a result of the polynomial fitting of data in Table 2, and the equation related to the distance is as follows:

$$H(s) = 10^3 \times [(-0.0003)s^3 + (0.0094)s^2 + (-0.1050)s + 12984]$$

$$\text{Residual of numerical fitting} = 657.6564 \quad (5)$$

This polynomial is the mathematical definition of the variation of matrix hardness related to distances, from the lowest hardness value corresponding to the most average-distant point from any reinforcement, to the closest average-distant point to the nearest reinforcement. The residual is the mathematical sum of the differences among the fitted points of the polynomial and the experimental points obtained with lab measurements. When a residual is low, statistically and numerically the result is considered acceptable, as it is this case, see Fig. 3. As a numerical result of programming, the data from Table 2 are done in convenient subroutines for curve-optimization. In Fig. 3, the graphics of this polynomial fitting is shown with detailed explanations. A polynomial approximation was chosen for initial simplicity, and it is pointed out that hardness is in HV units and the x-axis has a direct number of measurements in increasing order. If the Monte-Carlo [7] optimal distance is implemented, the shape of the curve would be different and another equation fitting would be the optimal numerical selection. Fig. 3 shows the numerical fitting of the 4-degree-polynomial with error plotting intervals of matrix experimental hardness in intervals of average Monte-Carlo distance from the center of the matrix to the next hardface spherical spot. This optimal distance is calculated with random measurements over the images instead of the classical Weibull statistical distribution, as shown in the previous images; the hardface polynomial fitting of the reinforcement hardness is better with a 3-degree polynomial equation. It is shown that the approximation is acceptable, with the exception of the beginning of the curve, i.e., these extreme dispersed values are usually discarded for model construction. Universal hardness (HU) and modulus of elasticity (E) were simultaneously determined according to the standard EN/ISO 14577-02 using the universal hardness tester 2.5/TS (Zwick). The applied load and the indentation depth were respectively 50 N and 100  $\mu\text{m}$ .

First, the Hutchings model was originally designed for plastic deformation. There are a number of formulas related to this model, from the simplest to the most complicated. This equation was selected for the sake of simplicity and clear understanding of the optimization method as follows:

$$W = \frac{K\rho U^2}{2H}, \quad (6)$$

where  $W$  is erosion rate,  $\rho$  is the density of the material being eroded,  $U$  is the initial particle velocity and  $H$  is the target surface hardness.  $K$  represents the fraction of the material removed from the indentation as wear debris and is also known as the wear coefficient. First, the value of  $K$  is optimized, which can be interpreted as a measure of the efficiency of the material removal process. In other words, the first step is to determine the optimal value of  $K$  for a random range around an interval of experimental measurements of SO3 material based on the lab tribotests of Tallinn University of Technology. That is direct application of

the Inverse Methods Theory in engineering. The second step is to simulate the model for a range of hardness and impact velocities in an interval around the experimental velocities of abrasive impact particles. These data are shown in Table 2. The objective function is a multi-objective least squares with  $L_2$  norm. The experimental hardness was set for optimization (43 measurements), and the K wear coefficient is the variable to be determined. According to eqn 4, the model of eqn 6 would be developed as follows:

$$\begin{aligned} \frac{dw}{ds} &= \frac{dw}{dH} \times \frac{dH}{ds} = (K\rho V^2) \times \left(\frac{-1}{2H^2(s)}\right) \times \left(\frac{dH(s)}{ds}\right) \\ &\text{integrating along all matrix average length} \\ \int_{w_0}^w dw &= \int_{s_0}^s (K\rho V^2) \times \left(\frac{-1}{2H^2(s)}\right) \times \left(\frac{dH(s)}{ds}\right) ds; \\ \int_{w_0}^w dw &= \int_{s_0}^s (K\rho V^2) \times \left(\frac{-p_1(s)}{p_2(s)}\right) ds; \\ &\text{with } p_{1,2}(s) \text{ as integrand polynomials;} \end{aligned} \tag{7}$$

Following the rationale, assuming that velocity is not constant, as it happens in practice, for instance, in the pipes with the stream of abrasive particles whose positive/negative accelerations depend on several streams [10]–[13]. Therefore, subject to these conditions, the integral-differential model becomes as follows:

$$\begin{aligned} dw &= \frac{\partial w}{\partial H} \partial H + \frac{\partial w}{\partial v} dv = (K\rho V^2) \times \left(\frac{-1}{2H^2(s)}\right) \times \frac{dH}{ds} \times ds + \left(\frac{K\rho}{2H}\right) \times (2v) dv = \\ &\text{integrating along all matrix Monte-Carlo average length,} \\ \int_{w_0}^w dw &= \int_{s_0}^s (k\rho V^2) \times \left(\frac{-1}{2H^2(s)}\right) \times \left(\frac{dH(s)}{ds}\right) ds; + \int_{v_0}^v \left(\frac{K\rho}{H}\right) \times (v) \times dv \end{aligned} \tag{8}$$

The matrix data from the lab measurements of matrix abrasive erosion are detailed in Table 2. Table 3 shows the numerical values of hardness from lab experimental measurements. Composition of alloy-reinforced experimental samples is 70 FeCrBSi, 30 WC-Co whose data was implemented for optimization of K wear coefficient in eqn 6. Particle size and energy is explained also [Tallinn University of Technology Laboratory].

Table 3: Complementary parameters for optimization.

| Number of measurement<br>(total measurements of matrix= 43) | Experimental data for model simulation/optimization [Tallinn University of Technology laboratory, Estonia] |  |
|---|--|--|
|   | Hardness [HV]  | Abrasive Particles Energy – AIEW<br>(abrasive impact erosion wear) |
| 4   | 861  | Particle size 0.1–0.3 mm   |
| 12  | 1027   | Density 1.4 mg/mm <sup>3</sup>                                     |
| 30  | 1161   | Low Energy Range   |
| 40  | 1219   |  |
| 4   | 861  | V=80m/s, experimental erosion ≈ 5mm <sup>3</sup> /Kg               |
| Experimental lab data for optimization                      | V=40m/s, experimental erosion ≈ 1 mm <sup>3</sup> /Kg  |  |

The first simulation of nonlinear least squares algorithm without constraints was designed with a classical formulation as follows:

$$\begin{aligned} & \text{minimize,} \\ & F(\vec{x}) = \sum_{i=1}^N \|H_i - f(\vec{x})\|^2; \text{ with, } f(\vec{x}) = \frac{K\rho v^2}{2W}, \end{aligned} \quad (9)$$

where  $H_i$  values are obtained through experimental, Table 2, and wear,  $w$ , was also experimentally determined.  $\rho$  is density,  $v$  velocity and  $K$  wear constant whose optimal value is determined by the programming software. This algorithm is developed for the first velocity, graphical determination of this objective function is shown in Fig. 3 and running program results are included in Table 3. The representation of the programming of eqn 9 is presented in Fig. 4. The objective function (OF) nonlinear optimization results for Table 1,  $N=43$ , and equation model of eqn 6. The impact velocity is 40m/s. Results are acceptable with a Global Minimum (GM) sharply determined and running time is lower than a second. GM is caught up by the cursor and residual is about 500, figure which can be considered acceptable. Constraints were not set in this program.

Table 4 shows detailed numerical data obtained that was obtained from nonlinear optimization of eqns 9 and 10. Experimental values, impact velocity, material density, and all parameters implemented are from laboratory measurements results. Additionally, in Fig. 5, the 3D surfactal simulation and graphical optimization results for Table 3 and model of eqn 6. The impact velocity is 40m/s. Results are acceptable with a Global Minimum and Global Maximum sharply determined that verifies the optimization software results. Matrices of imaging are 50x50. Range of simulation is around GM of algorithm of eqn 9, and hardness interval is [600 1300], which covers the experimental values of Table 3.

In Fig. 5, the results of 3D surfactal simulation and graphical optimization for Table 3 and model of eqn 6 are shown. The impact velocity is 40 m/s. Results are acceptable with a Global Minimum and Global Maximum sharply determined that verifies the optimization software results. Matrices of imaging are 50x50. Range of simulation is around Global Minimum of algorithm of eqn 9, and hardness interval is [600 1300], which covers the experimental values of Table 3.

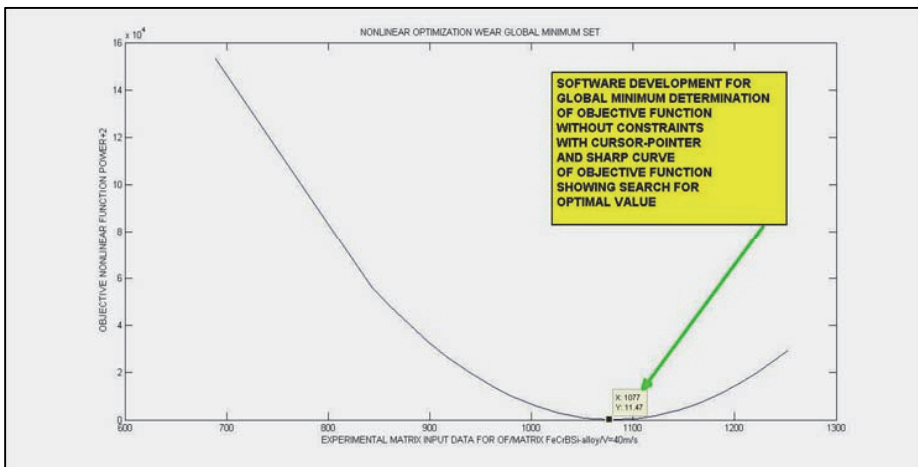


Figure 4: 2D graphical optimization result of eqn 9 with Global Minimum pointed.

Table 4: Constrained and unconstrained numerical optimization.

| <b>Simulation group 1</b> |   |   |                                       |
|---------------------------|---|---|---------------------------------------|
| <b>Search point</b>       | <b>Optimal k value (inverse method) v particles = 40m/s</b>                                     | <b>Residual of objective function (OF)</b>                      |                                       |
| X=1                       | 0.9646  | 838.8507  |                                       |
| X=5                       | 0.9646  | 838.8507  |                                       |
| X=20                      | 0.9646  | 838.8507  |                                       |
| Comments                  | Acceptable result for optimization low residual of OF global minimum exact for any search point |   |                                       |
| <b>Simulation group 2</b> |   |   |                                       |
| <b>Search point</b>       | <b>Optimal k value (inverse method) v particles = 80m/s</b>                                     | <b>Constraints, Intervals, LB: Lower bound, UB: Upper bound</b> | <b>Residual of objective function</b> |
| [20,15]                   | [0.7424, 3.0787]  | LB=[1/2, 0.2]<br>UB=[3/2, 4]                                    | 838.8507                              |
| [10,15]                   | [0.6334, 2.6265]  | LB=[1/2, 0.2]<br>UB=[1.5, 3]                                    | 838.8507                              |
| [1,15]                    | [0.7214, 2.9915]  | LB=[1/2, 0.2]<br>UB=[1.5, 3]                                    | 838.8507                              |
| Comments                  | Similar values but not equal, good residual   |   |                                       |

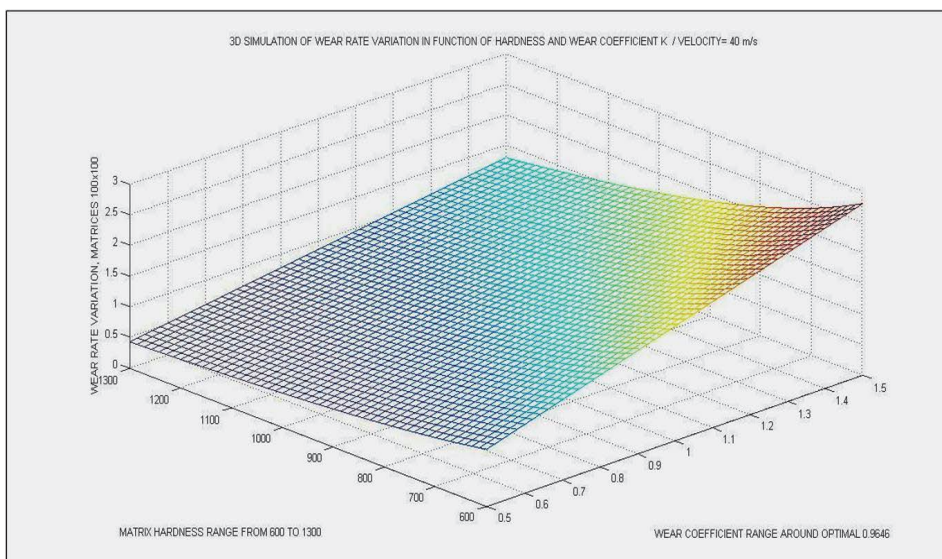


Figure 5: Graphical Optimization surfactal-programming implementation for eqn 9 (Casesnoves and Suzenkov [2]).

The second group of simulations with constraints in Table 4 is intended for using the same hardness data but with an extended wear interval for the wear rate whose central point is the experimental value obtained in tribotesting. The determination of  $K$  in the constraints is also in an interval centered in the value of  $K$  determined without constraints. What is meant here is the multiple options available for nonlinear optimization of a model. The mathematical algorithm was designed for the model with constraints, but in terms of simple formulation. The algorithm of the Objective Function with constraints reads as follows:

$$\text{minimize,} \\ F(\vec{x}) = \sum_{i=1}^{i=N} \|H_i - f(\vec{x})\|^2; \text{ subject to, } a_1 \leq K \leq b_1; a_2 \leq W \leq b_2; \text{ with, } f(\vec{x}) = \frac{K\rho v^2}{2W}, \quad (10)$$

where  $a_i$  and  $b_i$  are the lower and upper boundaries of the constraints. The result of programming of this algorithm with appropriate subroutines is not too complicated, although with the number of parameters in the multi-objective nonlinear optimization increasing, the search for global or even local minima becomes more difficult.

To summarize the graphical presentation, Fig. 6 shows the nonlinear optimization results of objective function (OF) for Table 3 and constrained optimization algorithm of eqn 10. The impact velocity is 80 m/s. Results are acceptable with a Global Minimum sharply determined and running time is lower than a second. However, the search with upper and lower constraints and 2 parameters does not always determine very close values.

According to the numerical values, graphical simulations and optimization of the equations, the mathematical development of the new model has been presented properly. When the number of variables optimization in the nonlinear least squares objective function increases, the different values for the minima vary, which occurs in particular when constraints are set.

#### 4 CONCLUSIONS

This article concentrates on the development of an integral-differential model of the matrix from selected alloy materials. The technical method used was based on experimental testing, with a new concept in the interpretation of the basic parameters that constitute an erosion model. The steps towards the modelling definition were justified with strict mathematical background, i.e., after the presented contribution, with Integral-Differential model and Graphical Nonlinear Optimization method. The model was built for the composite material, comprised of FeCrSiB alloy matrix and spherical WC-Co reinforcement (matrix/reinforcement ratio 70 % vol./30 % vol., respectively), assuming that hardness spatial distribution in the matrix may be numerically calculated by a 4-degree-polynomial. The computer simulation showed a proper compatibility of the proposed model with the results of the laboratory tests. This method is a mathematical approach. The details of the contributions to macroscopic yielding over the eroding surface which are directly related to hardness are not considered.

The study was complemented with computational software results for nonlinear optimization and simulations of the equations that are presented; numerical data were clarified for sharp learning in tables and images. The conclusions are related to new improvements in the second-subsequent generation of erosion-corrosion modelling methods, which are formed by continuous functions linked to the variation of metal-components in the surface/hardface of the materials that are under current industrial manufacturing. Our aim was intended to present the rationale of the Integral-Differential model and discuss its prospective/future applications in metallurgy material industrial processes.



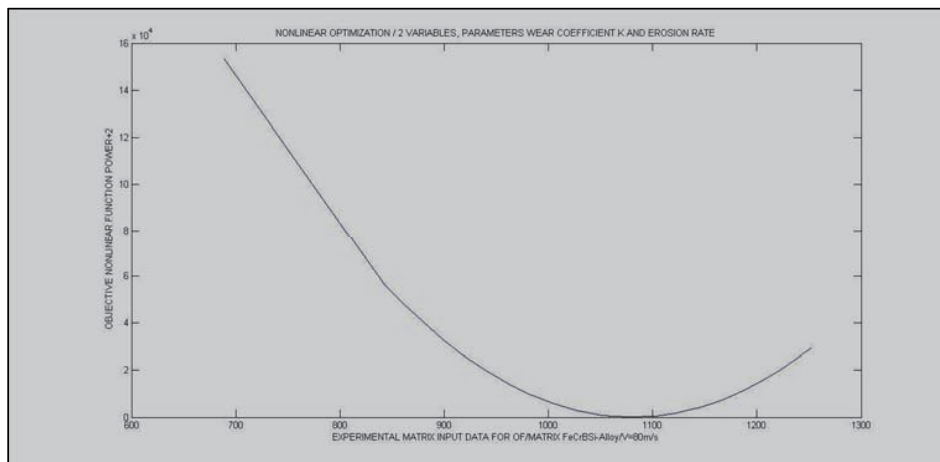


Figure 6: Constrained 2D graphical optimization results for eqn 10, with 80m/s of impact speed.

#### ACKNOWLEDGEMENTS AND SCIENTIFIC ETHICS STANDARDS

Tallinn University of Technology is gratefully acknowledged for all the facilities for research. Tallinn University of Technology Lab, measurements done by Taavi Simson, experimental supervised by Prof. Priit Kulu and Assistant Professor Andrei Surzhenkov. This study was conducted and their contents are realized according to the European Union Technology and Science Ethics. Reference, 'European Textbook on Ethics in Research'. European Commission, Directorate-General for Research. Unit L3. Governance and Ethics. European Research Area. Science and Society. EUR 24452 EN [23]. This article contains also unique numerical data and special new improved images based on standard-tested laboratory measurements and mechanical-experimental tribotesting equipment/apparatus. Any use of data from a source is adequately recognized. Ideas from previous publications were emphasized due to a clarification aim.

#### REFERENCES

- [1] Casesnoves F., Antonov, M. & Kulu, P., Mathematical Models for Erosion and Corrosion in Power Plants. A Review of Applicable Modelling Optimization Techniques. *57th International Scientific Conference on Power and Electrical Engineering of Riga Technical University (RTUCON)*, 2016.
- [2] Casesnoves, F. & Suzenkov, A., Mathematical Models in Biotribology with 2D-3D Erosion Integral-Differential Model and Computational-Optimization/Simulation Programming. *International Journal of Scientific Research in Computer Science, Engineering and Information Technology*, **2**(3), 2017. ISSN: 2456-3307.
- [3] Surzhenkov, A., Viljus, M., Simson, T., Tarbe, R., Saarna, M. & Casesnoves, F., Wear resistance and mechanisms of composite hardfacings at abrasive impact erosion wear. *IOP Conf. Series: Journal of Physics: Conf. Series 843*, 2017. 012060 doi: 10.1088/1742-6596/843/1/012060.
- [4] Casesnoves, F., Antonov, M. & Kulu, P., Mathematical Models for Erosion and Corrosion in Power Plants. *A Review of Applicable Modelling Optimization*



- Techniques. 2016// 57th International Scientific Conference on Power and Electrical Engineering of Riga Technical University (RTUCON), 2016.*
- [5] Kleis, I. & Kulu, P., *Solid Particle Erosion*, Springer, 2008.
  - [6] Casesnoves, F., A Monte-Carlo Optimization method in Numerical Reuleaux Method for the movement analysis of pseudo-rigid bodies. *10th SIAM Conference in Geometric Design and Computing joint to Approximation Theory Conference*, Texas, San Antonio, USA, 2007.
  - [7] Abramowitz, S., Handbook of Mathematical Functions, *Applied Mathematics Series*, **55**, 1972.
  - [8] Luenberger, G.D., *Linear and Nonlinear Programming*, 4th Edition, Springer, 2008.
  - [9] Casesnoves, F., Applied Inverse Methods for Optimal Geometrical-Mechanical Deformation of Lumbar Artificial Disks/Implants with Numerical Reuleaux Method. *2D Comparative Simulations and Formulation, Computer Science Applications*, **2(4)**, pp. 1–10.
  - [10] Balamanikandasuthan, K., Arun, K. & Palam, S.S., Design and fabrication of erosion protection shield for boiler tubes and its analysis. *International Journal of Mechanical and Materials Engineering*, **1(1)**, pp. 39–52, 2015.
  - [11] Hussainova, I., On micromechanical problems of erosive wear of particle reinforcement composites. *Proc. Estonian Acad. Sci. Eng.*, **11**, pp. 46–58, 2005.
  - [12] Kulu, P., Tarbe, R., Zikin, A., Sarjas, H. & Surženkov, A., Abrasive wear resistance of recycled hard metal reinforced thick coating. *Key Eng. Mat.*, **527**, pp. 185–190, 2013.
  - [13] Simson, T. et al., Optimization of reinforcement content of powder metallurgy hardfacings in abrasive wear conditions. *P. Est. Acad. Sci.*, **65**, pp. 90–96, 2016.
  - [14] Surzhenkov, A., Tarbe, R., Tarraste, M., Simson, T., Viljus, M. & Kulu, P., Optimization of hardmetal reinforcement content in Fe-based hardfacings for abrasive-impact wear conditions. *Proc. Eur. Conf. Heat Treat. 2016 and 3rd Int. Conf. Heat Treat. Surf. Eng. Automotive Applications, 11–13 May 2016*, Prague, Czech Republic.
  - [15] Chen, Q. & Li, D., Computer simulation of solid-particle erosion of composite materials. *Wear*, **255**, pp. 78–84, 2003.
  - [16] Antonov, M. & Renno, *Effect of oxidation on erosive wear behavior of boiler steels*.
  - [17] Hussainova, I., Kubarsepp, J. & Shcheglov, I., Investigation of impact of solid particles against hardmetal and cermet targets. *Tribology International*, **32**, pp. 337–344, 1999.
  - [18] Hussainova, I., Kubarsepp, J. & Pirso, J., *Mechanical properties and features of erosion of cermets*.
  - [19] Crocker, L., A review of current methods for modeling erosive wear. *NPL Report*, 2011.
  - [20] Casesnoves, F., Applied Inverse Methods for Deformable Solid Dynamics/Kinematics in Numerical Reuleaux Method (NRM). *International Journal of Numerical Methods and Applications*, **9(2)**, pp. 109–131, 2013.
  - [21] Woytowicz, P. & Richman, R., Modeling of damage from multiple impacts by spherical particles. *Wear*, pp. 120–133, 233–235, 999.
  - [22] Liao, H., Normand, B. & Coddet, C., Influence of coating microstructure on the abrasive wear resistance of WC/Co cermet coatings. *Surface and Coatings Technology*, **124**, pp. 235–242, 2000.
  - [23] European Textbook on Ethics in Research, European Commission, Directorate-General for Research, Unit L3. *Governance and Ethics. European Research Area. Science and Society*. EUR 24452 EN.





### **Paper III**

Kulu, P., Casesnoves, F., Simson, T., Tarbe, R. Prediction of abrasive impact wear of composite hardfacings. *Solid State Phenomena, Proceedings of 26<sup>th</sup> International Baltic Conference on Materials Engineering*. 2017, 267, pp. 201-206. (DOI:10.4028/www.scientific.net/SSP.267.201). 2017 Trans Tech Publications, Switzerland Online: 2017-10-10.



## Prediction of Abrasive Erosion Impact Wear of Composite Hardfacings

Priit Kulu<sup>a\*</sup>, Francisco Casesnoves<sup>b</sup>, Taavi Simson<sup>c</sup> and Riho Tarbe<sup>d</sup>

Department of Mechanical and Industrial Engineering, Tallinn University of Technology,  
Ehitajate tee 5, 19086 Tallinn, Estonia

<sup>a</sup>priit.kulu@ttu.ee, <sup>b</sup>frcase@ttu.ee, <sup>c</sup>taavi.simson@ttu.ee, <sup>d</sup>riho.tarbe@ttu.ee

**Keywords:** abrasive-erosive wear; impact wear; wear prediction; composite hardfacing.

**Abstract.** In this paper an attempt is made to consider for wear prediction apart from the plastic and brittle components also the fatigue component. As example, wear of the WC-Co hardmetal reinforced composite hardfacings under abrasive impact erosion wear conditions was calculated at low and high impact energy, accounting microcutting with surface fatigue for the wear of matrix and brittle fracture, surface fatigue and microcutting for the wear of reinforcement. Calculated wear rates are compared with data obtained from experimental tests. The results of the comparison show that the applied surface fatigue wear model is not applicable in the current case; the recommendations for the further improvement of the model are issued.

### Introduction

Abrasive impact erosion wear (AIEW) under extreme conditions (high hardness and velocity of erodent particles, cyclic impact loads, etc.) is a serious problem in industrial equipment, e.g. milling and mixing devices. Based on structural features and material properties, wear mechanisms may have various nature: in brittle solids, the direct fracture mechanism is dominating; in ductile ones, the microcutting and/or low-cycle surface fatigue mechanism prevails [1]. In AIEW that involves solid particle impact at the metal surface, plastic deformation occurs. The correspondent theories of erosion, which enable to find the wear rate at erosion, has been created and developed [2].

The concept of plastic deformation is also applicable to harder and more brittle materials, such as ceramics, but here the mechanism of plastic deformation is accompanied by the mechanism of brittle fracture. The question usually is, what mechanism is predominant [3]. Examples of wear comparison between the theory and experimental data may be found both for plastic [2] and brittle [3,4] materials, not looking to non-predictable parameters, such as fracture toughness of the erodent and the material to be tested, etc. A comparison of the experimental and calculation results demonstrated a satisfactory coincidence in the case of metallic materials [1,5].

Tribological materials and coatings are usually composite materials with a heterogeneous structure: hard particles in a relatively soft matrix. Most of the information available on their tribological properties has been derived from laboratory tests rather than from engineering applications. Attempts have been made to correlate erosion rates – experimental and calculated – with materials parameters [6]. In these models, hardness and fracture toughness emerge as the main material parameters that control erosion; a high hardness increases resistance to plastic deformation, while high fracture toughness increases resistance to fracture.

In papers [6,7] an attempt was made to predict the erosion wear of composite materials and to correlate erosion wear rates with experimental results and material parameters. The metal-matrix composite material containing about 20 vol.% WC reinforcement and thermal spray-fused NiCrSiB-alloy based composite coating containing about 20 vol.% WC-Co hardmetal reinforcement served as examples.

It is well known that there is a big difference between ductile and brittle materials, if the erosion wear rate is measured as a function of the impact angle [1]. Cermets and hardfacings have been considered sufficient to reduce scratching and micromachining damage of a surface, exposed to erodent particles at low impact angle, due to their hardness and stiffness. At the high impact angle, the exposed surface should be able to withstand repeated deformation, and material removal takes

place, after some critical deformation value is exceeded. Therefore the wear mechanism at high angles may be handled as a low-cycle fatigue [8,9].

The main aim of this study was to find out the possibility of prediction of wear of homogeneous and composite materials under combined wear mechanisms (microcutting, brittle fracture and surface fatigue).

### Used Mathematical Models

**Wear Modes and Studied Materials.** AIEW at low-energy (at oblique (30°) and normal (90°) impact angles) and high-energy (at normal impact angle) conditions was under the study (Fig. 1, Table 1). The choice of the impact angle and velocity values was dictated by the differences in the assumed wear mechanisms and intensities under small and high impact angles and velocities.

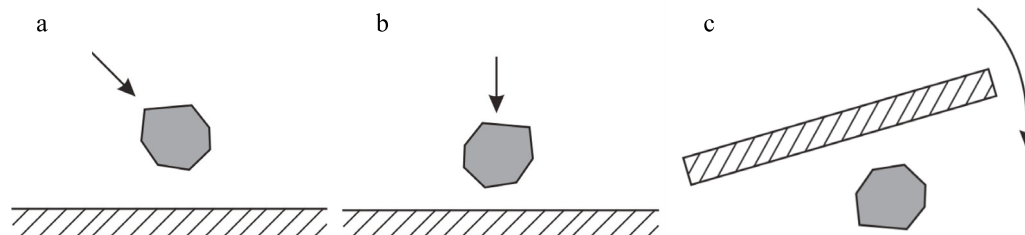


Fig. 1. AIEW conditions: a – oblique angle (30°) low-energy impact; b – normal angle (90°) low-energy impact; c – normal angle (90°) high-energy impact

Table 1. Abrasive impact erosion wear (AIEW) parameters

| AIEW type   | Abrasive type  | Abrasive hardness HV1 | Abrasive size [mm] | Impact angle [°] | Particle Velocity [m/s] | Particle Energy [J]  |
|-------------|----------------|-----------------------|--------------------|------------------|-------------------------|----------------------|
| Low-energy  | Granite sand   | 900–950               | 0.2 – 0.3          | 30; 90           | 40                      | $3.0 \times 10^{-5}$ |
|             |                |                       |                    |                  | 80                      | $1.2 \times 10^{-4}$ |
| High-energy | Granite gravel | 900–950               | 3.0 – 5.6          | 90               | 40                      | $1.4 \times 10^{-2}$ |
|             |                |                       |                    |                  | 80                      | $5.6 \times 10^{-1}$ |

As homogeneous materials, the wear resistant steel Hardox 400 and the unreinforced FeCrSiB hardfacing were used. As composite materials, iron-based self-fluxing alloy (FeCrSiB) matrix hardfacings with coarse (1.0 – 2.8 mm) WC-Co reinforcement were studied (Table 2).

Table 2. Studied materials

| Designation | Composition   | Hardness HV1       |
|-------------|---|--------------------|
| H400        | Steel Hardox 400 <sup>1)</sup>                                | 425 ± 25           |
| P1          | Unreinforced FeCrSiB <sup>2)</sup>                            | 870 ± 30           |
| C3          | 70 vol.% FeCrSiB <sup>2)</sup> + 30 vol.% WC-Co <sup>3)</sup> | Brought at Fig. 3. |
| S3          | 70 vol.% FeCrSiB <sup>2)</sup> + 30 vol.% WC-Co <sup>4)</sup> |                    |

<sup>1)</sup> wt.%, 0.25 C, 0.70 Si, 1.60 Mn, 1.00 Cr, 0.70 Ni, 0.80 Mo, 0.004 B, bal. Fe (SSAB Oxelösund)

<sup>2)</sup> wt.%, 2.07 C, 2.67 Si, 0.32 Mn, 13.72 Cr, 6.04 Ni, 3.40 B, 0.02 S, bal. Fe (Höganäs AB)

<sup>3)</sup> disintegrator milled angular hardmetal reinforcement (mixture of WC-3Co, WC-6Co, WC-10Co, WC-15Co), 1.0 – 2.5 mm (Tallinn University of Technology)

<sup>4)</sup> Ø2.8 mm spherical hardmetal reinforcement (WC-15Co; Wangsheng Cemented Carbide Ltd.)

For calculation of AIEW, models of plastic deformation, brittle fracture and surface fatigue were used.

**Wear at Plastic Deformation (Microcutting).** Eq. 1, proposed by Beckmann [2], was used for the calculation of the wear due to the horizontal component of impact velocity:

$$W_{cutting} = k_r \frac{3}{4\pi} \cdot \frac{\tau_0}{e_s} \cdot \left[ 6.81 \cdot \left( \frac{h_p}{R} \right)^{0.5} \cdot \frac{2\rho_2 v_0^2 \cos^2 \alpha}{3H_1} + 0.85 \cdot \left( \frac{h_p}{R} \right)^2 \right], \quad (1)$$

where  $k_r$  is the dimensionless coefficient (taken as  $k_r = 1.45$  [1]);  $\tau_0/e_s$  is the dimensionless ratio, taken from [1];  $h_p$  is the depth of an impact crater [mm];  $R$  is the average diameter of an erodent particle [mm];  $\rho_2$  is the density of the erodent [mg/mm<sup>3</sup>];  $v_0$  is the impact velocity [m/s];  $\alpha$  is the impact angle [°];  $H_1$  is the average static hardness of the target material [N/mm<sup>2</sup>].

**Wear at Surface Fatigue.** Wear due to the vertical component of the impact velocity by the surface fatigue mechanism was calculated by the Eq. (2), proposed by Hutchings [10]:

$$W_{fatigue} = 0.033 \cdot \frac{\alpha' \rho_1 \cdot \sqrt{\rho_2} \cdot v_0^3 \cdot \sin^3 \alpha}{\varepsilon_c^2 \cdot H_{dynamic}^3 / 2}, \quad (2)$$

where  $\frac{\alpha'}{\varepsilon_c}$  is a dimensionless ratio, taken from [10];  $\rho_1$  is the density of the target material [mg/mm<sup>3</sup>];  $H_{dynamic}$  is the dynamic hardness of the target material [N/mm<sup>2</sup>]; HV1 was used for calculations [11].

**Wear at Brittle Fracture.** Wear in the case of the brittle materials due to the vertical component of impact velocity was calculated by the Eq. 3, proposed by Gotzmann [4]:

$$W_{brittle} = 0.75 \cdot \sqrt{3} \frac{\rho_1}{\rho_2} \left( \frac{C_r}{R} \right)^2 \cdot \left( \frac{h_p}{R} \right)^{0.5}, \quad (3)$$

where  $C_r$  – the middle length of the radial crack.

**Calculation of Total Wear.** The wear of a ductile target material (steel and self-fluxing alloy) was calculated as

$$W_{ductile}^{total} = W_{cutting} + W_{fatigue}. \quad (4)$$

The total wear of a brittle target material (hardmetal) was calculated as

$$W_{brittle}^{total} = \left\{ [W_{brittle}(H_i) + W_{fatigue}(H_1)] \cdot P(H_i) + W_{cutting}(H_i) \cdot [1 - P(H_i)] \right\} \times f(H_i) \cdot \frac{\Delta H}{n}, \quad (5)$$

where  $H_i$  is the average hardness of a hardmetal hardness range [N/mm<sup>2</sup>];  $P(H_i)$  is the probability of a brittle fracture;  $\Delta H$  is the entire hardness range of hardmetal reinforcement;  $n$  is the number of ranges, taken as  $n = 4$ .

The total wear of the composite material is calculated as

$$W_{total} = W_{ductile}^{total} \cdot x + W_{brittle}^{total} \cdot (1 - x), \quad (6)$$

where  $x$  – the volume proportion of matrix.

**Experimental Wear Rates.** The wear tests were performed according to parameters, brought in Table 1. The centrifugal type tester CAK (Fig. 2 a) was used for the low-energy wear tests and disintegrator type tester DESI (Fig. 2 b) – for the high-energy ones.

The volumetric wear rate was calculated as:

$$W_{experimental} = \frac{360 \cdot \Delta m}{M \cdot \delta \cdot \rho_1}, \quad (7)$$

where  $\Delta m$  is the weight loss of the target material [mg];  $M$  is the total mass of the abrasive [kg];  $\delta$  is the target hit sector angle;  $\delta = 8.5^\circ$  in CAK and  $\delta = 9.4^\circ$  in DESI.

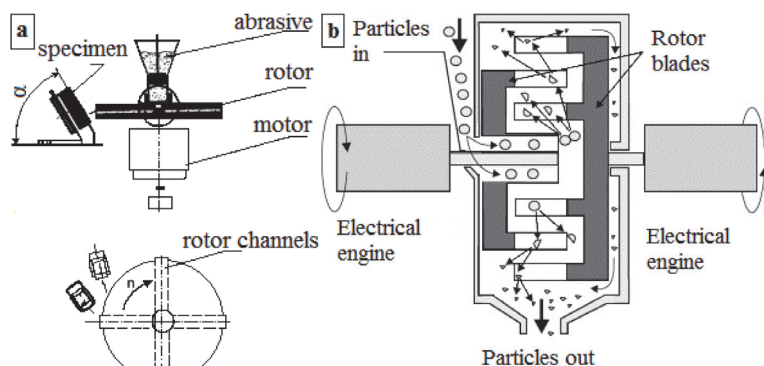


Fig. 2. Schematics of the wear testers: a – CAK; b – DESI

### Comparison of Calculated and Experimental Wear Rates

The wear rates were calculated, assuming that density of the erodent  $\rho_2 = 2.5 \text{ mg/mm}^3$ , Poisson's ratio of the erodent  $\mu_2 = 0.17$ , Young's modulus of the erodent  $E_2 = 90 \text{ GPa}$ , normal force  $F_n$  was  $0.19 \times 10^{-3} \text{ N}$  and  $0.85 \text{ N}$  at  $v_0 = 40 \text{ m/s}$  and  $0.75 \times 10^{-3} \text{ N}$  and  $3.45 \text{ N}$  at  $v_0 = 80 \text{ m/s}$  respectively under low-energy and high-energy AIEW conditions. The data of the materials, necessary for calculation of wear rates, is brought in Table 3 and Fig. 3.

Table 3. The input data of the materials to be studied

| Target material  | $\tau_0/e_s$ | Poisson's ratio $\mu_1$ | Young's modulus $E_{1,2}$ $\times 10^3 \text{ N/mm}^2$ | Density $\rho_1$ $[\text{mg/mm}^3]$ | Hardness HV1 $[\text{N/mm}^2]$ | Fracture toughness $K_{1C}$ $[\text{MPa}\cdot\text{m}^{-0.5}]$ |
|------------------|--------------|-------------------------|--|-------------------------------------|--------------------------------|--|
| H400             | 0.09         | 0.3                     | 185  | 7.85                                | 5250                           | –  |
| P1 <sup>1)</sup> | 0.19         | 0.26                    | 291  | 7.40                                | 6695                           | –  |
| C3 matrix        | 0.19         | 0.26                    | 291  | 7.40                                | 10990                          | –  |
| C3 reinforcement | 0.12         | 0.24                    | 430 – 650  | 14.1 – 15.3                         | 16800 – 24130                  | 10.5 – 19.5  |
| S3 matrix        | 0.19         | 0.26                    | 291  | 7.4                                 | 10460                          | –  |
| S3 reinforcement | 0.12         | 0.24                    | 430  | 14.1                                | 18100 – 24020                  | 19.5   |

<sup>1)</sup> Taken from Fig. 3.

Under the low-energy AIEW conditions, under the oblique impact angle the difference between the experimental and the calculated wear rates varies 1.4 – 2.1 times in the case of the homogeneous materials (Hardox 400 and FeCrSiB) and 3.3 times in the case of the composite material (C3; Table 4). However, under the normal impact angle the difference between the wear rates is generally remarkably different, being eleven orders of magnitude lower in the case of the homogeneous materials and 1.4 – 3.4 times higher in the case of the composite material (C3).

Under the high-energy AIEW conditions, the calculated wear rates were twelve orders of magnitude lower in the case of the homogeneous materials and 56 – 213 times lower, in the case of the composite material (S3), to be compared with the experimental results (Table 4).

The analysis of the calculated and the experimental wear rates, as well as of calculations themselves (not shown), demonstrates that the wear values, calculated by Eq. 4, are much lower to be compared with the experimental ones. There could be different reasons for that. The applied Hutchings' model ignores the shear deformation of the material [10]. However, multiple researchers reported the formation of "lips" at the walls of the impact craters, left by the erodent particles [15,16]. According to [16], they may be easily detached by the subsequent nearby impacts. Secondly, the size and shape of the particles is not taken into account, what results in, for example, the same values of wear rates for low-energy and high-energy AIEW (Table 4). Thirdly, this model does not take into account the residual stresses in the material, what may also influence the final result, especially in the case of composite structures [17,18].

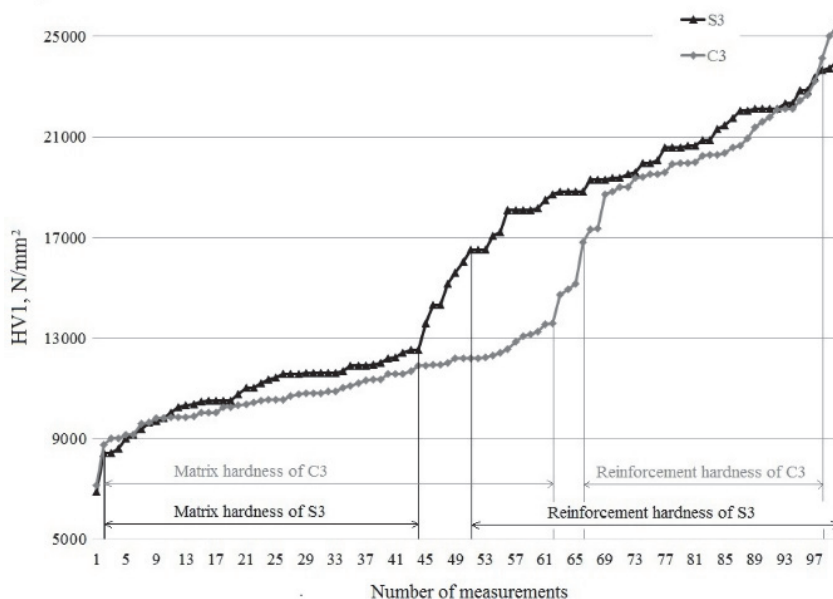


Fig. 3. Hardness distribution in C3 and S3

Table 4. Experimental wear rates, mm<sup>3</sup>/kg

| Material | Low-energy       |      |                       |      |       |      | High-energy           |      |                       |      |                       |       |
|----------|------------------|------|-----------------------|------|-------|------|-----------------------|------|-----------------------|------|-----------------------|-------|
|          | Velocity [m/s]   |      |                       |      |       |      |                       |      |                       |      |                       |       |
|          | 40               |      | 80                    |      |       |      | 40                    |      | 80                    |      |                       |       |
|          | Impact angle [°] |      |                       |      |       |      |                       |      |                       |      |                       |       |
|          | 30               |      | 90                    |      | 30    |      | 90                    |      | 90                    |      |                       |       |
|          | Calc.            | Exp. | Calc.                 | Exp. | Calc. | Exp. | Calc.                 | Exp. | Calc.                 | Exp. |                       |       |
| H400     | 3.8              | 7.9  | $6.0 \times 10^{-12}$ | 3.8  | 21.8  | 37.0 | $4.8 \times 10^{-11}$ | 30.0 | $6.0 \times 10^{-12}$ | 26.1 | $4.8 \times 10^{-11}$ | 85.4  |
| P1       | 4.6              | 3.2  | $2.7 \times 10^{-12}$ | 10.0 | 25.7  | 12.0 | $2.2 \times 10^{-11}$ | 21.5 | $2.7 \times 10^{-12}$ | 9.3  | $2.1 \times 10^{-11}$ | 29.5  |
| C3       | –                | –    | 1.1                   | 3.7  | 42.9  | 12.9 | 23.4                  | 16.7 | –                     | –    | –                     | –     |
| S3       | –                | –    | –                     | –    | –     | –    | –                     | –    | 0.4                   | 85.2 | 3.2                   | 180.7 |

## Summary

1. A good applicability of the used mathematical models was demonstrated for the oblique impact angle abrasive impact erosion wear (AIEW) conditions. Under the normal impact angle AIEW conditions, the used mathematical models, especially the Hutchings's model, proved to be unsuitable.
2. For a more accurate prediction of wear under the normal angle AIEW conditions, plastic deformation of the target material and, on the other hand, the geometry (size, angularity, etc.) of the erodent should be taken into account.

## Acknowledgements

This work was supported by the institutional research funding IUT19-29 „Multi-scale structured ceramic-based composites for extreme applications“ of the Estonian Ministry of Education and Research.

---

**References**

- [1] I. Kleis, P. Kulu, Solid Particle Erosion. Occurrence, Prediction and Control, Springer-Verlag, London, 2008.
- [2] G. Beckmann, I. Kleis, Abtragverschleiß von Metallen, VEB Deutscher Verlag für Grundstoffindustrie, Leipzig, 1983.
- [3] G. Beckmann, J. Gotzmann, Modelling blast wear on ceramic materials, Proc. Techn. Univ. Tallinn 609 (1985) 102-109.
- [4] J. Gotzmann, Modellierung des Strahlverschleißes an keramischen Werkstoffen, Schmierungstechnik, Fachzeitschrift für Tribotechnik, VEB Verlag Technik Berlin, 20 (1989) 324-329.
- [5] R.R.E. Ellermaa, Erosion prediction of pure metals and carbon steels, Wear 162 (1993) 1114-1122.
- [6] P. Kulu, R. Veinthal, Characterization and modelling erosion wear of powder composite materials and coatings, Int. J. Materials and Product Technology 28 (2007) 425-447.
- [7] R. Veinthal, Characterization and modelling of erosion wear of powder composite materials and coatings, PhD thesis, TUT Press, Tallinn, 2005.
- [8] I.M. Hutchings, Some comments on the theoretical treatment of erosive particle impacts, Proc. 5th Int. Conf. on Erosion by Liquid and Solid Impact, Cambridge, 3-6 of September 1979, paper 36.
- [9] I.M. Hutchings, Tribology: Friction and Wear of Engineering Materials, Cambridge, 1992.
- [10] I.M. Hutchings, A model for the erosion of metals with spherical particles at normal incidence, Wear 70 (1981) 269-281.
- [11] T. Simson, R. Tarbe, M. Tarraste, M. Viljus. Abrasive impact erosion of composite Fe-based hardfacings with coarse WC-Co reinforcement. Proc. 24<sup>th</sup> IFHTSE Congress European Conf. Heat Treatment and Surface Engineering, 26-29 of June 2017, Nice, France.
- [12] A.G. Evans, M.E. Gulden, M. Rosenblatt, Impact damage in brittle materials in the elastic-plastic response regime, Proc. Roy. Soc. Lond. A361 (1978) 343-365.
- [13] P. Kulu, A. Surzhenkov, M. Viljus, T. Simson, R. Tarbe, M. Saarna, Wear resistance and mechanisms of composite hardfacings at abrasive impact erosion wear. J. Phys.: Conf. Ser. 843 (2017) 012060.
- [14] T. Simson, P. Kulu, A. Surzhenkov, R. Tarbe, D. Goljandin, M. Tarraste, M. Viljus, Wear resistance of sintered composite hardfacings under different abrasive wear conditions, Materials Science (Medžiagotyra) (2017) (in press).
- [15] I.M. Hutchings, R.E. Winter, J.E. Field, Solid particle erosion of metals: the removal of surface materials by spherical particles, Proc. R. Soc. Lond. A348 (1976) 379-392.
- [16] M. Antonov, J. Pirso, A. Vallikivi, D. Goljandin, I. Hussainova, The effect of fine erodent retained on the surface during the erosion of metals, ceramics, plastic, rubber and hardmetal, Wear 354-355 (2016) 53-68.
- [17] I. Hussainova, On micromechanical problems of erosive wear of particle reinforced composites, Proc. Estonian Acad. Sci. Eng. 11 (2005) 18-30.
- [18] A. Surzhenkov, A. Vallikivi, V. Mikli, M. Viljus, T. Vilgo, P. Kulu, Wear resistant self-fluxing alloy based TiC-NiMo and Cr<sub>2</sub>C<sub>3</sub>-Ni hardmetal particles reinforced composite coatings, Proc. 2<sup>nd</sup> Int. Conf. Manufacturing Engineering & Management 2012, 5-7 of December 2012, Prešov, Slovakia, 33-36.

#### **Paper IV**

Casesnoves, F., Surzhenkov, A. mathematical models in biotribology with 2D-3D erosion integral-differential model and computational-optimization/simulation programming. *International Journal of Scientific Research in Computer Science, Engineering and Information Technology*, 2017, 2,3, pp. 329-356.



# Mathematical Models in Biotribology with 2D-3D Erosion Integral-Differential Model and Computational- Optimization/Simulation Programming

—a mathematical model construction based on experimental research

Francisco Casesnoves\*<sup>1</sup>, Andrei Suzenkov<sup>2</sup>

\*<sup>1</sup>Computational Engineering Researcher, Mechanical Engineering, TUT, IEEE (Electronics and Electrical Engineering Institute)  
Individual Researcher, Estonia, casesnoves.work.emailbox@gmail.com

<sup>2</sup>Assistant Professor, Mechanical Engineering, TUT, Estonia, andrei.surzhenkov@tut.ee

## ABSTRACT

Following from previous computational-research of biotribology models, the study of wear, abrasive wear, corrosion, and erosion-corrosion in bioengineering artificial implants, interior, exterior, partially-interior/exterior biomedical devices, or artificial-bone implants, is directly linked to the operationa-solution of their bioengineering/biomechanical difficulties. Additionally, this kind of deterioration could also involve external medical devices, prostheses, temporary prostheses or orthopaedic supplies, surgical permanent devices, and even surgery theatre devices or tools, causing a series of important associated functional difficulties. This usually happens during surgery and the post-operation stage, or rehabilitation time. The consequences of this industrial-biomedical design complexity are extent, from re-operation, failure of medical devices, or post-surgical discomfort/pain to complete malfunction of the device or prostheses. In addition to all these hurdles, there are economic loss and waste of operation-surgical time, re-operations and manoeuvres carried out in modifications or repair. The wear is caused mainly by solid surfaces in contact, abrasive or sliding wear with frictional resistance. Corrosion/Tribocorrosion of protective coatings also constitute a number of significant mechanical and bioengineering difficulties. Mathematical modelling through optimization methods, initially mostly developed for industrial mechanical systems, overcome these engineering/bioengineering complications/difficulties, and reduce the experimental/tribotesting period in the rather expensive manufacturing process. In this contribution we provide a brief review of the current classified wear, erosion and/or corrosion mathematical models developed for general biotribology—based on recent modelling international publications in tribology, as an introduction to research. Subsequently the aim focus on specific tribology for biomedical applications and references to optimization methods and previously published new graphical optimization for precise modelling with computational formul, programming presentation, and numerical-software practical recipes. Results comprise an initial review of tribological models with further simulations, computational optimization programming, new graphical optimization, and visual data/examples both in mechanical and biomechanical engineering. The corollary of this research is a mathematical integral-differential model for abrasive erosion is developed based on experimental laboratory data and previous mathematical modelling contributions. All in all, this study constitutes a contribution to modelling optimization in bioengineering with a model development and imaging optimization/simulation recent advances.

**Keywords :** Tribology, Erosion, Corrosion, Wear, Biomedical Devices, Erosion-Corrosion, Mathematical Modelling, Nonlinear Optimization, Advanced Programming And Software

## I. INTRODUCTION

Human life-biology constitutes a type of matter natural organization at earth with an special evolved cognitive

brain, together with animal, vegetal, atmosphere and mineral ones. This fact implies that any environmental physical-chemical phenomena that cause changes in the structure of all these kinds of material-structured

varieties involve common physical/chemical mathematical laws and parameters.

The engineering and science advances in modern research focused on tribology, biotribology and wear, erosion and corrosion are not an exclusive study of these phenomena. Natural earth surface has been modified by geophysics laws/parameters by wear, and erosion during periods of millions of years. Human/animal physical biomechanics and tissue-biology is linked to these physical-chemical changes along the lifetime of the natural beings. What is more, recent climate change has become an additional factor to modify previous natural conditions/stages of erosion and corrosion of earth, in such a way that today, for easy example, it is well-known that antarctic surface-glaciars are performing a significant objective modification in their structure and melting-volume. Secondly, the production results of the human industry is modified along their usability-time by tribological conditions, and even the increasing industrial residuals, specially non-biodegradable matter, and all kind of waste are subject of tribological constraints not only in the elimination/transformation phase but also during the storage of industrial-human and/or solid-residuals and waste.

As a logical consequence of all these phenomena, we can classify tribology and biomedical tribology among the groups natural, artificial, and natural-artificial. The interaction between/among these strands are evident, for instance, the modification of farming over the soil during the harvest grow or the links between the wood industry modification of natural spaces that yield the erosion of free land-surface alteration. An external biomedical implant directly causes influence over the surrounding muscles and tissues, since the biomechanics of that part of the human body is different as a result of the insertion of the medical device.

To summarize these environmental-human-tribocorrosion concepts, and prove the natural-artificial extensive interrelation, a logical example is the probably modification along the large-decades of the physiological temperature-control, due to the sudden climate changes and overlapping of the natural climate terms—in other words, in the same way that diet habits transformation during recent times have resulted in different body-shape of new generations, the external

conditions get similar influence. To guess akin phenomena, the skin physiological cycle of melanocytes could be become dissimilar for the long-term increase of the solar radiation, and the alike high-augment to electromagnetic radiation overall dose, e.g., cell-phones or comparable devices around radio-sensitive zones of head and neck, could result in decades in neural-axon transmission conversion to a new environmental circumstances.

Biomedical Tribology and Tribocorrosion constitutes a mixed up branch whose specialization shares parts of every group defined previously [8,9,13]. In other words, Biomedical Tribology involves artificial wear of medical implants and devices but also natural biochemical corrosion or wear of any medical device which is set into the human biomechanical system [8]. This fact implies that there are special and difficult mathematical, computational, numerical, physical, and chemical/biochemical conditions when the mechanical device of interest is biomedical and is surrounded by human/animal tissues. Another important evolution-factor is the biomedical technology advances linked to the progress towards a longer lifetime in human population. This incidence/prevalence fact implies that a significant percent of population will experience during their lifetime substitution(s) of body parts for a large number of pathological reasons, or traumatological-accidental causes [35,37,36,39]. It is not risky to pre-hypothesize that in the future decades the human body will experience changes along the life with increasing substitution of damaged/degenerated tissues/body-parts because the expectation of lifetime will be significantly longer [72].

Therefore, according to all these conditions/constraints, it is straightforward to guess and estimate the importance of the study/research of wear, erosion, and corrosion in technology and science as industrial-material, biomedical tribology essentials and environmental-geophysical factors. For built-up mechanized purposes, pure mechanical or biomedical, given the economic loss caused by erosion and corrosion in an extensive range of engineering/technology areas, the selection of materials became a must. As a result, a large number of technical approaches to deal this question have been put in practice, mainly since the beginning of the industrial era.

The advances during the XXth Century in mathematical methods towards their applicability in a large field of sciences that were not initially subject of strict-numerical objective determinations has supposed a quality jump in investigation, and not limited for this field but also extended, e.g., to social sciences, industry design/planification, classical agricultural/food-production techniques, physical-sport science, etc. Just the same occurred with materials engineering, whose classical trial-and-error testing involved a large series of defects and discarded intends in the field of machinery, metal coatings or power-energy stations, among many other areas.

The computational era of XXIst Century supposed a further upstep in research-applicable mathematical methods for engineering, and the selection/optimization of materials began to be subject of mathematical modelling and computational calculations—mainly accompanied with the electronics advances in microprocessors speed and memory quality standards. Complementary, the creation of simulators to avoid large laboratory investigation-terms supposed in these recent years a small revolution in scientific work methods [14,23,35,37,39,56].

The third leap-stage for mechanical materials engineering was the extension of the industry from first to next towards the manufacturing of medical devices. This fact was caused by the parallel advances of technology applied on medicine, surgery, and rehabilitation physical-therapy [23,35,37,39,56].

These objective real-world facts implied that investigation of biomaterials was born as a new specialization/branch within biomedical engineering. In other words, simulators, optimization methods, mathematical modelling and computational software constitute daily tools of advance in biomaterials investigation.

“Trial and error” methods, that is, the Forward Empirical Problem Technique, was found expensive, imprecise and time consuming [5,55]. In consequence, applications of the Inverse Problem methods were used to determine, *a posteriori*, the validation/refinement of theoretical mathematical models previously approximated [6,7,8,6,9]. In doing so, the modelling optimization time arose, in order to carry out an initial mathematical approximation for a subsequent

experimental choice of the most convenient materials [5,10]. Since the optimization task has become a routinary/compulsory task at daily research routine, [35,36], and not necessarily all the investigators got used to work with optimization programming and tools, graphical optimization, among several optional-practical methods arose in recent years—for instance, see section with images focused on graphical optimization with Freemat and Matlab.

In terms of general mechanics/machinery/devices, material coatings erosion,corrosion,deformation and stress cracks are considered an industrial hurdle that creates loss of budget, energy, reparation-time, and operating time. Material substrate, although important also and chemically/physically linked to these processes, does not constitute the primary problem. Statistically, a rate higher than 90%, of mechanical-machine failures are linked to fatigue, friction,and wear. Succintly, according to [11], the aggressive environments that cause degradation in general are, wear, corrosion, oxidation, temperature, gas-particle size/velocity [12,16,17,22,27], and any combination of these factors. In biomedical tribology the degradation is more specific, chemical factors take a fundamental role, and biomechanical forces that cause wear are also essential for durability of artificial implants, physiological acid-dase ions are fundamental in this phenomenon. Hence, the practical objective to find out engineering/bioengineering solutions is to use new/improved optimal materials for the technical design, in such a way according to precision of durability and functional operation of the mechanical system/device or group of any kind of apparatus/prostheses. Actually there is a number of mathematical models for tribology, biotribology, wear, erosion, corrosion, and combined erosion-corrosion or tribocorrosion. The objective of these modelling algorithms is to design accurate theoretical optimization models for initial search of optimal material characteristics, before passing on to the type of material testing/tribotesting with (approximated) those previous parameters- given as a solution of the theoretical model. In such a way, that mainly the coatings of the device, could be improved in durability, tribology/biotribology capabilities, and erosion-corrosion resistance.

Engineering solutions, as said, for these problems that cause economic loss, together with a waste of, e.g.,

functioning time and expensive reparations, re-operations in biomechanical and mechanical structures, power plants, bioengineering and mechanical apparatus/equipment are based on precision-design of both coating materials resistant to abrasion-erosion, and/or friction [1,3,4,6], and mechanical optimization of the operational structure of the device/mechanical system/mechanical-chain-group—in fact, temperature of components, e.g. hardmetal or cermets, constitutes also an important factor-and stress of materials also. Since materials testing apparatus have become more sophisticated and at the same time more accurate, the testing-process economical cost, therefore, has increased in recent times—we refer to them as the so-called tribotest in general [14,16]. Tribotests could be based on almost realistic simulations for all the components of the mechanical system, some of them, or a reduced number of them [16]—simplified-tests or single-component tests. As a result of the optimal variable-magnitude determinations with the mathematical model, it is imperative to link this objective data to perform, subsequently, experimental testing at lab. Then figure out a definite evaluation, in order to choose the optimal material usually for coatings or other structures [1,3]. Tribotests for biomedical wear and corrosion involve different and more uncommon/sophisticated conditions since the human physiology and biomechanics comprise different and rather more complicated parameters in several circumstances compared to classical mechanical systems [ref]. In other words, biomedical tribotests both *in vivo* and *in vitro*, involve a more complicated/constrained experimental conditions and even medical-ethical legal norms.

This contribution deals with an up-to-date modelling-presentation of tribology/biotribology wear,erosion, corrosion, and erosion-corrosion mathematical models, both from an objective and critical point of view. Complementary, in this article, we explained basic/functional nonlinear/linear optimization techniques to make an optimal choice of erosion and corrosion models, in order to minimize materials/machinery/device damage. The results and conclusions comprise a group of modern series of data, applicable in materials selection optimization, both for further research, and engineering design in the energy field. In general is a continuation of previous modeling contributions but complemented and developed

towards a biomedical and biotribology scope [35,36,37,39,72].

The simulations that are presented comprise both mechanical systems modeling for tribology and biomedical modeling also. Graphical optimization, [Casesnoves, 2017], is detailed with series of images and sharp conclusions that are evidenced by visual information. Optimization algorithms and computational examples are also shown with detailed and sharp-learning explanations. A group of highlights and important key points following all the article development from theory to computational practice are gathered at final sections to summarize the results of this research. The mathematical model developed constitutes a realistic presentation of a theoretical-experimental development of equation for hip implants wear [Casesnoves,2017].

## II. SIMPLIFIED CLASSIFICATION OF GENERAL MODELS FOR EROSION AND CORROSION

Erosion and corrosion concepts imply the interaction between/among physical structures that could be in any physical state, namely, solid, liquid-solid,deformable-solid, or metastates. There have been several classifications, developed for erosion and corrosion mathematical models, tribology and biotribology in general.

The interaction complexity is rather high, (Table 1). In the literature [17,10,55], it is possible to simplify the classification(s) on the basis that, given the rather large number of models, it is guessed that the extensive complexity of biotribology and specifically E/C causes the necessity to design particular models almost for every type of interaction.

Type1 and Type2 interactive classification constitutes a simple and fast practical use/selection of models in each

particular materials choice—proposal of authors previously published [55], Table 2. The predominant criterion of this classification is the practical engineering selection, that is, *for what is used every model*, and its advantages and limitations. The frame of classification is just the same for, biotribology, erosion, and corrosion. Therefore, it is defined as follows,

**Type 1 (T1)** Mathematical Tribology, Biotribology and specifically E/C Models.-Those ones that can be implemented for several applications/material-interactions.Degree of usage is from 1 (lowest application range) -4 (highest application range).

**Type 2 (T2)** Mathematical E/C Models.-Those ones that can be implemented, and are designed/optimized for a specific or super-specific physical application. Degree of usage 1.

**TABLE I**

| <b>BIOMATERIALS INTERACTION CONDITIONS FOR MECHANICAL TRIBOLOGY AND BIOMEDICAL TRIBOLOGY</b> |  |
|--|--|
| <b>Conditional Factor</b>  | <b>Variables/Parameters/Comments</b>   |
| State  | solid (cristallographyc variety),liquid,gas,metaestates  |
| Physical Magnitude   | particles velocity,kinetic energy,materials particle temperature                                     |
| Geometry   | rather difficult in most cases,particle impact angle(s),interaction angle(s), interaction surface(s) |
| Material Composition   | chemical,molecular,nano-quantum composition  |
| Material Structure   | physical-chemical and nanomaterial complexity  |
| Material Origin  | natural (unpredictable), artificial  |
| Environment  | temperature, humidity, thermal insulation, adiabatic and/or isothermal conditions                    |
| Residual Stress and Fatigue  | influence in erosion and corrosion rates and surface cracks  |
| Mutual Interaction   | any possible interaction among/between all the former factors  |
| Stress Residual and Strain in hip implants   | Stress and strain of prosthesis conditions for hip implant (modelled in equations)                   |
| Biomechanical Conditions   | For Biotribology and biomedical devices very important rather essential in engineering design        |
|  |  |

| <b>BIOMATERIALS INTERACTION CONDITIONS FOR MECHANICAL TRIBOLOGY AND BIOMEDICAL TRIBOLOGY</b>   |  |
|--|--|
| <b>Conditional Factor</b>  | <b>Variables/Parameters/Comments</b>   |
| <b>INTERACTIONS FLOW CHART</b><br><pre> graph LR     Physical[PHYSICAL] &lt;--&gt; Chemical[CHEMICAL]     Chemical &lt;--&gt; Physio[PHYSIOLOGICAL AND BIOCHEMICAL]         </pre> |  |
| Physiologic al-chemical- composition of plasme, blood flow, and surrounding tissue composition   | Very important for the tribocorrosion conditions and durability of the implant. Acid and base ions of plasma and surrounding chemical pH parameter constitutes a corrosion factor for metal/composites/plastic surfaces                                  |
| Associated diseases in the patient subject of biomechanical implant  | Any concomitant disease of the patient that is subject of biomedical device implant surgery is a factor interacting with the implant materials and biomechanics, e.g., osteoporosis, diabetes, clots, metasthesis, tumoral physical growth/pressure, etc |
| Biomechanical Specific Body-types  | Not all the patient anatomy and therefore biomechanical constitution are equal, and what is more, the particular physical activity of every person also is an important factor   |
| Histocompat ibility Contrast Internal External   | Internal devices are subject of biocompatibility Mandatory conditions, not the case for external implants, mixed requirements for internal-external [8]  |
| Medical Device Biomaterials personalizati on   | In not few cases, personalization of a medical device for special/complicated patients yields to the particular design of biomaterials   |

In Table 1 a general overview of Tribology and Biotribology definition of this classification is detailed—improved from previous publications [55].

**TABLE II**

| <b>TRIBOLOGY AND BIOTRIBOLOGY<br/>                     MATHEMATICAL MODELS<br/>                     CLASSIFICATION WITH DETAILS</b> |  |  |
|---|--|--|
| Group/Brand   | Model Type   | Definition Examples  |
| <b>TYPE 1 (T1)</b>  | Models with several applications   | Models for several E/C interactions in different conditions  |
| <b>TYPE 2 (T2)</b>  | Specific, and superspecific models with one application  | Precise or extremely-accurate design for a unique materials physical interaction   |
| <b>Mathematical Methods</b>   | Mathematical And Optimization Techniques applicable to characterize Type 1 and Type 2, linked to any model | Heuristic (H)<br>Empirical (E)<br>Random (Monte Carlo) (R)<br>Deterministic (D)<br>Mixed (M)<br>Finite Element (FE)<br>Dynamic Model (DM)<br>Others (O)<br>Degree of Usage (1-4)                 |
| <b>Flexible Classification</b>  | T1 and T2  | It is meant that an initial model in tribotesting stage/improvement could pass from T1 to T2, or vice-versa, derive in other models with new lab findings or be modified in optimization process |
| <b>DIAGRAM OF FLEXIBLE CLASSIFICATION OF MODELS</b>   |  |  |
|   |  |  |

**III. BIOMEDICAL  
 TRIBOLOGY/TRIBOCORROSION  
 MATHEMATICAL MODELS, AN  
 INTRODUCTION**

This section is mainly focused on hip prostheses models for femur acetabular joint replacement, and brief reference to other biomedical models. The predominant phenomenon in biotribology is not pure wear or corrosion. Since the environment in internal implants is human tissue, tribocorrosion is what mostly occurs. Tribocorrosion is defined as the degradation of material surfaces both physical and chemical—wear, cracking, corrosion, abrasion etc.

In Diagram 1, the process of model construction is briefly detailed. Tribocorrosion involves sliding among 2 or three bodies, which could be unidirectional or reciprocating, that is, corrosive wear or chemo-mechanical polishing. Fretting phenomenon happens in dentistry implants and body joints, just the same that occurs in rolling. Microabrasion is linked to rolling, grooving and slurry in general [9].

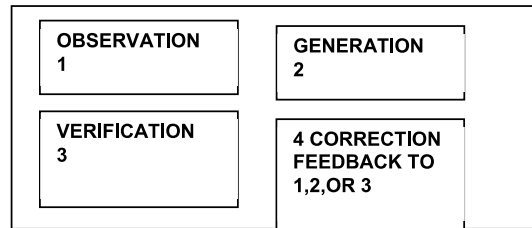


**Diagram 1.-**Basic construction and verification of a mathematical model

The reasons for more significant incidence/prevalence of biotribology linked to hip prostheses are multiple, from the high prevalence /incidence of hip articulation degradation/fracture or similar surgical/medical pathologies to traumatological or genetic malformations that involve severe biomechanical problems in hip articulation system. In fact, hip gait constitutes a fundamental part for walk, run and general mobility of the whole human anatomy. In other words, hip is the biomechanical mesh between the trunk and the legs walking muscular-articular system. No matter whether legs are functional or not, a mobility default in the hip causes such a complicated biomechanical consequences that all the inferior member of the body

could claudicate completely. In addition, load magnitudes on knee, taking into account tendons and ligaments forces during walk, are around 2000 N, and similar values can be expected in hip, both natural articulation or implant. This number gives an idea of the severe constraints/difficulties, both biomechanical and material characteristics (stress, strain, hardness, etc) when designing the prostheses [53,66]. Hip and knee are crucial biomechanical articulations for mobility, and the industrial focus of bioengineering medical devices sets an important part of activity/investigation in this field. A classical model for wear in hip arthroplasty is,

$$W = K \cdot (L X)/H$$

Equation [1]

where K is a wear parameter/constant, L is biomechanical load, X is sliding distance, and H is hardness of implant. This equation is optimized in computational section. Originally, this model was conceived with Flow-Pressure instead Hardness, although hardness can be approximated to flow-pressure. Besides, it is used as a basic formula to develop a mathematical model with a continuous hardness function of matrix in WC-Co reinforced composites to demonstrate an integral equation wear model [Casesnoves,2017]—provided the fact that Titanium-Titanium-Boride are the <sup>1</sup> histocompatible election composite choice [8]. This model reads as follows,with hardness defined as a continuous function H(s),

$$\frac{dw}{ds} = \frac{dw}{dH} \times \frac{dH}{ds} = (KLX) \times \left( \frac{-1}{H^2(s)} \right) \times \left( \frac{dH(s)}{ds} \right);$$

integrating along all matrix averagelength, Eq [2]

$$\int_{w_0}^w dw = \int_{s_0}^s (KLX) \times \left( \frac{-1}{H^2(s)} \right) \times \left( \frac{dH(s)}{ds} \right) ds;$$

or,

$$\int_{w_0}^w dw = \int_{s_0}^s (KLX) \times \left( \frac{-p_1(s)}{p_2(s)} \right) ds;$$

with  $p_{1,2}(s)$  as integrandpolynomials;

In the following it is developed two generic models that are basis for new derived types. One of the initial classifications of wear is the Barwell types, a follows,

<sup>1</sup> Integral-Differential Model was created by Francisco Casesnoves in December 2016 at Tallinn University of Technology based on Computational results from experimental lab data.

$$(1) \quad \Omega = \frac{\beta}{\alpha} [1 - e^{-\alpha T}];$$

$$(2) \quad \Omega = \alpha T;$$

$$(3) \quad \Omega = \beta e^{\alpha T};$$

Eq [2.1]

where  $\Omega$  is volume removed, alpha is a constant and T is the time. It is an initial overview useful for further research and development of models, applicable in biomaterials also. For friction in polymer-matrix composites or similar compounded materials, the Rhee model reads,

$$\Omega = K \times F^{(K_1)} \times V^{(K_2)} \times T^{(K_3)};$$

Eq [2.2]

where  $\Omega$  is volume removed, F load, V velocity, and T time, Ks are constants of laboratory experimental determination. Lubrication modeling in hip prostheses, [53], constitute also a base for development of mathematical formulation, and as an example we refer to Rabinowitsch model that reads,

$$\eta = \eta_{\infty} + \frac{\eta_0 - \eta_{\infty}}{1 + \left( \frac{\tau}{G} \right)^2};$$

Eq [3]

where mu is viscosity, and tau is shear-stress, the other parameters are constants determined by regression, [53]. And also the Carreau's and Cross model,

$$\eta = \eta_{\infty} + \frac{\eta_0 - \eta_{\infty}}{1 + \left( 1 + \left[ \frac{\dot{\gamma}}{\dot{\gamma}_c} \right]^2 \right)^{m/2}};$$

Eq [4]

where gamma is the notation for the shear rate. Actually hip arthroplasty constitutes an important branch of medical devices industry with several super-specialization branches for the extensive area of investigation. Lubrication is essential for several reasons, among them, the minimization of the surfaces

in contact wear, and other motive is the better mechanical performance of the implant.

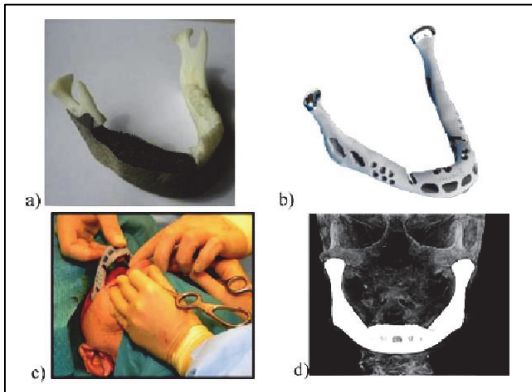


**Figure 1.**-From reference [8], excellent biomechanical sketch of Bartolo and Colls, [8], showing the recent progress in biomedical design-implants and surgery-implementation of an artificial mandible at surgical theatre. Projection of this kind of advances could involve/result in future towards a significant increase of lifetime with additional acceptable level of quality of life and personal-independence-capability standards. Note the well-overcome difficulty of that anatomical region, and the resolute solution with bioengineering design of muscles and tendons slits/holes to Insert them properly in the artificial implant [37]. That is, the mandible and neck-cranial group of muscles is a risky-complicated zone for surgery with important vascular parts, essential nerves and glandules.

Creep, [67], constitutes an additional parameter in rolling surfaces, for instance, for external implants. It is very usual the use of FE method which is essential in contact mechanics, specially in hip implants. One of the most important problems to be sorted to implement and obtain acceptable results is the biomechanical angle between the system acetabular-cup—femoral-head. If that angle would be 0°, modelling and biomechanical functioning would be easier. What is more, since this group of forces project its biomechanical consequences along the femur, which is the longest bone of the body, the results for the normal walk are significant. For basic contact mechanics and FE methods/models, contact radius and maximum stress have been modeled from Hertz theory, [66], namely, ....

$$A = \left[ \frac{3F_y R (1 - \nu^2)}{2E} \right]^{1/3};$$

$$\sigma_c = \frac{3F_y}{2\pi A^2};$$

Eq [5]

where R is the effective radius,  $\nu$  is Poisson ratio, and E is elasticity Modulus.

Mathematical models based on fundamental partial differential equations, [63], have been also used for hip replacement. For instance, by using heat transfer equation, Navier Stokes one, fluid dynamics flow, and stress-equilibrium PDEs [63]. Here it is detailed a primary formula of model for stress-equilibrium formula, which is used for implementation of FE models. Succintly,

$$\rho \frac{\partial^2 u}{\partial t} - \left( \frac{\partial \sigma_x}{\partial x} + \frac{\partial \sigma_{xy}}{\partial y} \right) = F_x; \sigma(\text{stress});$$

$$\rho \frac{\partial^2 v}{\partial t} - \left( \frac{\partial \sigma_{xy}}{\partial x} + \frac{\partial \sigma_y}{\partial y} \right) = F_y;$$

and,

$$\epsilon_x(\text{strain}) = \frac{\partial u}{\partial x}; \epsilon_y(\text{strain}) = \frac{\partial v}{\partial y}; \quad \text{Eq [6]}$$

$$\text{then, } 2\epsilon_{xy}(\text{strain}) = \frac{\partial u}{\partial y} + \frac{\partial v}{\partial x};$$

with the fundamental equivalence,

$$\begin{pmatrix} \sigma_x \\ \sigma_y \\ \sigma_{xy} \end{pmatrix} = \begin{pmatrix} d_{11} & d_{12} \\ d_{21} & d_{22} \\ & & d_{33} \end{pmatrix} \times \begin{pmatrix} \epsilon_x \\ \epsilon_y \\ \epsilon_{xy} \end{pmatrix};$$

where u and v are displacements in x and y directions respectively, F loads in x and y, and sigma and epsilon stress and strain classical tensors. These formulas are developed to obtain a larger equation for final implementation [63]. These mathematical formulism seem to be complicated but in modern FE software can be used fastly and obtain good imaging sketches of the complete result [13,15,19,22].

The wear of a hip prosthesis is a complicated phenomenon, which generally depends on the contact status between the ball and the cup (i.e., friction regime), characteristics of the tribocouple, physiological conditions [60], production quality of the

prostheses [61], lubricants [62], etc. For example, despite a low friction torque, the polymer-on-metal configurations exhibit higher wear, than metal-on-metal or ceramic-on-ceramic ones [63] due to the boundary lubrication regime between the wearing surfaces [64,65]. For the same reason, small-size metal-on-metal hip joints perform worse, than large-size ones [64]. Properly designed and manufactured metal-on-metal hip joint prosthesis work, *vice-versa*, under mixed lubrication regime [65], and ceramic-on-ceramic hip joints function even under hydrodynamic lubrication conditions [64], what provides extremely low friction—linked to the articular movement of acetabular hip, that is, number of rotations in a day is extremely high, arms and legs are basic in human daily movements.

The three principal wear mechanisms in hip joints were found to be adhesive wear, abrasive wear and fatigue wear [55], accompanied by tribocorrosion in the case of metal-on-metal configurations [60]. With time, one mechanism may change to another. For polymer-on-ceramic hip joints, adhesive wear of polymer with the subsequent formation of the tribolayer on the ceramic surface is characteristic. For polymer-on-metal configurations, both adhesive and abrasive wear mechanisms were reported, whereas the last was found to be more probable [61,62,63]. Surface fatigue in combination with three-body abrasion and tribochemical reactions was found to cause wear in the case of metal-on-metal tribocouples [60]. Despite the absence of clear literature data, for ceramic-on-ceramic configurations, surface fatigue and abrasion may be named as the most probable wear mechanisms.

For simulation of wear of a hip prostheses the Archard's wear law is usually applied [61,62]. Its is more convenient to present the integral equation from this model once obtained from the finite elements method mathematical development. According to it, the wear volume  $V$  ( $\text{mm}^3$ ), vanished from the contact surface, may be determined as

$$W = \int_{\Gamma_0}^{\Gamma_1} \int_{S_0}^{S_1} K_w \sigma \, dS \, dA \quad ;$$

Eq [7]

where  $\Gamma$  is the contact surface,  $\text{mm}^2$ ;  $S_t$  is the sliding distance,  $m$ ;  $k_w$  is the wear coefficient;  $k_w = (0.18-0.80) \times 10^{-6} \text{ mm}^3/\text{Nm}$  for the ultra-high-molecular-

weight polyethylene (UHMWPE) in tribocouple with the stainless steel [61,63], and  $k_w = 0.10-0.31 \times 10^{-6} \text{ mm}^3/\text{Nm}$  for UHMWPE in tribocouple with alumina ( $\text{Al}_2\text{O}_3$ ) [1];  $\sigma$  is the normal contact stresses (Hertz contact stresses),  $\text{N}/\text{mm}^2$ , which may be calculated by the corresponding formulas. The maximum normal force ( $F_N$ ) may be taken as  $F_N = 3500 \text{ N}$  [61] and the swing angle of foot is 23 degrees in the forward and backward directions. For the real simulations, the volumetric wear rate ( $\text{mm}^3/\text{year}$ ) is usually calculated. By the literature data, it is in the range of 5–50  $\text{mm}^3/\text{year}$ . The difference between the modeling of hip and knee is given mainly by the methods used. In knee implants, because of the extreme loads that are acting over a rather small bone surface, the usual method is Finite Elements modeling, with precise distribution of stress and strain magnitudes [47,51]. However, substitution of tibial parts are also made with metallic implants, e. g., titanium plasma spray coatings [47,51]. Archard's wear law has several formulii developments depending of the type of implementation an dis extensively applied in Tribology and Biotribology.

Spinal biomechanics modeling is also usually focused on Finite Elements Modeling, [Casesnoves, ref 12]. In spinal reconstruction, a large number of prostheses types are used given the complicated and risky system of the vertebral biomechanics. Finite elements are combined with other biomechanical constraints in order to obtain precision and functionality. All in all, in Tables IV, a succinct brief of biotribology are presented with advantages and inconvenients. The extension of the optimization/simulations of Appendix 1 will give in following publications additional algorithmic data for this important field of the Biotribology.

#### IV. NOTES OF NONLINEAR OPTIMIZATION METHODS AND ALGORITHMS

In previous publications, a modern review of main optimization methods was developed with numerical examples. In [55], these methods are described for complementary information and graphical optimization is set in its proper section. We refer the reader to that publication to find more data and complementary optimization simulation methods and erosion and corrosion models in Appendix 2.

**TABLE III**

| <b>SELECTED MEDICAL-BIOTRIBOLOGICAL MODELS</b>   |             |  |  |  |                     |   |
|--|-------------|--|--|--|---------------------|---|
| <b>BIOTRIBOLOGICAL MODELS/ALGORITHMS FOR HIP ARTHROPLASTY</b>  |             |  |  |  |                     |   |
| <b>NAME AUTHOR AND/OR REF</b>  | <b>TYPE</b> | <b>SETTING VARIABLES</b>   | <b>ADVANTAGES</b>  | <b>WEAKNESSES</b>                                | <b>USAGE GRAD E</b> | <b>COMMENTS</b>   |
| Classical General Model Jin and others [51]  | T1          | Hardness, Load, Rotation Velocity  | Simplicity   | Accuracy to be improved and specified            | 2                   | classic model for further developments  |
| Rabinowitsch Model for lubrication [53]  | T2          | Viscosity constants and shear-stress   | Specific for lubrication and minimize wear                       | Required precision in constants                  | 2                   | useful  |
| Carreau's Model [53]   | T2          | Viscosity constants and shear, shear rate  | Evolution of previous model with shear rate                      | Not useful totally for synovial fluid            | 2                   | Derived models are more improved  |
| Archard's wear model   | T1          | Finite Elements Integral equation  | Integral/Differential model precision                            | More computational time                          | 2                   | Step forward towards a infinitesimal model  |
| Integral-Differential model for basic Hip-Implant Wear Determination [Casesnoves, 2017]  | T2          | Direct empirical computational-determination of Hardness continuous function   | Integral-differential calculus applicable                        | Lab samples required, statistical requirements   | 2                   | This model is in mathematical development and validation actually   |
| Contact Mechanics Hertz parameters modelling   | T1          | Radius, Elasticity Modulus, and Poisson ration   | Implementation on FE methods                                     | Large computational-geometrical work             | 1                   | For FE methods but also applicable in contact biomechanics  |
| Stress-Strain Equational Model for Hip implants  | T1-T2       | Stress and strain matrices mostly  | Applicable also in TE methods                                    | Partial differential equation, not simple        | 1                   | Useful in several development, there are more similar models  |
| Barnwell Classification  | T1-T2       | All range of variables   | General to be improved   | Initial approach                                 | 1                   | First modelling   |
| Polymer-Matrix Model   | T2          | Load, velocity, timey  | applicability  | Only polymers                                    | 1                   | useful  |
| <b>BIOTRIBOLOGICAL MODELS/ALGORITHMS FOR KNEE ARTHROPLASTY (THOSE MODELS ARE USUALLY DEVELOPED WITH SPECIFIC FINITE ELEMENTS GENERIC METHOD)</b> |             |  |  |  |                     |   |
| <b>NAME</b>  | <b>TYPE</b> | <b>SETTING VARIABLES</b>   | <b>ADVANTAGES</b>  | <b>WEAKNESSES</b>                                | <b>USAGE GRAD E</b> | <b>COMMENTS</b>   |
| Finite Elements Modelling  | T1          | Physical variables   | Extensive and multifunctional applications                       | Errors at implementation                         | 2                   | Simulation processes feasible   |
| Corrosion Models applied on solid metallic implants for knee [52]  | T2          | Chemical parameters  | Specific accuracy  | For durability of metal-coated knee implants     | 1                   | useful  |
| <b>BIOTRIBOLOGICAL MODELS/ALGORITHMS FOR SPINAL ARTIFICIAL IMPLANTS</b>  |             |  |  |  |                     |   |
| Dynamics of deformable Compliant Artificial Intervertebral-Lumbar Disks [Casesnoves 2017]  | T1-2        | THE NUMERICAL REULEAUX METHOD APPLIED ON ARTIFICIAL DISKS [Casesnoves, 2007] Synergic model for deformation-biomechanical-stress of artificial disks | Applicability on deformable solids dynamics/kinematics           | Computational algorithms And framework necessary | 2                   | Connected with Deformable solid theory and General Numerical Reuleaux Method (Casesnoves, 2007) Modelling |
| Finite Elements Modeling   | T1          | Corrosive activity,time, and force acting on the oxide layer   | Both corrosion and erosion determination Extensive applicability | Specific for tubes and boilers                   | 2                   | Largely developed by Ots with series of equations   |

## V. MATHEMATICAL METHODS FOR NUMERICAL-GRAPHICAL NONLINEAR OPTIMIZATION WITH ALGORITHMS

This section is intended to explain several new/improved methods for direct approximated graphical optimization. Advantages of this method are the nimble/fast search of the global/local minima/maxima and the sharp imaging visualization of the objective function shape and spatial geometry-distribution along the selected interval. Inconvenients are the limitation to 2 variables in plane x/y, and the strict necessity of simulation-graphical accurate software instead simple numerical-programming software, e.g., a FORTRAN compiler. Then it is defined,

**Definition 1** [Casesnoves, 2017].-Graphical nonlinear optimization<sup>2</sup> is a constructive approximated method to set the global/local minima/maxima of an Objective Function provided two strict conditions,  
-computational graphical simulation of the objective function is precise and imaging software is sufficiently proved as accurate in its imaging algorithms.  
-Objective Function mathematical development and constraints, are strictly mathematically linked to the graphical implementation.

**Proposition 1.-Approximated Optimization by Separation of Variables** [Casesnoves, 2017].-Any OF can be developed/expanded by variables separation method, to obtain several approximations kinds of equations to fastly calculate minima/maxima and set the surfactal imaging-representation of that OF.

**Proof:** beginning with a classical  $L_2$  OF, and for simplicity taking one-term,

$$F(\bar{x}_i) = \|\bar{a} - f(\bar{x}_i)\|^2 = \|\bar{a}\|^2 + \|f(\bar{x}_i)\|^2 - 2\|\bar{a}\| \|f(\bar{x}_i)\| \cong [\text{separation of variables expansion}]; \quad \text{Eq [8]}$$

And the expansion divide the minima calculation in a series of independent terms which are multiplied or summed, giving several options to get further

<sup>2</sup> Graphical-3D Nonlinear Optimization Method was created by Francisco Casesnoves at Tallinn University of Technology in December 2016. The method was a result of the numerical-mathematical study with Fortran and F# Software of lab experimental data.

minimization/maximization approximations [23,35,36,37,39,56,72].

## VI. COMPUTATIONAL SIMULATIONS OF BIOTRIBOLOGY AND MECHANICAL MODELS WITH PROGRAMMING RECIPES

The beguine of this section is with 3d graphical optimization examples and Region of Interest selection methods. We continue with previous research models both for simplicity and clarification in learning. This example of 2 variables simulation is done with the Menguturk and Sverdrup (1979) model, developed as an empirical erosion model for carbon steel material eroded by coal dust. The model shows that erosion is largely a function of particle impact velocity and angle. It is important to remark that what is shown with is model is totally applicable on any bioengineering mathematical model. The selection of this algorithm is justified for primary new 3D simulations with surfaces in an attempt to demonstrate the practical materials engineering/bioengineering usage of this kind of 3D representation—in other words, the cursor of the software can give the numerical desired values for lab or experimental of any type. The model for small and large particle impact angles is given as a easy tool to carry out a graphical optimization, as follows,

$$E = v^{2.5} \times \left[ (1.63e - 6 \cdot (\cos \alpha)^{2.5}) + (4.68e - 7 \cdot (\sin \alpha)^{2.5}) \right];$$

This is the simplest equation valid for particle impact angles  $\geq 22.7^\circ$ . For angles  $< 22.7^\circ$ , the model formulation reads],

$$E = v^{2.5} \times \left[ \left( 1.63e - 6 \cdot (\cos \alpha)^{2.5} \cdot \sin \left( \frac{180}{45.4} \alpha \right) \right) + (4.68e - 7 \cdot (\sin \alpha)^{2.5}) \right];$$

Eqs [9]

where E is the erosion rate in  $\text{mm}^3 \text{g}^{-1}$ , and impact velocity and angle  $\alpha$ , measured in  $\text{m s}^{-1}$  and radians, respectively. The volumetric erosion rate ( $\text{mm}^3 \text{g}^{-1}$ ). That is, 2 variables. This simple equation illustrates the following series of computational simulations, because the implementation of programming matrices algebra-operations is fast, although the application of the matrix-algebra concepts in programming requires special calculations to obtain

accurate/realistic/precise results.

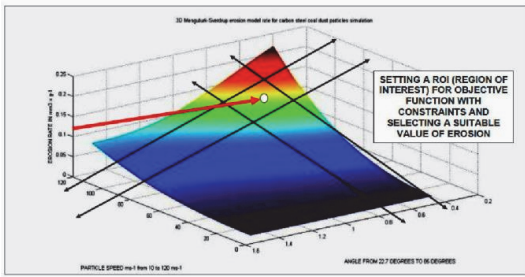


**Fig 2.-** [Enhanced in Appendix 1] Mathematical-geometrical Method of selection of graphical optimization values for a ROI, (region of interest), within the objective function with constraints [Casesnoves,2017]. The picture is a matrix-simulation for a velocity range from 10–120  $\text{ms}^{-1}$  of the model and matrices 1000x1000, quite large numerical imaging programming—running time around 4 seconds, perspective-imaging change time about 10 seconds, taking into account the large matrices. The projection of this kind of graphical optimization onto large series of different models is realistic and mathematically acceptable—for instance, the subsequent simulations of the hip implant wear equation. The setting of constraints in this type of optimizations yields to a new concept in ROIs selection to save time and lab tribotesting.

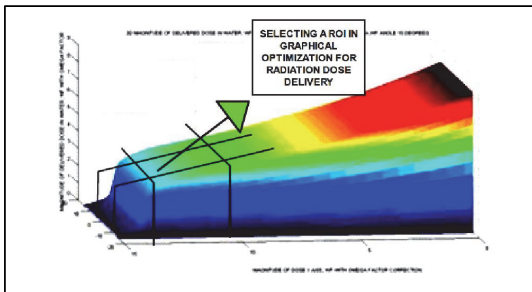


**Fig 3.-** Graphical 3D optimization example, [Casesnoves,2017], of a radiotherapy dose delivery selection of a Region of Interest with constraints in Matlab—enhanced in Appendix 1. Any numerical data within the ROI can be determined with the design of the software, and selection of the optimal values are straightforward.

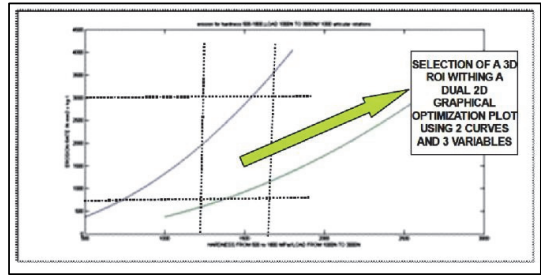


**Fig 4.-** Graphical 2D-3D optimization example, [Casesnoves,2017], of a hip implant simulation with a selection of a Region of Interest with constraints in Matlab—enhanced in Appendix 1. This software is more complicated for the subroutine to conform the optimal graph to select further the ROI. Any numerical data within the ROI can be determined with the design of the software, and selection of the optimal values are straightforward. Note that the choice of the ROI is essential to get comparison sharing all variables.

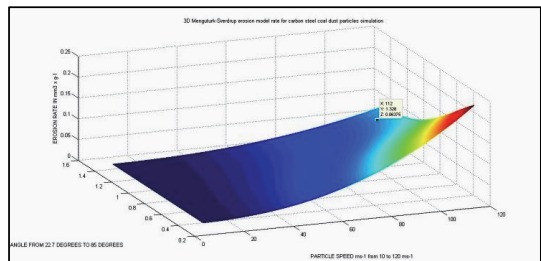


**Fig 5.-** Pictured with cursor-magnitude-inset, the narrowly-same numerical Matlab-2009-10, jpg format, surface-matrix-simulation for a velocity range from 10–120  $\text{ms}^{-1}$  of Menguturk and Sverdrup (1979) model and matrices 1000x1000, quite large numerical imaging programming. Cursor indicates speed 112  $\text{ms}^{-1}$ , angle of particle 1.326 radians, and erosion rate about 0.084  $\text{mm}^3 \text{g}^{-1}$ . The choice of the imaging perspective is intended to show the smooth surface growth towards the maximum speed and angle optimal value that gives the maximum erosion magnitudes for the model. Note the the practical utility of the cursor to search optimal experimental-theoretical values for modeling research both for simulation and nonlinear optimization.

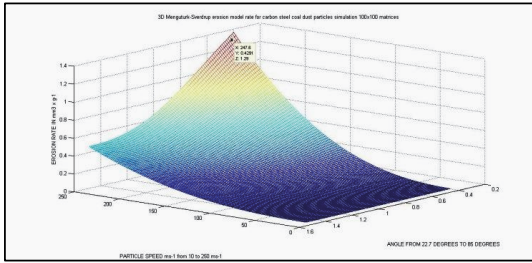


**Fig 6.-** This simulation shows maximum-model cursor-values of speed about  $247 \text{ ms}^{-1}$ , angle of particle  $0.4291$  radians, and erosion rate about  $1.29 \text{ mm}^3 \text{ g}^{-1}$ . So pictured with inset-cursor it is a different simulation of the previous figure in also different angles, to show the surface extension, jpg format, a matrix-simulation for a velocity range from  $10\text{--}250 \text{ ms}^{-1}$  of the model and matrices  $100 \times 100$ , rather simple numerical imaging programming—running time around 2 seconds, perspective-imaging change time about 1-3 seconds, taking into account in this case the small matrices. Cursor in at peak of The choice of the imaging perspective is intended to show better the smooth surface growth towards the maximum-peak speed and angle optimal value, with the surface-sheet totally pictured, that gives the maximum-medium-minimum erosion magnitudes for the model, and also the surface part for minimum values.

Following with 2D type of simulations., this example of 2 variables simulation is developed with the classical wear of hip implants prosthesis mainly. It is simpler programming and can be easily executed both in Freemat or Matlab as it is here presented.

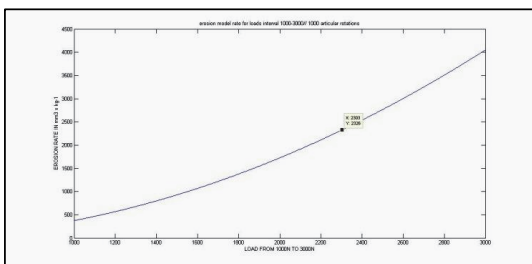


**Fig 7.-**In this 2D-simulation-program for hip implant in Equation [1], the load range was  $[1000,3000]$  in MPa. This program was designed for erosion rate versus load with Matlab subroutines for 1000 rotations. The simulation with inset cursor is showing selected data in

the plotted curve. It was selected a cursor-point with higher than average load value. The matrices of imaging programming are  $1000 \times 1000$ .

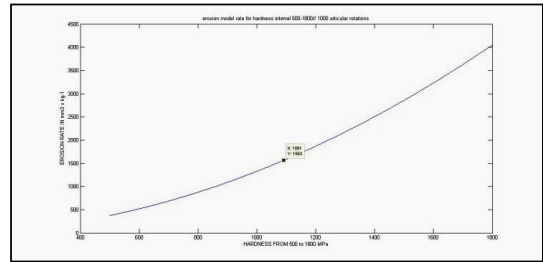


**Fig 8.-**In this 2D-simulation-program for hip implant in Equation [1], the hardness range was  $[500,1800]$  in MPa. This program was designed for erosion rate versus hardness for 1000 rotations. The simulation with inset cursor is showing selected data in the plotted curve. It was selected a cursor-point with middle-hardness value. The matrices of imaging programming are  $1000 \times 1000$ .

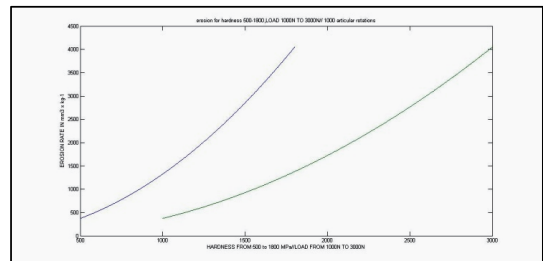


**Fig 9 [enhanced in Appendix 1].-**In this 2D-simulation-program the software was specially designed to show both previous images in the same graph for comparison—ranges are just the same. Hardness range was  $[500,1800]$  in MPa. This program was designed for erosion rate versus hardness and load for 1000 acetabular-cup rotations. The simulation with inset cursor could show selected data in the plotted curves. The matrices of imaging programming are  $1000 \times 1000$ . In Matlab, as it also happens in Freemat, this is not the unique subroutine that can be used for 2D graphs.

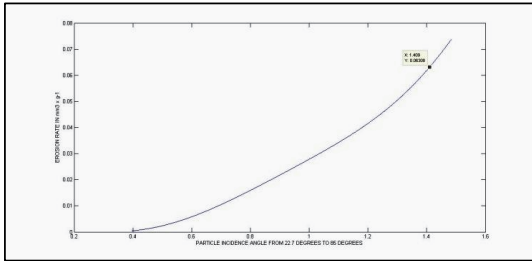


**Fig 10.**-In this 2D-simulation-program the speed range was from 10-120  $\text{ms}^{-1}$ —Menguturk and Sverdrup (1979) model. This program was designed for erosion rate versus angle range of particle incident. The simulation with inset cursor is showing angle of 1.409 radians and erosion rate about  $0.063 \text{ mm}^3 \text{ g}^{-1}$ . It was selected a cursor-point with rather extreme incident-angle value. The matrices of imaging programming are  $1000 \times 1000$ . Note the cosine and sine variations and exponentials low values in the model according to changes within the velocity/angles range.

To summarize this section, in Appendix 1, pictured table, a series of optimization trials in non-linear least squares for wear in biotribological hip prostheses and mechanical systems—usually done with `lsqnonlin` subroutine or similars. This group of data is an improvement of computational work presented in previous publications. The laboratory measurements were set randomly, and the most important is the well-performance of the subroutines of Matlab for nonlinear optimization. The hip implants materials are selected as significantly different, with hardness interval from metal to the highest values of ceramic-ceramic implants [51, 61, 62]. In Freemat there are also a number of subroutines with nearly similar applications, or the reader can find a Freemat program example for Newton-Rapson method with Hutchings model from previous contributions [55].

## VII. IMAGING AND GRAPHICAL NONLINEAR OPTIMIZATION METHODS WITH SPECIFIC HIP IMPLANTS 3D SETTINGS

In this section global-local minima with a random simulated laboratory measurements are computed in order to obtain a 2D plot series of global minimum visual location. In the same way, a number of imaging

optimization pictures are shown with additional comments.

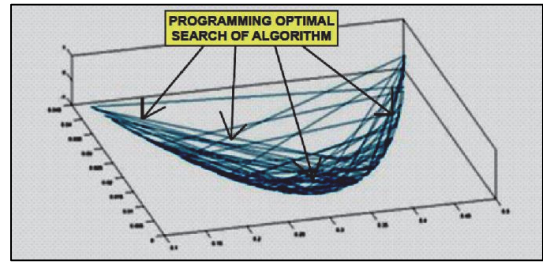


**Fig 11.**-In this Freemat 3D-simulation-program the classical Hutchings model search for the minimum with random simulations is shown. The programming search for global minimum is seen sewing points of the curve. Since values of simulations are stochastic, the program is joining these curve model points in the neighbourhood of the minimum. This picture is intended to show both the several alternatives in nonlinear optimization software, e. g., Matlab and Freemat, and the easy use of all this number of subroutines with sharp intuitive-visual interpretation—in other words, for non-specialized researchers in optimization, only with basic learning of concepts the practical caption of the results is caught up.

The new practical concepts in approximated/constructive optimization have derived from the current available software facilities and applications. A model of hip implants is developed and simulated in 3D with graphical sharp images. It is not unfrequent that lab experimental requires fast calculations, roughly speaking approximated, to try tentative trials or get a quick view of maximum and minimum, usually local, optimal values of a model with/without constraints. From Proposition 1 and Lemma 1, it can be guessed the availability to represent any 3D Objective Function with/without constraints in a graphical way.

The significant improvements of the 3D/2D graphical software and the extensive choice of tools available in the graphics prompts, obtain the maximum of a function in a previously selected range with the simple program and parameters range takes a few seconds. Complementary, errors, residuals and even with a few improvements in the program determinations coefficients can be calculated.

For example, in previous figures the approximated local maximum of the function is easily determined by the use of the cursor. Just the same approach for the approximated local minimum determination can be done, and further ROIs of constraints can be calculated.

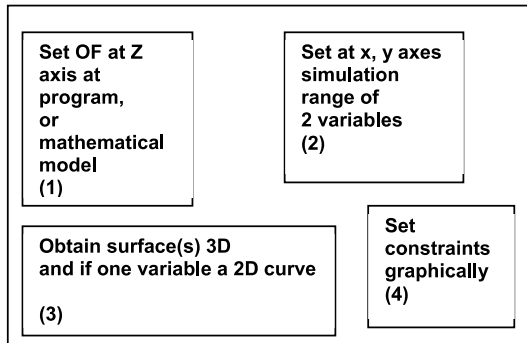


**Diagram 2.**-Basic application of graphical optimization and setting of objective function.

Furthermore, it is possible to try a constructive approximation with straight lines and even curves, so settings constraints or constraints groups in 3D. That is, fixed a value for one variable, we drag the cursor in that direction to find the maximum or minimum of the z axis objective function obtaining at the same time the optimal local value of the other axis variable. That is, we have set an upper graphical constraint for one parameter and found the search for both optimal values in the other parameter and the z-axis objective function. In Figs 16,17 an even more evident instance is shown with a radiotherapy dose distribution of radiation dose distribution—from the author’s previous publication, with new software in Freemat, that has very explicit imaging simulations examples [36,54]. The global maxima line of the radiation dose distribution is sharply found and just the same occurs for the global minima—minima and maxima are in a line since the distribution in 3D is symmetric. Therefore, to use this method when, for example, we are designing further programs of simulations/optimization and the need is to get a caption of approximate values is suitable and practical—and this happens usually in engineering fast experimental works/trials.

Advantages of this method are a quite series ones, provided that the program for simulation is precise and accurate—and this is a mandatory condition. The fastest method to check whether a simulation is

accurate is to carry out random calculations and verify all the interval ranges precisely.

Not all the laboratory staff are experts in programming and optimization, and instead they can get sharp learning from this graphical method. In addition, it is not necessary to design more optimization codes, e. g., a multiobjective optimization program, to obtain a local minimum for any selected interval. Other significant advantage is the fact, provided the accuracy of the simulation, that to use a searching-optimization program could yield wrong results from an inconsistent choice of the initial search. However, using the graph, if there are several concavities in the objective function surface, to locate the local minimum is visually fast/precise instead.

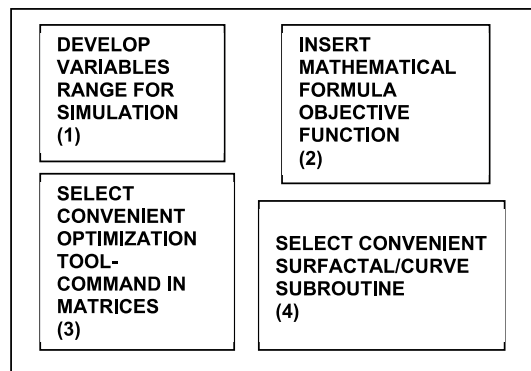


**Diagram 3.**-Flow chart of a graphical optimization program (basic).

Definitely, the constant progress/improvements in software for simulations or optimization graphs justify this usage for practical engineering trials and experimental. Disadvantages of this method exist obviously, since it is an approximated method, are the simplification/approximation of data obtained, and the limitation of the function to 3D and a closed interval range of parameters. In conclusion, it is suggested this method for fast and visual optimization with simple computational programming and convenient tolls at prompt.

While using Matlab software, for instance, the cursor can determine the optimal point of intervals, but with Freemat it is not possible, only to get a general overview of the surface objective function and guess the regions of maxima and minima. However, imaging

both in Matlab and Freemat is overall acceptable and good for their respective subroutines.

In the following, a series of figures with 3D plots are shown and commented—both for hip implant equation and a Triple Gaussian Model in radiation therapy.

According to previous simulations, we pass on proper biomedical models such as hip implants wear basic formula. This deals with direct imaging software results of objective function representation of hip implant equation [1] subject to realistic experimental data from references. Each image has specific software developed to prove the utility of the presented mathematical-graphical method(s). The formula developed in the following series of simulations, Eq [1], reads,

$$W = K \cdot (L X)/H ;$$

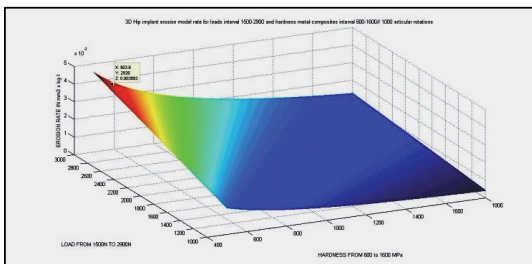


**Fig 12.-** [Enhanced in Appendix 1] Maximum of Equation (1) model for hip implants with cursor inset showing numerical values. Matrices are 1000x1000, and Matlab sharpness of this image is very good, and running time is acceptable.

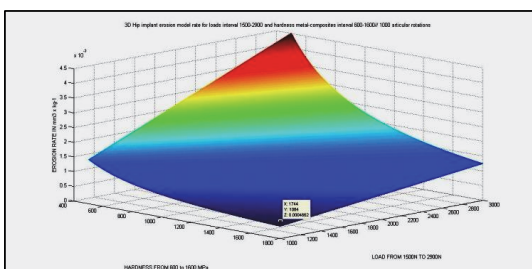


**Fig 13.-** [Enhanced in Appendix 1] Minimum of Equation [1] model for hip implants with cursor inset showing minimum numerical values. Matrices are 1000x1000, and sharpness of this image is very good, and running time is acceptable.

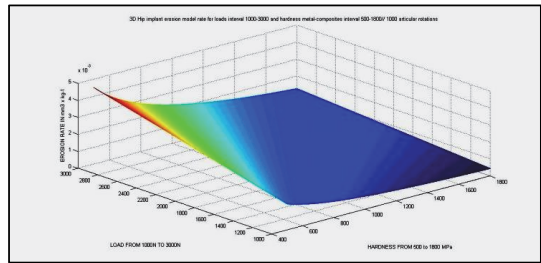


**Fig 14.-**Maximum of Equation (1) model for hip implants without cursor but convenient angle showing numerical values for erosion rate. Matrices are 1000x1000, and Matlab sharpness of this image is very good, and running time is acceptable.

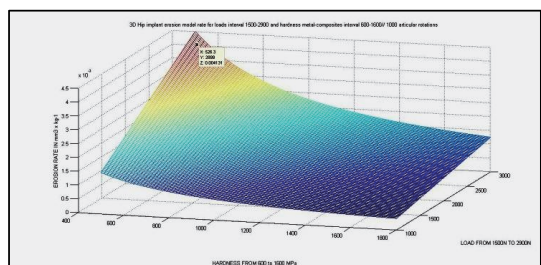


**Fig 15.-** Simulation of Equation [1] maximum of Equation [1] model for hip implants with cursor inset showing numerical values. Matrices are 100x100, and sharpness of this image is very good, with running time is acceptable.

To support all these arguments with additional-variety mathematical development, a graphical radiotherapy simulation is shown in next picture. It corresponds to a Triple-Gaussian radiotherapy model, so-called AAA, analytic anisotropical algorithm, algorithm. In particular, a corrected model representation for a wedge filter at depth of 15cm and 18Mev beam physical parameters. This image was done with Freemat instead of Matlab, as used in previous radiotherapy contributions, [36,54], to prove the adaptation of the designed simulation-optimization software on several types of programs.

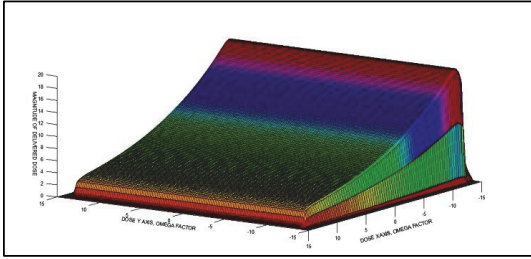


**Fig 16.-A** Freemate 4.1 (Samit Basu General Public License), 3D objective symmetric-function of radiotherapy photon-dose surface with clear determination of the straight marginal lines of global minima/maxima in radiation delivery dose distribution. Matrices are 150 x 150, and with Freemate 4.1 the running time is longer than Matlab—at the same time the matrices size for normal running-time is lower in standard microprocessors. This simulation is Freemate original based on previous computational contributions [refs].For 150 x 150 matrices imaging view setting takes about 5 seconds, and spatial-changes of imaging-set about 7 seconds. If 50x50 matrices are used, the time is reduced around 2 seconds.

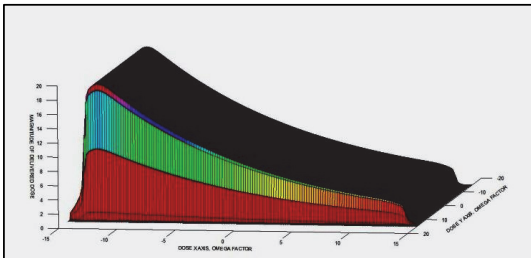


**Fig 17.-A** Freemate 4.1 (Samit Basu General Public License), 3D objective symmetric-function of radiotherapy photon-dose surface with clear determination of the straight marginal lines of global minima/maxima in radiation delivery dose distribution. Matrices are 150 x 150, and with Freemate 4.1 the running time is longer than Matlab—at the same time the matrices size for normal running-time is lower in standard microprocessors. This simulation is Freemate original based on previous computational contributions [refs].For 150 x 150 matrices imaging view setting takes about 5 seconds, and spatial-changes of imaging-set about 7 seconds. If 50x50 matrices are used, the time is reduced around 2 seconds.

## VIII. BRIEF MARKS OF F# FUNCTIONAL PROGRAMMING APPLICATIONS IN COMPUTATIONAL SIMULATIONS

F# programming, [73], a non-classic programming language, shows advantages and inconvenients to simulate some kind of formulation. This language, for instance, in a Visual Studio compiler, can download a number of packages to carry out several options to be included in the codes—and also interact with web information and html programming. Inconvenients, again, of F#, apart from cyber-security questionable use when programming design, are its limitation in numerical methods compared to other specific software, whether as it is a different construction sometimes simpler, whether in other cases results more complicated, related to other languages—namely the powerful-precise FORTRAN in numerical methods [37,56].

In the following, a hip implant extremely simple code is shown, [Casesnoves,2017], for a tentative program to be developed in double precision and more extensive features in F#. In addition, it is presented the F# interactive output at prompt, that gives the random simulation values of the program.

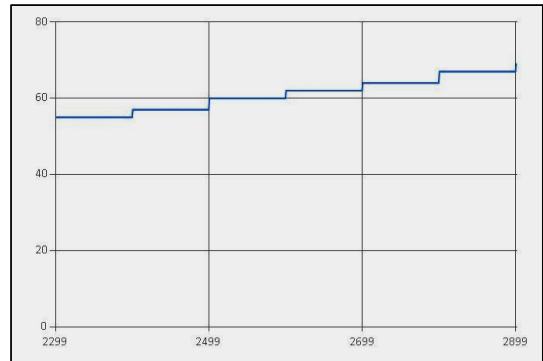


**Fig 18.-A** F# chart developed with functional programming software in visual studio for a hip implants erosion model simulation. It is seen sharply the good image given by the compiler, although other types of programming software facilities could make better and faster plots without downloading chart-F# specific packages. This program was developed in F# by the authors originally [Casesnoves,2016].

```

open FSharp.Charting
open FSharp.Charting.ChartTypes
//approximate value of grup of constants.We simulate a chart of
implant wear with loads from 2300 to 2900
//taking k value approximated as 37e-2. X axis is load and y axis is
wear mm3 after 10e6 cycles of
//biomechanical movement and we remark that this is a simulated
approximation according to references values studied.
Chart.Line([for x in 2300 .. 2900 -> x,(x/100)*12*2/10]).ShowChart()

//
let randomPoints = [for i in 0 .. 1000 -> rand(), rand()]

Chart.Point randomPoints

let randomTrend1 = [for i in 10.0 .. 0.1 .. 200.0 -> i, 5.1*sin i *
rand()]/velocity
let randomTrend2 = [for i in 10.0 .. 0.1 .. 10.0 -> i, sin i *
rand()]/density

```

**Fig 19.-A** F# simple code to generate random hip implant simulation, for further improvements in formul and double-precision. It was developed with functional programming software in visual studio for model simulation.It is seen sharply in previous picture the good image given by the prompt interactive, although other types of programming software facilities could make better windows and faster debugs. This program was developed in F# by the authors originally [Casenoves,2016].

```

val randomTrend1 : (float * float) list =
[(10.0, -0.140462546); (10.1, -2.293313682); (10.2, -0.4796590218);
(10.3, -2.565416881); (10.4, -3.606794148); (10.5, -2.266275941);
(10.6, -3.395426854); (10.7, -3.575901385); (10.8, -4.231986696);
(10.9, -2.471837757); (11.0, -4.917858253); (11.1, -1.521487212);
(11.2, -3.408112815); (11.3, -4.787778867); (11.4, -3.27653312);
(11.5, -3.014259536); (11.6, -2.358532016); (11.7, -3.058279046);
(11.8, -1.725775824); (11.9, -1.913584685); (12.0, -1.997005739);
(12.1, -2.074145695); (12.2, -1.627197885); (12.3, -0.7537396874);
(12.4, -0.2311859042); (12.5, -0.2119616309); (12.6, 0.1217366107);
(12.7, 0.5814583174); (12.8, 0.1765334274); (12.9, 1.4074383317);
(13.0, 1.451865481); (13.1, 2.394991471); (13.2, 1.429399311);
(13.3, 3.175968384); (13.4, 0.78170315); (13.5, 3.459728222);
(13.6, 1.188891998); (13.7, 3.893001325); (13.8, 2.549692091);
(13.9, 0.2632960671); (14.0, 0.3871546167); (14.1, 2.572510299);
(14.2, 1.413911938); (14.3, 4.93114415); (14.4, 1.78025936);
(14.5, 4.518372979); (14.6, 3.205197617); (14.7, 3.445987855);
(14.8, 3.587155339); (14.9, 0.7329472398); (15.0, 0.9765795428);
(15.1, 1.060163802); (15.2, 2.307318118); (15.3, 1.762342793);
(15.4, 0.6408115451); (15.5, 0.1538954116); (15.6, 0.4554263128);
(15.7, 0.0232679747); (15.8, -0.1788710209); (15.9, -0.2241753176);
(16.0, -1.167613296); (16.1, -1.51640736); (16.2, -1.409758032);
(16.3, -0.576836707); (16.4, -2.633927112); (16.5, -0.1485404028);
(16.6, -3.28121609); (16.7, -3.212352085); (16.8, -3.479961159);
(16.9, -4.050878599); (17.0, -1.979813082); (17.1, -3.610775974);
(17.2, -1.297272757); (17.3, -2.217823597); (17.4, -2.68504735);
(17.5, -1.119521787); (17.6, -3.032619744); (17.7, -4.23063458);
(17.8, -0.884402902); (17.9, -1.351877714); (18.0, -3.52988045);
(18.1, -3.165478399); (18.2, -2.68622658); (18.3, -2.527956556);
(18.4, -0.773001439); (18.5, -0.5477665466); (18.6, -1.250058038);
(18.7, -0.457750870); (18.8, -0.1302467619); (18.9, 0.01555350602);
(19.0, 0.01155143649); (19.1, 0.882452538); (19.2, 0.8071007276);
(19.3, 0.664913319); (19.4, 0.6879986614); (19.5, 0.2876200617);
(19.6, 3.198532586); (19.7, 0.2878878552); (19.8, 0.7074857359);
(19.9, 1.418490008); ...]
val randomTrend2 : (float * float) list = [(10.0, -0.1776498577)]

```

**Fig 20.-A** F# simple output in interactive from the previous program [Casenoves,2017]. Data in prompt is well-presented and storage of files and execution usually does not show too many complications compared to other software programming in numerical methods, such as Freemat.

## IX. INTEGRAL-DIFFERENTIAL MATHEMATICAL MODEL CONSTRUCTION FOR WC-Co REINFORCED METAL COATINGS, EXPERIMENTAL-THEORETICAL METHOD

This section is focused on general fundamental steps to develop a mathematical model starting from experimental and heading towards the theory. Biomedical implants are manufactured with a large type of materials. Among them, metal coatings constitute an important variety used in manufacturing both in medical devices and internal/external biomedical implants, subjected to histocompatibility always—provided that this condition is applicable on contact tissue-material surfaces, particularly well-accomplished by titanium. There are two essential requirements for biomaterials, specially when implants are internal, namely, biocompatibility or histocompatibility, and biodegradability [8]. Additional desirable/compulsory properties are appropriate porosity, bioactivity, mechanical strength, adequate surface finish, and easily manufactured and sterilization conditions. Among this kind of biomaterials, the promising shape memory/development, and geometrical-conformally-adapted materials are creating a new specific branch of applications in biomedical engineering.

Recently, [8], reinforcements are used to increase titanium hardness, such as titanium boride in a titanium matrix—explicitly Ti-TiB<sub>w</sub>. Published results show that this kind of composite is not cytotoxic and has an acceptable hemolysis level.

The material of this model-example, composite Fe-based hardfacings with coarse WC-Co reinforcement types are used in industry but closely similar materials are manufactured also for medical devices with the constraint of histocompatibility when they are internal ones.

In this example the model construction in its principal outlines is detailed for Fe-based self-fluxing alloy (FeCrBSi) with spherical WC-Co hardmetal reinforcement. In biomedical implants this kind of composites are used but with histocompatible metal titanium, when the implant is internal [8].

Conceptual mathematical an analytic geometry problem in this kind of coatings is the non-constant

hardness distribution, phenomena that occurs in the matrix, hardface, and at interface—absolutely necessary to remark in this point that interface constitutes an essential part linked to the binding between matrix and reinforced hardface. This implies that if hardness is not constant, wear is not also. Therefore, the material modelling is more complicated. What is meant here is a method to construct a model that can be generalized with different equations/algorithms.

Taavi Simson and Colls, Tallinn University of Technology Lab]. The matrix average distances from the minimum hardness points to the borders of hardface are measured randomly using images and, for instance, Monte-Carlo Method [Casesnoves, 2017, refs]. Images of composite obtained with scanning electron microscope (SEM) EVO MA-15 at Tallinn University of Technology Lab. Interface crown is sharply seen at the right-upper corner inset. Although minimum is coating-surface extension, interface is essential in the binding and cohesion of the composite.

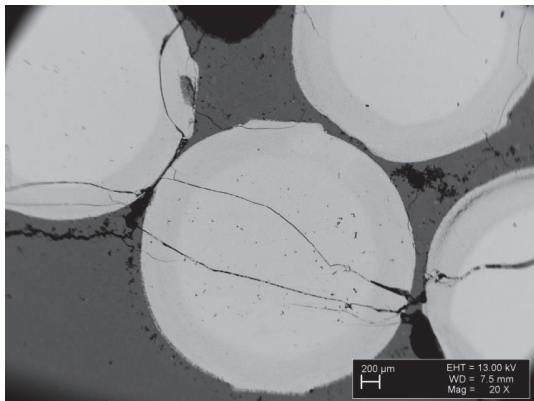


**Fig 19.**-Image of matrix, hardface and transition zone in composite Fe-based hardfacings with coarse WC-Co reinforcement [Andrei Surzhenkov, Taavi Simson and Colls, Tallinn University of Technology Lab]. Images of composite obtained with scanning electron microscope (SEM) EVO MA-15 at Tallinn University of Technology Lab.

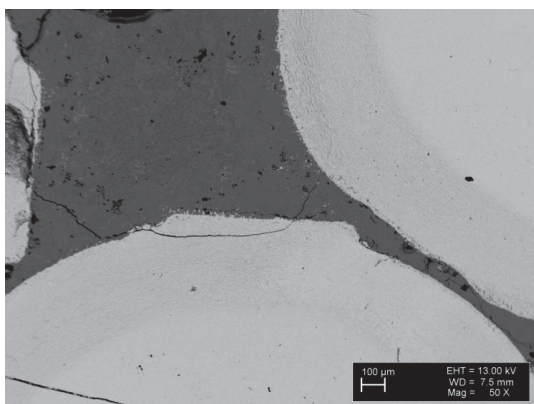


**Fig 20.**- Enhanced image of matrix, hardface and transition zone in composite Fe-based hardfacings with coarse WC-Co reinforcement [Andrei Surzhenkov,

**TABLE IV**

| Type of component | Type of material                      | Chemical composition [wt.%]  |
|-------------------|---------------------------------------|--|
| Matrix            | Fe-based self-fluxing alloy (FeCrBSi) | 13.72 Cr, 2.67 Si, 0.32 Mn, 2.07 C, 0.02 S, 3.40 B, 6.04 Ni, bal. Fe |
| Reinforcement     | Spherical WC-Co hardmetal             | 85 WC, 15 Co   |

**Table 4** .-Detailed composition of the laboratory sample for modeling construction. The geometry of the reinforcement in this case is spherical, not angular. The spherical hardmetal size in this manufactured composite can be considered rather high, which is a geometrical advantage for the model construction.

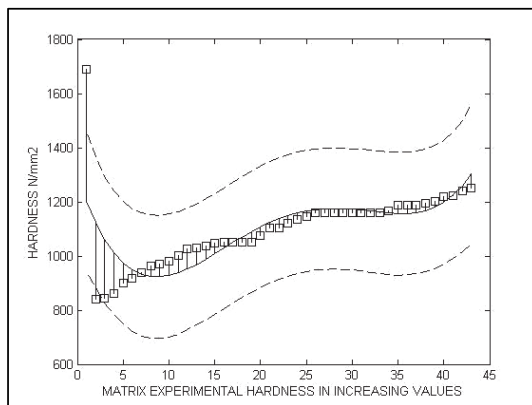


**Fig 21.**-Pictured, Matlab 4-degree-polynomial numerical fitting with error plotting intervals of matrix experimental hardness in intervals of average distance from center of matrix to the next hardface spherical spot. This is calculated with random measurements

over the ultramicroscopic images instead the classical Weibull distribution [1,9,23,37]. It is seen sharply the acceptable goodness of the approximation, with the exception of the beginning of the curve—these extremal-dispersed values are usually discarded for model construction. In the x axis 43 increasing measurements that correspond each one to an statistically distance calculation from matrix center geodesic to interfaces around hardfaces.

**TABLE V**

| EXAMPLES OF EXPERIMENTAL DATA FOR MODEL DEVELOPMENT [TALLINN UNIVERSITY OF TECHNOLOGY LABORATORY, ESTONIA] |                |
|--|----------------|
| NUMBER OF MEASURE  | HARDNESS [MPa] |
| 1  | 689            |
| 2  | 841            |
| 4  | 861            |
| 30   | 1161           |
| 35   | 1189           |

**Table 5** .-Experimental data examples of matrix hardness carried out at Tallinn University of Technology Mechanics Lab. These 43 values were implemented to construct the mathematical model for matrix.

The mathematical development begins with the assumption that hardness is not constant as a result of the polynomial fitting of data of Fig , and its equation related to distance reads,

$$H(s) = 10^3 \cdot [(-0.0003)x^3 + (0.0094)x^2 + (-0.1050)x + 12984];$$

Residual of numerical fitting = 657.6564 ;

Therefore, for the model in matrix, it is straight to guess that hardness in classical hip implants, with similar materials, has a nonlinear distribution according to distance from WC-Co reinforcement spherical spots. The formulation gets modified,

$$W = K \cdot (L X)/H(s) ;$$

As a first approximation, considering K, L, and X constants, it is reasonable to take derivatives of wear respect to distance, [Casesnoves, Integral-Differential model, 2017], reads,

$$\frac{dw}{ds} = \frac{dw}{dH} \times \frac{dH}{ds} = (KLX) \times \left( \frac{-1}{H^2(s)} \right) \times \left( \frac{dH(s)}{ds} \right);$$

integrating along all matrix average length,

$$\int_{w_0}^w dw = \int_{s_0}^s (KLX) \times \left( \frac{-1}{H^2(s)} \right) \times \left( \frac{dH(s)}{ds} \right) ds;$$

Eqs [10]

Which is the total wear for all the matrix length, and a part of the total wear of the composite metal. This type of numerical-differential modelling, is applicable on Composite Fe-based Hardfacings with coarse WC-Co reinforcement, and also in titanium-varieties histocompatible coatings, usually Titanium-Boride composites, of this material type for hip implants. What is clear, as guessed, is the development from the experimental to the theoretical modelling of this rather difficult metals given their complex chemical composition, increased for the geometrical-spatial distribution of every constituent.

The construction of the model follows straightforward from this equation since the hardness at matrix is a continuous and differentiable function, instead a series of discrete values. Given the Hardness Function, the insertion of the function into any other suitable model of wear, subject to constraints, constitutes a new method for erosion rate determination.

The evolution of this model in its differentiable equation will be continued in next contributions since the development to obtain useful calculations could be extent and its applications at least substantial.

## X. DISCUSSION AND CONCLUSIONS

An objective analysis of mathematical models for erosion, corrosion, and tribocorrosion in bioengineering was presented with introductory ideas and appendices of general mechanical engineering tribology models. The evolution of the concept of investigation method in Biotribology was enlightened and justified.

The mathematical development of a model for the matrix of a composite metal Fe-based coating was

determined and sharply explained with mathematical formulation, lab images, and explicit equations—Integral-Differential Model. Graphical Optimization Methods, with/without constraints in region of interest, was explained and linked to clear imaging-computational pictures and software details.

In summary, according to the volume of new research and innovative optimization methods presented, the advances of this study could be considered acceptable and well-backgrounded with special nonlinear optimization procedures.

## XI. ACKNOWLEDGEMENTS AND SCIENTIFIC ETHICS STANDARDS

TUT is gratefully acknowledged for all the facilities for research. This study was carried out, and their contents are done according to the European Union Technology and Science Ethics. Reference, 'European Textbook on Ethics in Research'. European Commission, Directorate-General for Research. Unit L3. Governance and Ethics. European Research Area. Science and Society. EUR 24452 EN. This research was completely done by the authors, the software, calculations, images, mathematical propositions and statements, reference citations, and text is original for the authors. The research publication in United States is exclusive. This article contains also unique numerical data and special new-improved images. The principal sketches were made originally, and the figures, tables, or data that corresponds/developed-from previous papers is properly clarified. When anything is taken from a source, it is adequately recognized [58]. Ideas from previous publications were emphasized due to a clarification aim.

## XII. REFERENCES

- [1] Kulu, P, Zimakov, S. Wear resistance of thermal sprayed coatings on the base of recycled hardmetal. *Surface and Coatings Technology* 130 2000 46-51.
- [2] I. Hussainova, On micromechanical problems of erosive wear of particle reinforcement composites, *Proc. Estonian Acad. Sci. Eng.* 11 (2005) 46-58.
- [3] P. Kulu, R. Tarbe, A. Zikin, H. Sarjas, A. Surženkov, Abrasive wear resistance of recycled hardmetal reinforced thick coating, *Key Eng. Mat.* 527 (2013) 185-190.
- [4] T. Simson, P. Kulu, A. Surženkov, R. Tarbe, M. Viljus, M. Tarraste, D. Goljandin, Optimization of reinforcement content of powder metallurgy hardfacings in abrasive wear conditions, *P. Est. Acad. Sci.* 65 (2016) 90-96.
- [5] A. Surzhenkov, R. Tarbe, M. Tarraste, T. Simson, M. Viljus, P. Kulu, Optimization of hardmetal reinforcement content in Fe-based hardfacings for abrasive-impact wear conditions, *Proc. Eur. Conf. Heat Treat. 2016 and 3rd Int. Conf. Heat Treat. Surf. Eng. Automotive Applications*, 11–13 May 2016, Prague, Czech Republic.
- [6] Antonov, M, Renno Veinthal Elina Huttunen-Saarivirta Irina Hussainova, Ahto Vallikivi, MartynasLelis, Jelena Priss. 'Effect of oxidation on erosive wear behaviour of boiler steels'. *Tribology International* 68 (2013) 35–44.
- [7] Matthews, S Franklin and K Holmberg.' Tribological coatings: contact mechanisms and selection'.
- [8] Bartolo, P and collaborators. Biomedical production of implants by additive electrochemical and physical processes. *CIRP Annals - Manufacturing Technology*.2012.
- [9] Kleis, I, Kulu, P. *Solid Particle Erosion*. Springer. 2008.
- [10] Ots, A. *Oils Shale Combustion*. Trukitud Tallinna Raamatrutukikojas. Tallinn 2004.
- [11] Shin J, Jeon Y, Maeng, Kim, J. Ro. Analysis of the dynamic characteristics of a combined-cycle power plant. *Energy* 27 (2002) 1085–1098.
- [12] Casesnoves, F. 'Computational Simulations of Vertebral Body for Optimal Instrumentation Design'. *ASME Journal of Medical Devices (Research Paper)*. Author: F Casesnoves .*Journal of Medical Devices*. June 2012. Volume 6. Issue 2/021014.11 pages.<http://dx.doi.org/10.1115/1.4006670>.
- [13] Ožbolt J; Sola E and Balabanić G. Accelerated Corrosion of Steel Reinforcement in Concrete: experimental Tests and Numerical 3D FE Analysis. *ASCE Conference Proceedings. Concreep 10*.
- [14] Chen Q, Li D. Computer simulation of solid-particle erosion of composite materials. *Wear* 255 (2003) 78–84.
- [15] Mackerle J. Finite-element analysis and simulation of machining: a bibliography (1976–

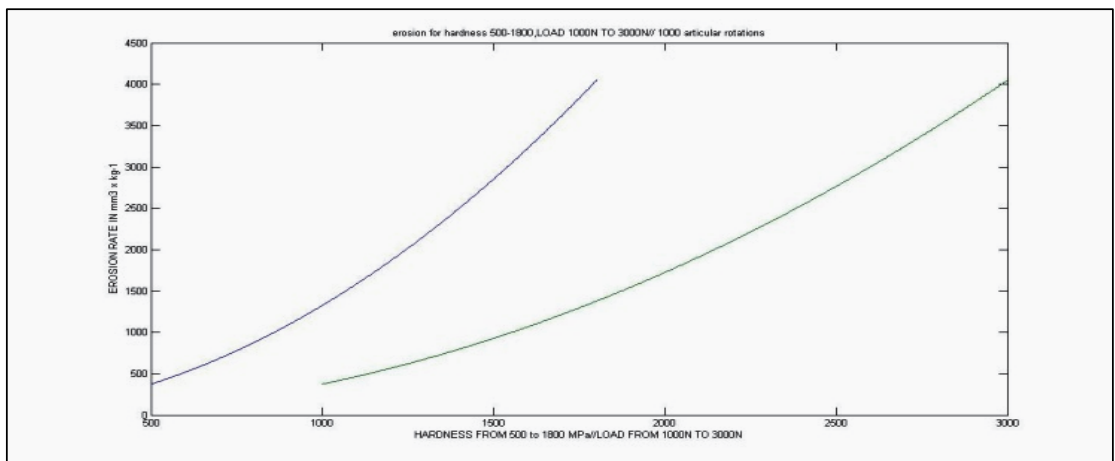
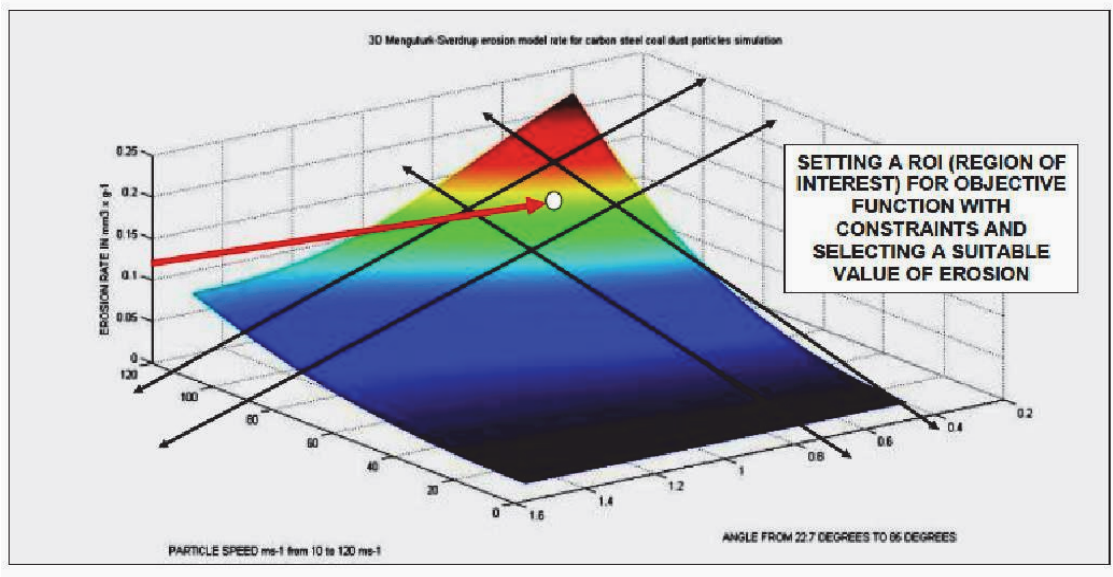
- 1996). *Journal of Materials Processing Technology* 86 (1999) 17–44.
- [16] Antonov, M. Assessment of Cermets Performance in Aggressive Media. Doctoral Dissertation, thesis. thesis on mechanical and instrumental engineering e29.TUT Press. 2006.
- [17] Antonov, Renno, and collaborators. Effect of oxidation on erosive wear behavior of boiler steels.
- [18] Irina Hussainova Jakob Kubarsepp Igor Shcheglov. Investigation of impact of solid particles against hardmetal and cermet targets. *Tribology International* 32 (1999) 337–344.
- [19] Hussainova, Jakob Kubarsepp, Juri Pirso. Mechanical properties and features of erosion of cermets.
- [20] Antonov, Hussainova, and collaborators. Effect of temperature and load on three-body abrasion of cermets and steel.
- [21] Antonov, M Remigiusz Michalczewski, Rihard Pasaribu and Witold Piekoszewski. Comparison of a tribological model and real component test methods for lubricated contacts. *Estonian Journal of Engineering*, 2009, 15, 4, 349–358.
- [22] Shimizu K, Noguchi T, Seitoh H, Okadab M, Matsubara Y. FEM analysis of erosive wear. *Wear* 250 (2001) 779–784.
- [23] Abramowitz, Stegun. *Handbook of Mathematical Functions*. Applied Mathematics Series. 55.1972.
- [24] Nielsen J. Heuristic Evaluation. Usability Inspection Methods. Chapter 2.
- [25] Machery E. Concept empiricism: A methodological critique. *Cognition* 104 (2007) 19–46.
- [26] ElTobgy M, Ng E, Elbestawi M. Finite element modeling of erosive wear. *International Journal of Machine Tools & Manufacture* 45 (2005) 1337–1346.
- [27] Ashby F. *Materials Selection in Mechanical Engineering*. Butterworth-Heinemann.2000.
- [28] Crocker, L. A review of current methods for modeling erosive wear. NPL Report. 2011.
- [29] Li L, Li D. Simulation of corrosion-erosion of passive metals using a micro-scale dynamical model. *Wear* 271 (2011) 1404–1410.
- [30] Melchers R. Mathematical modelling of the diffusion controlled phase in marine immersion corrosion of mild steel. *Corrosion Science* 45 (2003) 923–940.
- [31] Tribocorrosion: research, testing, and applications. Selected Technical Papers. International Standards Worldwide. ASTM, STP#1563.
- [32] Creager M, and Paris C. Elastic field equations for blunt cracks with reference to stress corrosion cracking.
- [33] IMechE. The reliability of mechanical systems. Second Edition. Mechanical Engineering Publications Ltd. Institution of Mechanical Engineers., London.1994.
- [34] Todinov, M. *Reliability and Risk Models*. Wiley. 2005.
- [35] Luenberger, G D. *Linear and Nonlinear Programming*. Fourth Edition. Springer.2008.
- [36] Casesnoves, F. 'Large-Scale Matlab Optimization Toolbox (MOT) Computing Methods in Radiotherapy Inverse treatment Planning'. High Performance Computing Meeting. Nottingham University. January 2007.
- [37] Casesnoves, F. 'A Monte-Carlo Optimization method for the movement analysis of pseudo-rigid bodies'. 10th SIAM Conference in Geometric Design and Computing, Texas, San Antonio, USA. Contributed Talk. November 2007.
- [38] Derrick O. Njobuenwu, Michael Fairweather. Modelling of pipe bend erosion by dilute particle suspensions. *Computers and Chemical Engineering* 42 (2012) 235–247.
- [39] Casesnoves, F. 'Applied Inverse Methods for Deformable Solid Dynamics/Kinematics in Numerical Reuleaux Method (NRM)'. INTERNATIONAL JOURNAL OF NUMERICAL METHODS AND APPLICATIONS. VOLUME 9(2) 2013 .Pages 109-131. Peer-Reviewed International Mathematical/Computation Journal Article. print/Online. <http://www.pphmj.com/abstract/7688.htm>. This article is specially innovative in Inverse Problems applications for deformable solids kinematics/dynamics, further publications are included in United States Congress Library [ref 64] and Numerical Reuleaux Method is accepted by scientific community as an innovative dynamics method in deformable solids with mechanical, biomechanical and aerospace applications. New applications of this method will be probably found significantly in future.

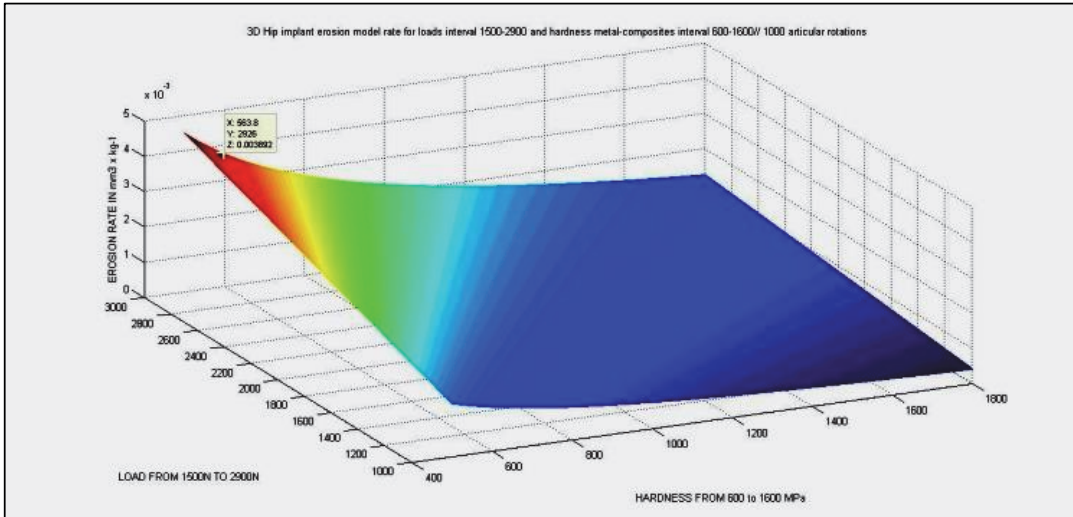
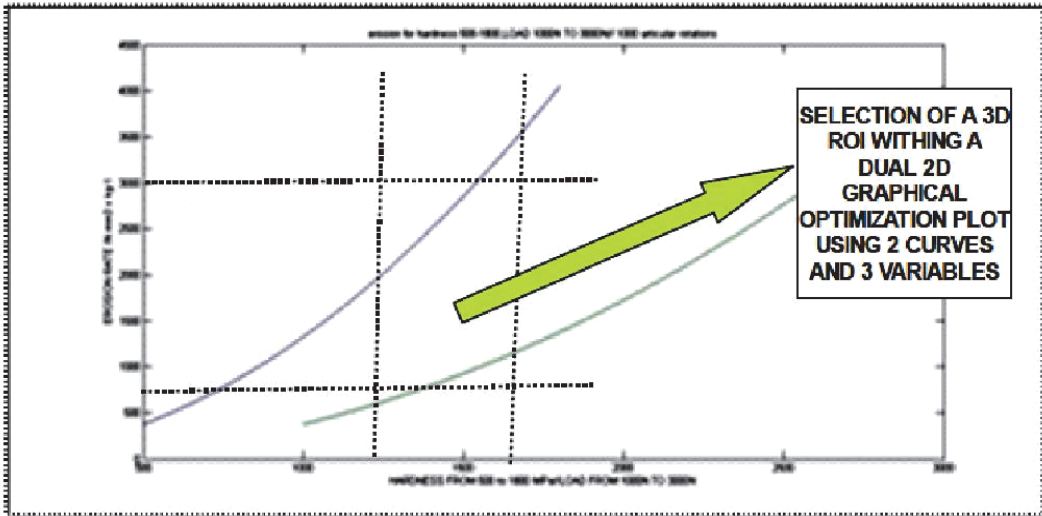
- [40] Mayusama, F. 'History of Power Plants and Progress in Heat Resistant Steels'. International Journal of the Iron and Steel Institute of Japan ISIJ International, Vol. 41 (2001), No. 6, pp. 612–625.
- [41] Duan, V. Y. Karelin. abrasive erosion and corrosion of hydraulic machinery. world Scientific Publishing Co. Pte. Ltd.2002.
- [42] Wood R J. The sand erosion performance of coatings. Materials and Design 20 \_1999. 179-191.
- [43] Martin, J. Materials for Engineering. 4<sup>th</sup> Edition. CRC Press.2006.
- [44] Lewis, R, Oloffson, U. Wheel Rail Interface Handbook. CRC Press. 2009.
- [45] Mellor, B G. Surface coatings for protections against wear. CRC Press. Woodhead Publishing in Materials. 2006.
- [46] Woytowitz ,P, Richman R. Modeling of damage from multiple impacts by spherical particles. Wear 233–235 .999. 120–133.
- [47] Li D, Elalem K, Anderson M, Chiovelli S. A microscale dynamical model for wear simulation. Wear 225–229 .1999. 380–386.
- [48] Matthews A, Franklin S, and Holmberg K. Tribological coatings: contact mechanisms and selection. J. Phys. D: Appl. Phys. 40 (2007) 5463–5475.
- [49] Liao H, Normand B, Coddet C. Influence of coating microstructure on the abrasive wear resistance of WC/Co cermet coatings. Surface and Coatings Technology 124 (2000) 235–242.
- [50] Melchers R, Jeffrey R. Early corrosion of mild steel in seawater. Corrosion Science 47 (2005) 1678–1693.
- [51] 'European Textbook on Ethics in Research'. European Commission, Directorate-General for Research. Unit L3. Governance and Ethics. European Research Area. Science and Society. EUR 24452 EN.
- [52] Galante, J, Rostoker, W. Wear in Total Hip Prostheses. Acta Orthopaedica Scandinavica. 43:sup145, 1–46, DOI: 10.3109/ort.1972.43.suppl-145.01.
- [53] L. Mattei, F.DiPuccio, B.Piccigallo, E.Ciulli . Lubrication and wear modelling of artificial hip joints: A review. Tribology International 44 (2011) 532–549.
- [54] Casesnoves, F.. 2016. Exact Integral Equation Determination with 3D Wedge Filter Convolution Factor Solution in Radiotherapy. Series of Computational-Programming 2D-3D Dosimetry Simulations. International Journal of Scientific Research in Science, Engineering and Technology (ijsrset.com). 2016 IJSRSET | Volume 2 | Issue 4 | Print ISSN: 2395-1990 | Online ISSN : 2394-4099 Themed Section: Engineering and Technology.
- [55] Casesnoves, Antonov, Kulu. Mathematical Models for Erosion and Corrosion in Power Plants. A Review of Applicable Modelling Optimization Techniques. 2016// 57th International Scientific Conference on Power and Electrical Engineering of Riga Technical University (RTU CON). 2016.
- [56] Casesnoves, F. 1.-'Theory and Primary Computational Simulations of the Numerical Reuleaux Method (NRM)',Casesnoves,Francisco. Published in International-Scientific Peer-Reviewed Journal, International Journal of Mathematics and Computation. <http://www.ceser.in/ceserp/index.php/ijmc/issue/view/119>.Volume 13,Issue Number D11.Year 2011.Peer reviewed paper, both in Print and Online. 23 pages with extent mathematical Formulation, Proofs and References.
- [57] Z.M. Jin, M. Stone, E. Ingham, J. Fisher. Mini-symposium: biomechanics for the frcs orth exam.(v) biotribology. Current Orthopaedics (2006) 20, 32–40.
- [58] Lucien Reclaru, Pierre-Yves Eschler, Reto Lerf, Andreas Blatter. Electrochemical corrosion and metal ion release from Co-Cr-Mo prosthesis with titanium plasma spray coating. Biomaterials 26 (2005) 4747–4756.
- [59] L. Mattei, F.DiPuccio, B.Piccigallo, E.Ciulli. Lubrication and wear modelling of artificial hip joints: A review. Tribology International 44 (2011) 532–549.
- [60] J.-P. Hung, J. S.-S. Wu. A comparative study of wear behaviour of hip prosthesis by finite element simulation. Biomedical Engineering - Applications Basis & Communications, 2002, 14 (4), 139–148.
- [61] M.E. Müller. The benefits of metal-on-metal total hip replacements. Clinical Orthopaedics and Related Research, 1995, 311, 54–59.
- [62] S.C. Scholes, A. Unsworth, R.M. Hall, R. Scott. The effects of material combination and lubricant

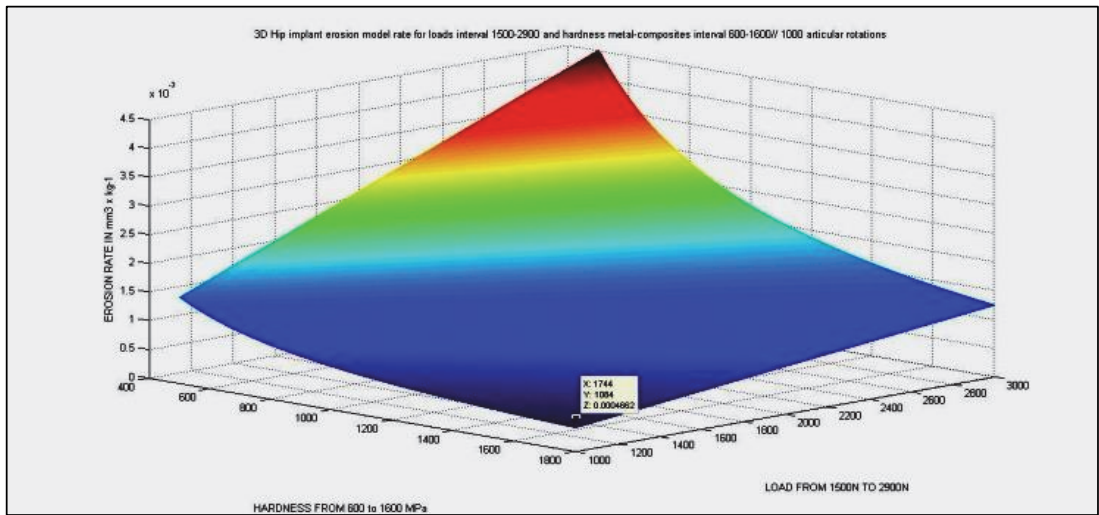
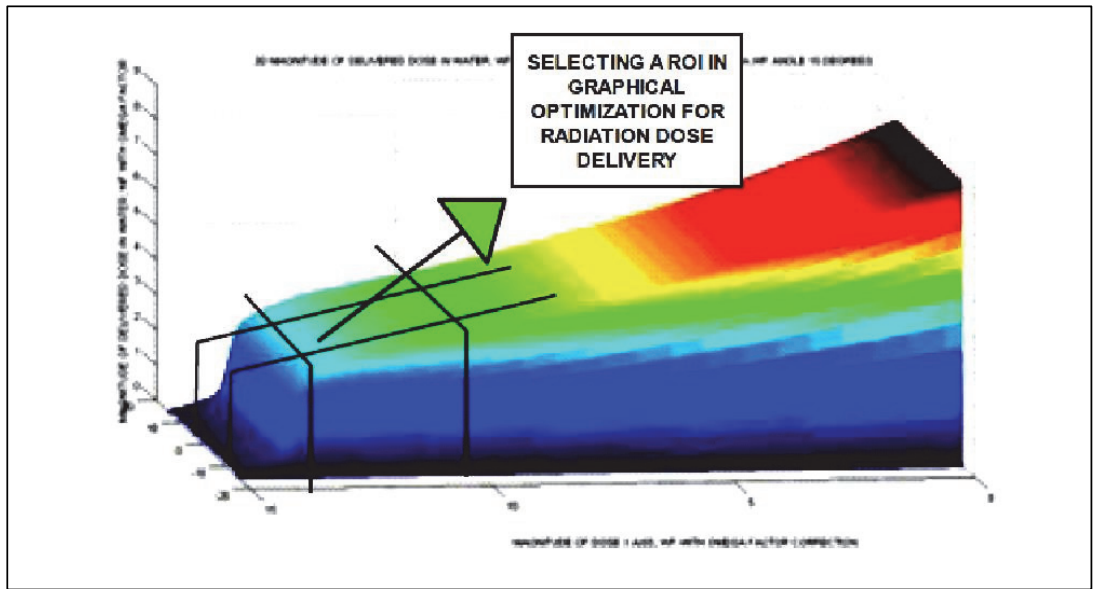
- on the friction of total hip prostheses. *Wear*, 2000, 241 (2), 209–213.
- [63] Srimongkol, S. A review of mathematical modeling in total hip replacement. *International Mathematical Forum*, Vol. 7, 2012, no. 52, 2561–2569.
- [64] D. Downson, F.C. Wang, W.Z. Wang, Z.M. Jin. A predictive analysis of long-term friction and wear characteristics of metal-on-metal total hip replacement. *Proceedings of the Institution of Mechanical Engineers, Part J: Journal of Engineering Tribology*, 2007, 221 (3), 367–378.
- [65] D. Downson, Z.-M. Jin. Metal-on-metal hip joint tribology. *Proceedings of the Institution of Mechanical Engineers, Part H: Journal of Engineering in Medicine*, 2006, 220 (2), 107–118.
- [66] M.A. Wimmer, J. Loos, R. Nassutt, M. Heitkemper, A. Fisher. The acting wear mechanisms on metal-on-metal hip joint bearings: in vitro results. *Wear*, 2001, 250 (1–2), 129–139.
- [67] Ali, M, Mao, K. Modelling of Hip Resurfacing Device Contact under Central and Edge Loading Conditions. *Proceedings of the World Congress on Engineering 2012 Vol III*.
- [68] P. Hung, C.-S. Shu, J.-H. Chen. The computer simulation of wear behaviour appearing in total hip prosthesis. *Computer Methods and Programs in Biomedicine*, 2003, 70, 81–91.
- [69] Telliskivi, T. Simulation of wear in a rolling-sliding contact by a semi-Winkler model and the Archard's wear law. *Wear* 256 (2004) 817–831.
- [70] F. Liu, I. Leslie, S. Williams, J. Fisher, Z. Jin. Development of computational wear simulation of metal-on-metal hip resurfacing replacements. *Journal of Biomechanics*, 2008, 41 (3), 686–694.
- [71] V. Saikko. A multidirectional motion pin-on-disk wear test method for prosthetic joint materials. *Journal of Biomedical Materials Research*, 1998, 41 (1), 58–64.
- [72] Casesnoves, F. Applied Inverse Methods for Optimal Geometrical-Mechanical Deformation of Lumbar artificial Disks/Implants with Numerical Reuleaux Method. 2D Comparative Simulations and Formulation. *Computer Science Applications*. Volume 2, Number 4, pp. 1-10. [www.ethanpublishing.com](http://www.ethanpublishing.com). This article is registered as original method published by Francisco Casesnoves in Philadelphia 2015 in United States Congress Library.
- [73] Daniel Jebaraja. F # Succintly, 17. SynCFusion. Technology Resource Portal. Apress.2009.

## APPENDIX 1

### NON-LINEAR OPTIMIZATION SIMULATUION SFOR BIOTRIBOLOGICAL AND MECHANICAL SYSTEMS AND INAGING ENHANCED PICTURES







**APPENDIX 2 PROGRAMMING SOFTWARE WITH NUMERICAL NONLINEAR OPTIMIZATION RESULTS COMPLEMENTED**

| <b>NON-LINEAR OPTIMIZATION NUMERICAL DATA FOR BIOMEDICAL/MECHANICAL TRIBOLOGY WEAR/EROSION MATHEMATICAL MODELS</b>      |   |  |                     |                         |  |
|---|---|--|---------------------|-------------------------|--|
| <b>MATLAB SUBROUTINES USED LSQNONLIN, FMINCON INTERIOR POINT AND ACTIVE SET ALGORITHMS, MATLAB OPTIMIZATION TOOLBOX</b> |   |  |                     |                         |  |
| <b>MODEL TYPE AND SIMULATION #</b>  | <b>NUMBER OF OPTIMIZATION VARIABLES</b> | <b>NUMBER OF RANDOM SIMULATED LAB MEASUREMENTS</b> | <b>SEARCH POINT</b> | <b>OPTIMAL SOLUTION</b> | <b>APPLIED DOUBLE PRECISION AND COMMENTS</b> |
| Hutchings   | 2, k v                                  | 50   | (0.2,10)            | 0.0003, 12.0            | N  |
| Hutchings   | 2, k v                                  | 100  | x=(0.2 ,10)         | 0.0005 9.9919           | N  |
| Hutchings   | 2, k v                                  | 10000  | x= (1, 14)          | 0.0003 13.8600          | N,running fast                               |
| Hutchings   | 2 k v                                   | 1000   | x=( 0.2, 10)        | 0.2821 0.4159           | N  |
| Hutchings   | 2 k v                                   | 1000   | x=( 0.3, 10)        | 0.2834 0.4159           | N  |
| Menguturk and Sverdrup  | 2, v, angle 25 degrees                  | 10000  | X=5                 | 138.4362                | N  |
| Menguturk and Sverdrup  | 2, v, angle 25 degrees                  | 1000   | X=5                 | 139.0728                | Y  |
| Menguturk and Sverdrup  | 2, v, angle 25 degrees                  | 10000  | X=1                 | 138.3685                | N, precision                                 |
| Menguturk and Sverdrup  | 2, v, angle 25 degrees                  | 10000  | X=4                 | 138.2630                | N  |
| hip metal implant   | 1, k, Hardness 350 MPa                  | 10000  | X=5                 | 5.5802e-04              | Y, search point not too much influence       |
| hip metal implant   | 1, k, Hardness 350 MPa                  | 10000  | X=2                 | 5.6087e-04              | Y  |
| hip metal implant   | 1, k, Hardness 350 MPa                  | 10000  | X=2.5               | 5.6087e-04              | N  |
| hip metal-coated implant $C_0C_RM_0$  | 1, k, Hardness 884 MPa                  | 10000  | X=5                 | 0.0014                  | N  |
| ceramic implant 2300  | 1, k, Hardness 2300 MPa                 | 10000  | X=4                 | 0.0037                  | N  |
| ceramic implant 2300  | 1, k, Hardness 2300 MPa                 | 10000  | X=7                 | 0.0037                  | N acceptable results                         |
| ceramic implant 2300  | 1, k, Hardness 2300 MPa                 | 10000 at interval [1,5]                            | X=7                 | 0.0368                  | N  |
| ceramic implant 2300  | 1, k, Hardness 2300 MPa                 | 10000  | X=6                 | 0.0368                  | N  |

**CONCLUSIONS:** Initially acceptable optimization results conditioned to further improvements, however further improvements will be done in next contributions.

## **Paper V**

Casesnoves, F., Surzhenkov, A. Inverse methods for computational simulations and optimization of erosion models in power plants. *IEEE Proceedings of RUTCON2017 Power Engineering Conference*. 2017, paper 139. (DOI:10.1109/RTUCON.2017.8125630. Electronic ISBN:978-1-5386-3846-0. USB ISBN: 978-1-5386-3844-6. ISBN: 978-1-5386-3847-7).



# Inverse Methods For Computational Simulations And Optimization Of Erosion Models In Power Plants

## A numerical-sufactal Nonlinear Optimization of Modelling

Francisco Casesnoves<sup>1\*</sup> MSc MD, Andrei Surzhenkov<sup>2</sup> PhD

<sup>1</sup>Computational Engineering Researcher, IEEE Individual Member, Tallinn University of Technology, Ehitajate tee 5, 19086 Tallinn, Estonia; [fricase@ttu.ee](mailto:fricase@ttu.ee) (corresponding author)

<sup>2</sup>Department of Mechanical and Industrial Engineering, Tallinn University of Technology, Ehitajate tee 5, 19086 Tallinn, Estonia

**Abstract**—Simulations and Linear/Nonlinear Optimization mathematical methods constitute presently the choice of preference in getting improvements for erosion and corrosion simulations/determinations in general tribology, biotribology and tribocorrosion. This criterion is also applicable for engineering-reliability functional efficacy/efficiency during energy-power plants lifetime—with important consequences in the probabilities of operating failure of power-plant. Their running essential parts study-control is carried out with the necessary tribotests for the definite validation of the models specifically considered in their mechanical-electromechanical-systems. In previous contributions, an extent review of erosion and corrosion models applicable on energy power plants machinery was presented. In this new contribution a subsequent research stage towards formal simulation and optimization of those models is shown. In other words, Inverse Applied Methods, carried out computationally, are used in modern mathematical approaches for accurate selection/fitting of the optimized modeling results, fact that happens in a large number of science-engineering branches, and also in energy power plants operation. Stepping forward in this research-line, this article deals with initial programming simulations series of selected model-formulations, and mathematical analysis in new graphical simulation-optimization methods. In doing so, subsequently nonlinear optimization programming techniques are developed, to conclude with the presentation of a hardface metal-coatings design for W-Co composites types. That model overview is related to experimental abrasive-erosion tribotests performed at laboratory. The deliberation of the second generation of functional tribology models was detailed with computational-mathematical scopes. Finally, an objective discussion of the numerical results and data/graphs series was presented in summary.

**Keywords**—*power engineering, functional power-plants, nonlinear optimization, inverse problems theory/applications, engineering reliability operational probabilities*

### I. INTRODUCTION AND BASIC CONCEPTS

The concept of Inverse Problems,(IP), became significantly important during the past century, and was extended to a large number of branches of science and engineering. In the past, trial and error methods were the main technique to improve or develop mathematical formulation. However, it was soon guessed/understood in practice that empirical data should be used to make the configuration of the mathematical model instead to adapt the formulation directly on the experimental measurements through successive proofs/intends. In plain

language, IPs abstract idea is applicable in most of the human/animal knowledge branches, namely, from science, engineering, economy, to philosophy or sociology. Any observer/electro-mechanical system is surrounded and continuously receiving signals, both mental (biological-cognitive case specifically) and physical, with amounts of information/data from an extensive number of sources. These intense flows/streams of information are formed by signals of different nature, from electromagnetic waves/fields to social structures, emotional perceptions, market-economy fluctuations, radiological imaging shapes for medical diagnosis, a chemical reaction at lab, an erosion experiment at lab, etc. Each one possesses an specific type of records. IPs technique rationale/consistence is based on the usage of this empirical data to perform an approximated analysis of the emitting real-source configuration/characteristics, and if it were possible, guess precise algorithms and computational analysis of them—which is done with applied mathematical methods usually. The obsolete, although not in all cases, rather complementary forward method, was to try in consecutive trials to check/validate any algorithm-functionality through the insertion of the received database within any kind of tentative equations.

In this situation of study advances, developed in XX Century yet, a number of algebraic methods arose to match large series of equations over the experimental database. The stage was similar, for illustrating the point with an instance, to XIX century, whith the high-level/complication-hurdles for the mathematical analysis in differential equations. That is, researchers focused all the effort to find exact/perfect analytical solutions, before the discovery of numerical methods that guided them to a useful technical saving time/work in applied mathematics.

Later on, the engineering and science mathematical formulation became so large and diverse that the algebraic methods by themselves appeared evidently to be insufficient to carry out accurate IP methods in practice—the computers were the necessary instruments to perform such a large-scale of computational work. Therefore, the development-route/history of IPs was linked since that stage to computational methods and extensive numerical analysis [1–4]. The amount of database necessary to develop new formulation in science and mathematical methods improvements was the rutinary work load in standard investigation. An important branch of mathematics, both

theoretical and applied, linked to the IPs theory, was the Optimization. Optimization methods have experienced an extent expansion all over any branches of engineering and technology, because the continuous requirement in research and industry is to obtain an accurate link between any model and the variable empirical data with/without direct application of IPs recipes. Therefore, all these concepts are specifically applicable on energy industry since power engineering constitutes a point of convergence for multidisciplinary branches of engineering.

In Power Engineering and Tribology, today, up to quarter of all the tube failures at the coal-fired power plants is caused by the erosion-corrosion wear at the elevated temperatures [5]. Tube replacement accounts for up to 75% of the total downtime of such plants, increasing the energy production costs up to 54 % [6]. The erosion action is due to the ash constituents, such as quartz ( $\text{SiO}_2$ ), corundum ( $\text{Al}_2\text{O}_3$ ) and iron oxide ( $\text{Fe}_2\text{O}_3$ ), whereas the most severe wear is caused by the first [7]. For the ash with a high quartz content, the gas flow velocities inside the tubes have to be limited to 12–13 m/s, despite the decrease in the power plant production efficiency (for a less erosive ash, the gas flow velocities of 18–20 m/s are allowed) [8]. In its turn, the corrosion component of the wear process is induced by the temperatures inside the tubes. The typical range is from 380 to 538 °C [9]. In addition to its absolute value, the cyclic character of the heating should be taken into account [10], as it may cause the spallation of the oxide films and thus accelerate the wear [7].

So far, the trial-and-error approach has been applied in the industry [9]. However, field tests are very expensive, take much time and are hard to track and evaluate [7]. Therefore it is important to develop mathematical models in order to estimate and prognosticate the erosion-corrosion rates.

This contribution deals with the subsequent steps following previous publications of mathematical models for power plants in erosion, corrosion, and tribocorrosion. A number of models have been optimized with computational software, and presented with database of laboratory description and a series of 2D-3D graphical works for sharp learning.

Results comprise mathematical formulation/models for erosion optimized, proof of fitting residuals, graphs of global minima of objective functions and 3D special graphical optimization. The complementary section of this paper was intended to explain a brief introduction to the new generation of mathematical modeling in engineering of general tribology, based on functional models.

## II. MATHEMATICAL-COMPUTATIONAL METHOD(S)

This study method(s) were focused on practical optimization and nonlinear inverse problems applications in erosion models useful for power plants with mechanical systems and machinery. The selected models are appropriate to be applied for wear, and abrasive wear in some components—and the most important in this study is the demonstration of the technique applicable to a large number of models.

In general, most of the tribological models, mainly for abrasive wear erosion, are nonlinear equations, since their

research origin had to be fitted on an extent empirical/experimental database. This fact has consequences in the choice of most appropriate subroutines for optimization. In this research some of them are implemented to obtain accurate optimization of models and their usage is sharply presented in numerical tabulation and 2D-3D graphical optimization images.

In other words, let's suppose that obtained laboratory measurements data,  $D_i$  are trustworthy statistically and the objective is to fix the optimal parameters of a selected model,  $M_i$ , by using IPs with nonlinear optimization methods. What is meant here is an extremely simple/basic example of the paper-standard methodology.

If those data numbers  $D_i$  were corresponding exactly to the model equation  $M_i$ , we would have the equality,

$$D_i = M_i \text{ (function of } x, y, z, \dots \text{ parameters of model),}$$

$x$  could be particle speed,  $y$  density of hardface, etc,

That is, for every measurement  $M_i$  inserted within the model equation, the exact result would be equal to  $D_i$ . However, this is totally irreal in engineering practice, power engineering included, that is, in the attempt to set the model, initially we get,

$D_i \neq M_i$  ; and it is strictly necessary to carry out approximations for  $x, y, z, \dots$  etc, so passing  $M_i$  on to left side,

$D_i - M_i \neq 0$ , as said,  $D_i$  are lab fixed numbers, and  $M_i = M_i(x, y, z, \dots \text{ parameters of model to be optimized})$ . Therefore, the very-basic IP methods, in plain language, is to make software/algorithms to find the solution of the equation

minimize,

$$\sum_{i=1}^N \|D_i - M_i(x, y, z, \dots)\|^2 \text{ ; with, } M = \text{selected model;} \quad (1)$$

with the objective to make,

$$D_i \cong M_i \text{ (approximately equal),}$$

and NOT  $D_i \neq M_i$

This example was intended as introductory illustration for sharp learning of the following research sections. The square power in this kind of formula ( $L_2$  Norm formally) is done, among many mathematical-optimization reasons, to guarantee all the curves to be at the positive quadrants in 2D and 3D.

## III. COMPUTATIONAL-PROGRAMMING INVERSE NONLINEAR OPTIMIZATION RESULTS

The simulations and optimization series of several models are included in this section. Each model simulation one has the same structure, namely, numerical simulation, graphical simulation, and nonlinear optimization. Experimental values are taken from Tallinn University of Technology (TUT) and are real—sometimes approximations are necessary. The mathematical-computational designed method for showing inverse nonlinear optimization and 3D-Graphical Nonlinear

Optimization/simulations, is almost equal for all the model equations selected. What is meant, and important, is the general methodology, which is more significant than the type of models selected applicable for power plants erosion/corrosion. The Hutchings model originally was designed for plastic deformation. There is a number of formulas related to Hutchings model, from simplest to the most complicated [11]. The initial formula to be simulated [12], for the sake of sharpness, is

$$E = \frac{K\rho U^2}{2H} \tag{2}$$

where  $\rho$  is the density of the material being eroded,  $U$  is the initial particle velocity and  $H$  is the target surface hardness.  $K$  represents the fraction of material removed from the indentation as wear debris and is also known as the wear coefficient. What is going to be optimized at first is the value of  $K$ , that can be interpreted as a measure of the efficiency of the material removal process. In other words, the first step is to determine the optimal value of  $K$  for a random range around an interval of experimental measurements of the composite material (70 vol.% FeCrSiB, 30 vol.% WC-Co; Table 1) based on lab tribotests of TUT. That is direct application of Inverse Methods. The second step is to simulate the model for a range of hardness and impact velocities in interval around the experimental velocities of abrasive impact particles. All this data is set in Table 2. The objective function is a multiobjective least squares with  $L_2$  norm. The experimental hardness is set for optimization (31 measurements), and the  $K$  wear coefficient is the variable to be determined.

TABLE I

**Table 1.-**Composition of alloy-reinforced experimental samples whose data was implemented for optimization of  $K$  wear coefficient in Eq. 2.

| COMPOSITION [VOL.%]  | REINFORCEMENT SHAPE |
|----------------------|---------------------|
| 70 FeCrBSi, 30 WC-Co | Spherical           |
| 50 FeCrBSi, 50 WC-Co | Spherical           |

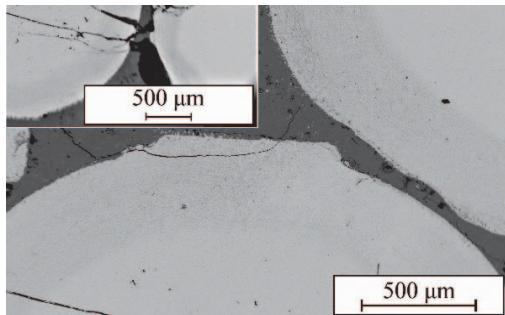


**Figure 1.** Microstructure of the studied hardfacing (50 vol.% spherical WC-Co reinforcement). The numerical hardface data that was implemented in Eqs. 1,2 for optimization corresponds to this kind of material.

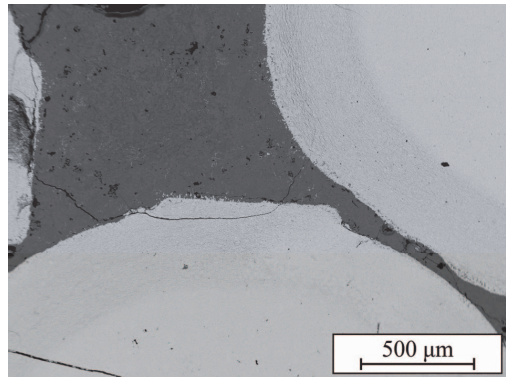


**Figure 2.** Microstructure of the studied hardfacings (50 vol.% WC-Co reinforcement; reinforcement-matrix view). The numerical hardface data that was implemented in Eqs. 1,2 for optimization corresponds to this kind of material.

TABLE II

| EXAMPLES OF EXPERIMENTAL DATA FOR MODEL DEVELOPMENT |  |   |
|---|--|---|
| NUMBER OF MEASUREMENTS (TOTAL 31)                   | HARDNESS [10×MPa]                                  |   |
| 1   | 1653   |   |
| 2   | 1653   |   |
| 16  | 1881   |   |
| 22  | 1954   |   |
| 29  | 2060   |   |
| EXPERIMENTAL LAB DATA FOR OPTIMIZATION              | wear rate<br>3 mm <sup>3</sup> /kg<br>(v = 40 m/s) | wear rate<br>18 mm <sup>3</sup> /kg<br>(v = 80 m/s) |

**Table 2.-** Numerical values of hardface hardness and wear rates from experimental measurements (70 vol.% FeCrSiB, 30 vol.% WC-Co).

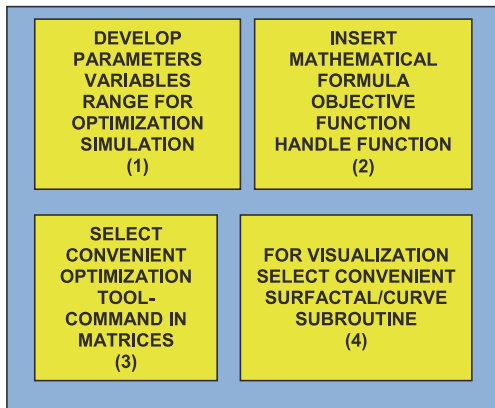


Diagram 1.-Flow chart of a graphical optimization program (basic).

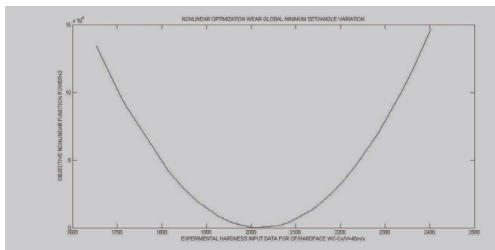


Figure 3.-Objective function (OF) nonlinear optimization results for Table 1 and Eq. 2 model, Matlab 2009-12. The impact velocity is 40 m/s. Results are acceptable with a Global Minimum sharply determined and running time is lower than a second.

TABLE III

| SEARCH POINT | OPTIMAL K/<br>HARDNESS VALUE<br>(INVERSE METHOD)<br>V = 40 m/s                                   | RESIDUAL OF<br>OBJECTIVE<br>FUNCTION (OF) |
|--------------|--|---|
| X=1          | 0.5297/2008  | 1.4135e+3                                 |
| X=5          | 0.5297/2008  | 1.4135e+3                                 |
| X=20         | 0.5297/2008  | 1.4135e+3                                 |
| COMMENTS     | Acceptable result for optimization low residual of OF global minimum exact for any search point. |   |

Table 3.-Numerical data that was obtained from nonlinear optimization of Eq. 2.

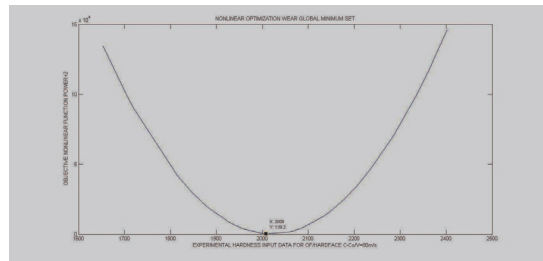


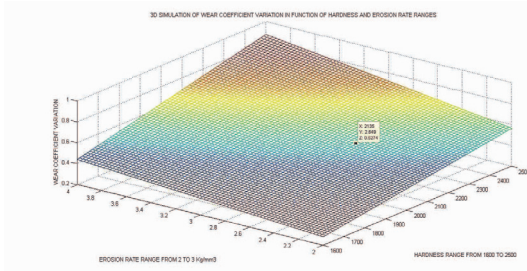
Figure 4.-Objective function (OF) nonlinear optimization results for Table 1 and Eq. 2 model, Matlab 2009-12. The impact velocity is 80 m/s. Results are acceptable with a Global Minimum sharply determined and running time is lower than a second.

TABLE IV

| SEARCH POINT | OPTIMAL K/<br>HARDNESS VALUE<br>(INVERSE METHOD)<br>V = 80 m/s  | RESIDUAL OF<br>OBJECTIVE<br>FUNCTION (OF) |
|--------------|---|---|
| X=20         | 0.7945/2008   | 1.6135e+3                                 |
| X=-1         | 0.7945/2008   | 1.4735e+3                                 |
| COMMENTS     | Acceptable result for optimization low residual of OF global minimum exact for any search point, even negative points |   |

Table 4.-Numerical data that was obtained from nonlinear optimization of Eq. 2 (erodent particle velocity v = 80m/s).

The subsequent simulations are intended to verify numerically the goodness of the K wear coefficient that was obtained by optimization, (firstly for v = 40 m/s, and then for v = 80 m/s). This is performed with software for 3D graphical simulation/optimization. In Figure 3 it is shown a simulation of K value for a range of hardness and erosion around the experimental laboratory data. The range of hardness is in the interval [1600,2500], and the range of simulated erosion in [2,10]. The cursor search verifies the data of optimal K value of 0.5297, since it indicates the approximation for that value at the optimization values obtained for an erosion magnitude of 3 kg/mm<sup>3</sup>. Cursor indicates a magnitude K = 0.5274, for erosion rate around 3 and hardness around 2000, even more accurate values can be reached with more tentative search at 3D graphics.



**Figure 5.**-3D surfactal simulation results for Table 3 and Eq. 2 model (erodent particle velocity 40 m/s). Results are acceptable with a Global Minimum sharply determined by cursor that verifies the optimization software results. Matrices of imaging are 75x75.

Following the same type of simulation, the next is to verify the value of the K coefficient for  $v = 80$  m/s. In Figure 4, pictured with cursor values inset, it is detailed the simulation for this velocity and a range of erosion around experimental values [13,14]. The accuracy of the simulation is determined by cursor K magnitude, which is 0.7919 almost equal to the optimal value of 0.7945.

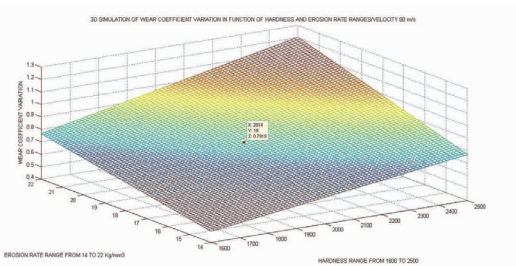


**Figure 6.**-3D surfactal simulation results for Table 4 and Eq. 2 model (erodent particle velocity 80 m/s). Results are acceptable with a Global Minimum sharply determined by cursor, 0.7919, that verifies the optimization goodness software results. Matrices of imaging are 75x75—with Matlab it is possible to reach 1000x1000, dimensions, with Freemat the maximum size is nearby 400x400 for acceptable running image-perormance time.

Finally, to summarize this model optimization/simulation, an additional image of Fig. 4 programming with matrices 500x500 high definition is presented.

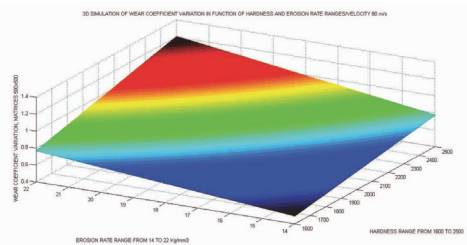


**Figure 7.**-3D surfactal simulation results for Table 4 and Eq. 2 model (erodent particle velocity 80 m/s). Results are acceptable with a Global Minimum that can be sharply determined by cursor (0.7919), that verifies the optimization goodness software results. Matrices of imaging are 500x500. High imaging-surfactal definition is reached at this matrices-size.

After this model, the next proof of optimization/simulation is done with the same experimental data but a more precise formulation derived from the previous model, namely

$$E = \frac{K \rho [V \sin \alpha]^{2.5}}{H} \tag{3}$$

where all the parameters are the same of Eq. 2 but the impact angle  $\alpha$  and the power of the velocity is different. This model was designed specifically for cutting wear, in such a way that the power of the velocity range is from 2 to 2.5.

The formulation that was implemented for the matrix of this model, Eq. 3, was in the same way that is was done with model of Eq. 2, the graphical optimization/simulation is shown in the following for model of Eq. 3. In Figure 10, it is seen that for the hardness values corresponding to minimum of least squares objective function, there are several options for combinations of impact angle and wear coefficient.

TABLE V

| SIMULATION DATA EQUATION M-2 | PARAMETERS        |                |                             |
|------------------------------|-------------------|----------------|-----------------------------|
|                              | IMPACT VELOCITY V | IMPACT ANGLE K | EROSION EXPERIMENTAL VALUES |
| OPTIMIZATION 1               | 40 m/s            | variables      | 3                           |
| OPTIMIZATION 2               | 80 m/s            | variables      | 18                          |

**Table 5.**-Optimization parameters for Eq. 3 model. This optimization is more complicated as it involves two variables, and one of them is a sine, a trigonometric function.

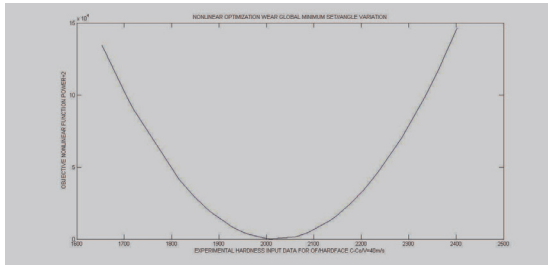


**Figure 8.**-Objective function (OF) nonlinear optimization results for Table 6 and Eq. 3 model, Matlab 2009-12 (erodent particle velocity 40 m/s). Results are acceptable with a Global Minimum sharply determined and running time is lower than a second.

| SEARCH POINT | OPTIMAL K/ HARDNESS AND IMPACT ANGLE VALUE (INVERSE METHOD) V =40m/s   | RESIDUAL OF OBJECTIVE FUNCTION (OF) |
|--------------|--|-------------------------------------|
| X=[1,0.5]    | 0.0343/74.2107°  | 1.4155e+3                           |
| X=[0.8,0.2]  | 1.0473/86.0262°  | 1.8135e+3                           |
| X=[0.5,0.9]  | 0.0952/79.5778°  | 1.4135e+3                           |
| X=[0.5,0.8]  | 0.9029/85.7850°  | 1.6135e+3                           |
| COMMENTS     | Acceptable but variable result for optimization two variables, low residual of OF global minimum exact for any search point, angle of sine has influence |                                     |

**Table 6.**-Numerical data that was obtained from nonlinear optimization of Eq. 3. Here the impact angle makes variations according to search point.

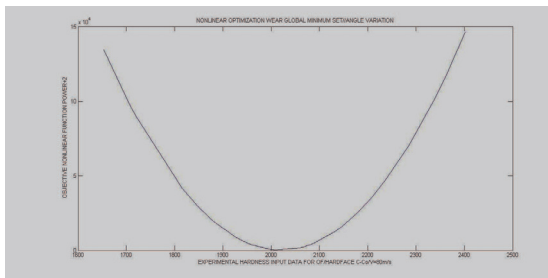


**Figure 9.**-Objective function (OF) nonlinear optimization results for Table 7 and Eq. 3 model, Matlab 2009-12 (erodent particle velocity 80 m/s). Here the impact angle makes variations according to search point.

| SEARCH POINT | OPTIMAL K/ ANGLE VALUE (INVERSE METHOD) V = 80 m/s  | RESIDUAL OF OBJECTIVE FUNCTION (OF) |
|--------------|---|-------------------------------------|
| X=[0.8,0.9]  | 0.0015/74.4507°   | 1.4235e+3                           |
| X=[0.85,0.9] | 1.0439/85.9286°   | 1.5135e+3                           |
| X=[0.4,0.9]  | 1.9295/86.8127°   | 1.4135e+3                           |
| COMMENTS     | Acceptable result for optimization low residual of OF global minimum exact for any search point, sine angle and search point show that OF is not totally convex, it is a product of variables in OF |                                     |

**Table 7.**-Numerical data that was obtained from nonlinear optimization of Eq. 3 (erodent particle velocity v = 80 m/s).

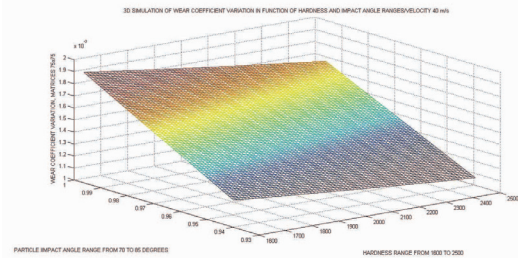


**Figure 10.**-3D surfactal simulation results for Table 5 and Eq. 3 model. The impact velocity is 40m/s. Range of angles for Eq. 3 is [70°,85°]. Range of hardness is [1600,2500]. Results corroborate the Tables 6,7 numbers. That is, a global minimum is not totally well-defined. Matrices of imaging are 75x75.

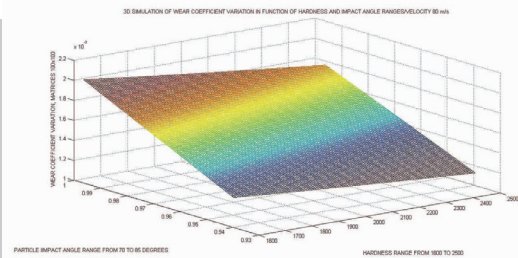


**Figure 11.**-3D surfactal simulation results for Table 5 and Eq. 3 model (erodent particle velocity 80 m/s). Range of angles for Eq. 3 is [70°,85°]. Range of hardness is [1600,2500]. A global minimum is not totally well-defined, among other reasons, because of there is a product of variables in objective function. Matrices of imaging are 75x75.

According to simulations and optimization results shown, the practical conclusion is that not all objective functions are well-defined in convexity. The graphical 3D optimization is a good

tool to find coherent values for variables when their number increases—specially when there is a product of consecutive variables. In the following section, models with continuous functions are overviewed.

#### IV. THE SECOND GENERATION OF TRIBOLOGY MATHEMATICAL MODELS, NEW ASPECTS IN MODERN TRIBOLOGY

After the recent decades of extent development in number and varieties of tribology models, e.g., wear, erosion, corrosion, tribocorrosion, abrasion etc, the current times in investigation of engineering-manufactured materials, have resulted in non-singular-compounded materials production/use—for example, hardmetal reinforced metal composites [15]. This, specifically in power engineering plants, is the consequence of new requirements for multi-functional materials in industry, plants design/construction, and the emerging large number of an extent variety of options at every branch of any kind of industry. For instance, from the automobile to energy plants pipes, it is possible to find a considerable choice of different types for each particular necessity.

Therefore, since requirements of hardness, plastic deformation with/without fatigue magnitudes, cutting erosion, or brittle resistance involve a large number of situations, the search for mixed materials, e.g., carbides, composites, kind of reinforcements, or similar compounds, has experienced a significant industrial-compounds development—with the additional effect of multi-varied manufacturing options and industrial expansion [16].

To date, the classical mathematical models in tribology based on discrete or single-valued parameters can be considered rather obsolete, since new materials are compounded by several phases of different chemical-physical conditions. This fact implies that the surface exposed to abrasion wear damage for particles, for instance, is not homogeneous in wear resistance/rate, because the fluence of abrasive particles impact is probabilistically distributed over the non-equal spatial compounded material surface—and just the same concept is applicable for corrosion, biotribology, or tribocorrosion.

It is straightforward guessed that the parameters of the models should become at least differentiable-integrable functions for every type of compounded material, in spatial-surface and thickness, rather than a series of discrete numerical values or an average approximated valued for all the surface.

The new generation of tribology mathematical models conceived to obtain improved/precise determinations of tribology engineering-values should be formed by continuous functions of parameters, derivable and integrable for the material mathematical-numerical range conditions [1,17].

As a result, a number of nonlinear optimization, stochastic optimization, statistical-probabilistic variables have concentrated their effect on the design of new generation of tribology models for future high-precision applications [1,17].

An important complementary subject in this type of materials production, is the group of constraints to be taken into account for improvements in circular economy. This, in particular at European Union conditions/legislation, constitutes a key point for a sustainable environmental-industrial development.

Therefore, to conclude this section, it is sharply meant the new steps towards the subsequent generation of tribology models for future-extensive applications/improvements.

#### V. DISCUSSION AND CONCLUSIONS

This contribution supposes a continuation of the study started in a previous article of initial mathematical description of tribology, erosion and corrosion models, with some brief numerical optimization examples. However, this step forward research was focused on nonlinear optimization and direct applications of inverse problems theory. The models that were presented for optimization were detailed to demonstrate the method of inverse nonlinear optimization with specific software. All the selected models in this study are appropriate/suitable to be implemented on any other more complicated equation, no matter the number of variables to be optimized—large-scale multiobjective optimization could be carried out with the programming designed properly [1,4,17]. In particular, graphical 3-D optimization/simulation surfaces were shown for sharp learning of this new technique.

Results are considered accurate and acceptable, conditioned to serial lab experimental validation in future research. The practical applications in erosion/corrosion models for power plants, energy industry, and circular production, follow straightforward form the proven method with adequate software.

#### ACKNOWLEDGMENTS AND SCIENTIFIC ETHICS STANDARDS

This work was supported by institutional research funding IUT19-29 Multi-scale structured ceramic-based composites for extreme applications of the Estonian Ministry of Education and Research. This study was carried out, and their contents are done according to the European Union Technology and Science Ethics. Reference, 'European Textbook on Ethics in Research'. European Commission, Directorate-General for Research. Unit L3. Governance and Ethics. European Research Area. Science and Society. EUR 24452 EN [18]. This research was completely done by the authors, the software, calculations, images, mathematical propositions and statements, reference citations, and text is original for the authors. This article contains also unique numerical data and special new-improved images. When anything is taken from a source, it is adequately recognized. Ideas from previous publications were emphasized due to a clarification aim.

## REFERENCES

- [1] Casesnoves F, Suzenkov A. Mathematical Models in Biotribology with 2D-3D Erosion Integral-Differential Model and Computational-Optimization/Simulation Programming. *International Journal of Scientific Research in Computer Science, Engineering and Information Technology*, 2017, **2**(3), 329–56.
- [2] Surzhenkov A, Viljus M, Simson T, Tarbe R, Saarna M, Casesnoves F. Wear resistance and mechanisms of composite hardfacings atabrasive impact erosion wear. *IOP Conf. Series: Journal of Physics*, 2017, **843**, 012060.
- [3] Abramowitz M, Stegun IA. Handbook of Mathematical Functions with Formulas, Graphs and Mathematical Tables. Dover, New York, 1972.
- [4] Casesnoves F. Applied Inverse Methods for Deformable Solid Dynamics/Kinematics in Numerical Reuleaux Method (NRM). *International Journal of Numerical Methods and Application*, 2013, **9**(2), 109–131.
- [5] Balamanikandasuthan K, Arun K, Sharath Sekar Palam. Design and fabrication of erosion protection shield for boiler tubes and its analysis. *International Journal of Mechanical and Materials Engineering*, 2015, **1**(1), 39–52.
- [6] Higuera Hidalgo V., Belzunce Varela J., Earilles Menéndez A., Poveda Martinez S. High temperature erosion wear of flame and plasma sprayed nickel chromium coatings under simulated coal-fired boiler atmospheres. *Wear*, 2001, **247**, 214–222.
- [7] Antonov M, Veinthal R, Huttunen-Saarivirta E, Hussainova I, Vallikivi A, Lelis M, Priss J. Effect of oxidation on erosive wear behaviour of boiler steels. *Tribology International*, 2013, **68**, 35–44.
- [8] Erosion in fluidized-bed boilers. In: High-temperature corrosion and materials applications, Lai GY (ed.), ASM International, Materials Park, 2007, 307–314.
- [9] Erosion and erosion-corrosion. In: High-temperature corrosion and materials applications, Lai GY (ed.), ASM International, Materials Park, 2007, 235–248.
- [10] Power Plant Life Management and Performance Improvement. Oakey JE (ed.), Woodhead Publishing Ltd., Cambridge, 2011.
- [11] Casesnoves F, Antonov M, Kulu P. Mathematical models for erosion and corrosion in power plants. A review of applicable modelling optimization techniques. Proceedings of the 57th International Scientific Conference on Power and Electrical Engineering of Riga Technical University RTU CON 2016, 13–14 October 2016, Riga, Latvia, art. no. 7763117.
- [12] Crocker LE. A review of current methods for modelling erosive wear. National Physical Laboratory Report MAT 52, 2011.
- [13] Kleis I, Kulu P. Solid Particle Erosion. Occurrence, Prediction and Control. Springer Verlag, London, 2008.
- [14] Hussainova I, Kubarsepp J, Shcheglov I. Investigation of impact of solid particles against hardmetal and cermet targets. *Tribology International*, 1999, **32**, 337–344.
- [15] Kulu P, Tarbe R, Zikin A, Sarjas H, Surzhenkov A. Abrasive wear resistance of recycled hardmetal reinforced thick coating, *Key Engineering Materials*, 2013, **527**, 185–190.
- [16] Kulu P, Hussainova I, Veinthal R. Solid particle erosion of thermal spray coatings. *Wear*, 2005, **258**(1–4), 488–496.
- [17] Casesnoves F. Applied inverse methods for optimal geometrical-mechanical deformation of lumbar artificial disks/implants with numerical reuleaux method. 2D comparative simulations and formulation. *Computer Science Applications*, 2015, **2**(4), 1–10.
- [18] European Textbook on Ethics in Research. Publications Office of the European Union, Luxembourg, 2010.

**Francisco Casesnoves** is computational-engineering/physics researcher, MSc-BSc, Physics/Applied-Mathematics (Eastern-Finland-University), Graduate-with-MPhil, in Medicine and Surgery (Madrid University Medicine School), and PhD Candidate at TUT. Casesnoves education/scientific vocation was motivated young, by Profs Candida Navamuel and Isabel Vela, in Renaissance-Humanism ideas. His research, 61 international publications, is Computational-mathematical Nonlinear/Inverse Optimization. Casesnoves best-achievement is the Numerical Reuleaux Method in dynamics and nonlinear-optimization.

**Andrei Surzhenkov** received his MSc in Product Development and Production Engineering from Tallinn University of Technology (TTU) in 2007 and PhD from TTU in 2011. Since 2016 he is a teaching assistant at the Department of Mechanical and Industrial Engineering (TTU). His principle research interests lie in the areas of thick wear resistant coatings (obtained by thermal spraying or cladding) and surface duplex treatment (laser hardening of PVD coated steels, etc.).

# Curriculum vitae

## Personal data

Name: Francisco Jose Casesnoves Granado Lopez de Haro

Date of birth: 4/4/1959

Place of birth: Madrid City

Citizenship: Political Asylum Process in USA

## Contact address

e-mail: frcase@taltech.ee

## Education

2016–2018, Tallinn University of Technology, PhD

2017–October, Mektory Aerospace Center Satellite Program course

2017–September, TalTech Cybersecurity studies, ITC0004, Oxford University Certificate

2017–July, Mektory, TalTech, Tech Innovation Startup

2017–January, TalTech, 20-hours Course, Visual Components/Phyton Programming

2010–July, Princeton University, Institute in Mathematics, Utah

2005–2009, PhD Researcher, Optimization, Nottingham University

1998–2001, MSc, Eastern Finland University, Physics/Applied Mathematics

1997–2001, BSc, Eastern Finland University, Physics/Applied Mathematics

1995–European Union License for Physician Practice in any EU and associated countries

1985–MPhil in Medicine and Surgery, Medical Physics, Radioprotection

1983–1985, Researcher, Radio-Dosimetry at Medical Physics Dept, Madrid University

1976–1983, Graduate in Medicine and Surgery, Madrid University, 6 years career.

Training in medical and surgical practice at Clinical Madrid Hospital (1979–1981) and Central Defence Madrid Hospital (1981–1983)

1970–1976, Public High School ALVIMAR (today Public Gran Capitan Institute, with Honors)

## Language competence

A2 Estonian Language Innove Examination, February 2018, 55 %

A2 AtlasNet Diploma, January 2018, 60 %

A1 Estonian Language and Culture course, TalTech, HLE0050, 2017, A Level

A2 Estonian Language Academy, EU-Project, 2018, 51 %

A1 Estonian Course 2017, Ministry of Education, 17/25 points

English-Fluent, IELTS, International English language Testing System, Band 6.5, British Council Evaluation 2004, reading, writing, listening, and speaking

Madrid Languages School, 1996, 4<sup>th</sup> English course

Madrid Languages School, 1996, English language for bachelor (1<sup>st</sup>, 2<sup>nd</sup>, 3<sup>rd</sup> courses)

Madrid Languages School, 1977–1979, English language for professors (1<sup>st</sup>, 2<sup>nd</sup>, 3<sup>rd</sup> courses)

5 years of American English as resident in USA, 2011–2016; British English as resident in UK, 2005–2011; 5 years basic Finnish, 1996–2001

## Professional employment

2016 September–2017 June, Researcher, Department of Mechanical and Industrial Engineering, TalTech

2017 July, EIT European Union Innovation and Technology Program scholarship for medical devices engineering-computational design. Professional scholarship in Tartu University (European Union EIT-Health Technology)

2007 spring, Assistant Teacher at Machine Dynamics Problems Dep., Nottingham University

2006 autumn, Assistant teacher at Thermofluids Laboratory, Nottingham University.

2005 October–2009 October, EPSRC-Award (Engineering and Physical Science Research Council UK), Scholarship, Post-graduate in Computational bioengineering optimization, Nottingham University

2003–2005, Researcher-collaborator at Electromagnetism Department, Madrid University

1995–1996, Researcher-collaborator at Experimental surgery unit at Gregorio Marañón Hospital, Madrid NHS

1983–2005, Physician licensed at Madrid Medical Council working at NHS Madrid

1984–1995, Medical practice at National Health System, Madrid community

Membership of scientific societies: SIAM (Society for Industrial and Applied Mathematics), 2007–2008, 2019–2010. SIAG (SIAM Group Geometrical Design and Computing), 2010–2012). ASME (American Society of Mechanical Engineers), 2010–2013. IIIS, (International Institute of Informatics and Systemics), 2014–2015. IEEE (International Institute of Electronics and Electrical Engineers), 2013–2014, 2016–2017. IAAM (International Association of Advanced Materials), 2017– Permanent membership

# Elulookirjeldus

## Isikuandmed

Nimi: Francisco Jose Casesnoves Granada Lopez de Haro

Sünniaeg: 4/4/1959

Sünnikoht: Madrid

Kodakondsus: Poliitiline varjupaigamenetus USAs

## Kontaktandmed

E-post: frcase@taltech.ee

## Hariduskäik

2016–2018, Tallinna Tehnikaülikool, doktoriõpe

2017–Okt., Mektory Kosmoseagentuuri Satelliitprogrammi kursus

2017–Sept., TalTech, Küberjulgeoleku uuringud, ITC0004, Oxfordi Ülikooli sertifikaat

2017–Juuli, Mektory, TalTech, Tech Innovation Startup

2017–Jaan., TalTech, 20-tunniline kursus, Visual Components/Phyton Programmeerimine

2010–Juuli, Princetoni Ülikool, Matemaatika Instituut, Utah

2005–2009, PhD Teadlane, Optimeerimine, Nottinghami Ülikool

1998–2001, MSc, Ida-Soome Ülikool, füüsika / rakenduslik matemaatika

1997–2001, BSc, Ida-Soome Ülikool, füüsika / rakenduslik matemaatika

1995–Euroopa Liidu tegevusluba arstipraktikale kõikides ELi ja assotsieerunud riikides

1985– MPhil meditsiinis ja kirurgias, meditsiiniline füüsika, kiirguskaitse

1983–1985, Teadlane, Raadio-dosimeetria meditsiinifüüsika osakonnas, Madridi Ülikool

1976–1983, Meditsiini ja kirurgia lõpetaja, Madridi Ülikool, 6-aastane karjäär. Koolitus

Madridi kliinikus asuvas haiglas meditsiinis ja kirurgias (1979–1981) ja Madridi Sõjaväe Peahaiglas (1981–1983)

1970–1976, Avalik keskkool ALVIMAR (praegu Avalik Gran Capitan Instituut, Autasuga)

## Keelteoskus

A2 Innove Eesti keele eksam, veebruar 2018, 55 %

A2 AtlasNet diplom, jaanuar 2018, 60 %

A1 Eesti keele ja kultuuri kursus, TalTech, HLE0050, 2017, A tase

A2 Eesti keele akadeemia, EU-projekt, 2018, 51 %

A1 Eesti keele kursus, 2017, Haridus- ja Teadusministeerium, 17/25 punkti

Inglise keel-suurepärase, IELTS tase 6.5, Briti Nõukogu hinnang, 2004, lugemine, kirjutamine, kuulamine ja rääkimine

Madridi keeltekool, 1996, 4. inglise keele kursus

Madridi keeltekool, 1996, 1.-3. inglise keele kursused (bakalaureus tase)

Madridi keeltekool, 1977–1979, 1.-3. inglise keele kursused (professori tase)

Ameerika inglise keele praktika, 5 aastat, (elanik USA-s 2011–2016); Suurbritannia inglise keele praktika, (elanik Suurbritannias 2005–2011); soome keele praktika (elanik Soomes 1996–2001)

### **Teenistuskäik**

2016 september–2017 juuni, Teadlane, Mehaanika ja tööstustehnika instituut, TalTech  
2017 juuli, EIT Euroopa Liidu innovatsiooni- ja tehnoloogiaprogrammi stipendium meditsiiniseadmete insener-arvutusliku disaini jaoks. Tartu Ülikooli erialastipendium (Euroopa Liidu EIT-tervishoiutehnoloogia)

2007 kevad, Õpetaja assistent, Masina dünaamika probleemide osakond, Nottinghami Ülikool

2006 sügis, Õpetaja assistent, Termovedelikute laboratoorium, Nottinghami Ülikool

2005 oktoober–2009 oktoober, EPSRC-auhind (Engineering and Physical Science Research Council, Suurbritannia), aspiranti stipendium, Arvutuslik bioinseneerne optimeerimine, Nottinghami Ülikool

2003–2005, Teadur Elektromagnetismi osakonnas, Madridi Ülikool

1995–1996, Teadur Eksperimentaalse kirurgia üksuses, Gregorio Marañón Hospital, Madrid NHS

1983–2005, Madridi arstide nõukogus litsentseeritud arst, NHS Madrid

1984–1995, Meditsiinipraktika riiklikus tervisesüsteemis, Madridi kogukond

Teadusühiskonna liikmelisus: SIAM (Society for Industrial and Applied Mathematics), 2007–2008, 2019–2010. SIAG (SIAM Group Geometrical Design and Computing), 2010–2012. ASME (American Society of Mechanical Engineers), 2010–2013. IIS, (International Institute of Informatics and Systemics), 2014–2015. IEEE (International Institute of Electronics and Electrical Engineers), 2013–2014, 2016–2017. IAAM (International Association of Advanced Materials), 2017– püsiv liikmelisus